Modeling and Analysis of the Effects of Impairments in Fiber Optic Links

Surachet Kanprachar

Thesis submitted to the Faculty of the
Virginia Polytechnic Institute and State University
in partial fulfillment of the requirements for the degree of

Masters of Science
in
Electrical Engineering

Dr. Ira Jacobs, Chair
Dr. Anbo Wang
Dr. Brian D. Woerner

September 14, 1999
Blacksburg, Virginia

Modeling and analysis of the effects of impairments in fiber optic links

by

Surachet Kanprachar

Dr. Ira Jacobs, Chairman

Electrical Engineering

(ABSTRACT)

In digital communication systems, several types of impairments may be introduced to the signal. These impairments result in degraded system performance; for example, high bit-error-rate or power penalty. For optical communication systems, in this thesis, these impairments are categorized into four types; that is, thermal noise, shot noise, signal-dependent noise, and intersymbol interference (ISI). By using a Gaussian approximation, effects of the first three impairments are analyzed. It is shown that signal-dependent noise introduces an error floor to the system and the bit-error-rate is considerably degraded if a nonzero-extinction ratio is applied to the system. It is shown that if the decision threshold at the decision circuit is set improperly, more received power is required to keep the bit-error-rate constant.

Three main components in the system (i.e., transmitter, optical fiber, and receiver) are modeled as Butterworth filters. ISI from this model is determined by computer simulation. A high ISI is from a small system bandwidth. It is shown that a minimum power penalty can be achieved if the transmitter and receiver bandwidths are matched and fixed, and the ratio of fiber bandwidth to bit rate is 0.85. Comparing ISI from this model to ISI from raised cosine-rolloff filters, it is shown that at some particular bandwidths ISI from raised cosine-rolloff filters is much lower that that from this model. However, if the transmitter and receiver bandwidths are not matched and are not equal to these bandwidths, ISI from this model is lower than ISI from raised cosine-rolloff filters.

Acknowledgments

I would like to express my deeply felt gratitude to Dr. Ira Jacobs, my advisor and mentor, whose erudition in the field is unequaled, who provided generous advice and extensive feedback on the manuscript, considerably polishing the final version. I dedicate this thesis to him with affection and respect.

I am especially indebted to Dr. Brian D. Woerner and Dr. Anbo Wang for their serving on my graduate committee.

Finally, grateful thanks go to my family and my girlfriend for their immeasurable understanding and encouragement.

Table of Contents

List of Illustrations

1.0 Introduction

In communication systems, there are three main components; that is, transmitter, channel, and receiver. To send information from one place to another these components are combined together, each has particular functions. First, input information is passed through a transmitter to transform into an appropriate format for sending through a channel. The channel then carries the transmitted signal from a transmitter to a receiver. There are many kinds of channel; for example, a telephone line, an optical fiber, and free space. At a receiver, a received signal is detected and converted back to its original format. Some signal processings may be added at the transmitter and/or the receiver to improve system performance.

For optical communication systems, the three main components are optical transmitters, optical fibers, and optical receivers. The main function of optical transmitters is to convert an input electrical signal into an optical signal and then launch it into an optical fiber. The major component of the optical transmitters is an optical source, which is generally divided into two types; that is, light-emitting diodes (LEDs) and semiconductor lasers. An optical fiber acts like a channel of the system. The optical signal launched from the optical transmitter propagates along the optical fiber to an optical receiver. The main component in an optical receiver is a photodetector. This component will convert the received optical signal into a photocurrent. This current is

then sent to an electrical amplifier and a decision circuit for receiving the transmitted information.

Along these components, many types of impairments are added to the signal. These impairments result in a fluctuation to the signal; thus, the statistical properties of the signal are changed. In this thesis, the impairments are categorized into four types; that is, thermal noise, shot noise, signal-dependent noise, and intersymbol interference. Thermal noise arises from the random movement of the charge carriers in electronic devices in the system. Thermal noise is modeled as a Gaussian random process [1]. This noise is the major limitation for a system using p-i-n photdetectors.

Shot noise is the quantum noise due to the fact that the received signal is actually a series of photons [3]. The number of received photons during each bit period varies randomly from one bit to another bit, and is Poisson distributed. This random nature of received photons leads to a fluctuation on the photocurrent; thus, shot noise. Some experimental measurements of shot noise have been performed by Bachor [6], Bacon et al. [7], and Tsai and Liu [8]. In [7], Bacon et al. have shown that the power of shot noise is proportional to the received optical power.

Signal-dependent noise is divided into three types; that is, modal noise, mode partition noise, and relative intensity noise. Modal noise is from the interference among the various propagating modes in a multimode fiber. This interference results in a time-varying speckle pattern at the end face of the fiber; hence, a fluctuation on the received signal. In [9] to [16], the effects of modal noise on the system performance have been studied. Hjelme and Mickelson [10] and Das et al. [13] have shown that microbending and fiber misalignments can enhance modal noise and reduce the signal-to-noise ratio of the received signal. The effect of a longitudinal gap between two multimode fibers on modal noise has been studied by Das et al. [12]. In [15], it has been shown that modal noise can lead to a bit-error-rate floor to the system.

An intensity fluctuation among the longitudinal modes of a multimode semiconductor laser and different propagating velocities caused by fiber dispersion result in a fluctuation of the signal at the receiver end. This fluctuation introduces a noise called mode partition noise. This noise has been measured experimentally by Okano et al. [17] and Ogawa et al. [19]. The measurements indicate that mode partition noise causes degradation of the

bit-error-rate performance. The analysis of mode partition nosie has been done by Ogawa [18], Miller [21,22]. In [18], Ogawa has shown that the signal-to-noise ratio due to mode partition noise is independent of the signal power but depends on the fiber dispersion and half width of the laser diode spectrum. Laughton [20] has shown that partition noise from a low-coherence laser such as a gain-guided laser has a strong effect on the performance of a multimode optical system.

Another type of signal-dependent noise is relative intensity noise (RIN). This noise is from a fluctuation induced by the spontaneous emission in semiconductor lasers. The optical feedback from multiple reflections along the fiber path can increase the effect of this noise. The effect of optical feedback that is fed back into a laser cavity has been studied experimentally by Fujita et al. [23]. It is shown that, for the same amount of optical feedback, the increase of intensity noise depends on the optical feedback phase. Port and Ebeling [24] have shown that the intensity noise under moderate optical feedback depends on the injection current and the cavity length of lasers. Nakano et al. [27] have shown that the excess intensity noise induced by external reflection in gain-coupled distributed feedback lasers is less than that of the index-coupled distributed feedback lasers, if the optical feedback is restricted below 1 percent. Independent of the optical feedback reflected back into lasers, the optical feedback from multiple reflections along the fiber path can cause the phase-to-intensity noise conversion, which also enhance RIN at the receiver. This type of RIN enhancement has been studied by Gimlett [26], [28], and [29]. It has been shown that multiple reflections of a few percent per connector/splice can give unacceptable system degradation.

The last impairment is intersymbol interference. This type of impairment arises from overlapping between pulses caused by the pulse broadening and distortion induced by components in the system. This overlap can cause a wrong decision at the decision circuit at the receiver; thus, increase of bit-error-rate. Equalization is a way to solve this problem. Liu et al. [31] have calculated the bit-error-rate from three types of equalizers for different amounts of intersymbol interference. They have found that the use of a proper equalizer can significantly improve the bit-error-rate performance and the best choice of an equalizer depends on the input waveform, amount of intersymbol interference, and the APD gain.

The intent of this thesis is to model the impairments in fiber optic systems and to examine the effect of impairments on system performance. In chapter 2, the theory and results from [1] to [31] for all impairments are summarized. The characteristics of these impairments are explained. Some techniques to reduce these impairments are given.

In chapter 3, the mathematics describing the effect of impairments on system performance are presented. The effect of extinction ratio is also included. The Gaussian approximation is used in this chapter to calculate the system performance. The error probability, the required average number of photons per bit, and the power penalty are described mathematically and graphically.

Chapter 4 deals with the effect of system bandwidth on intersymbol interference. In this chapter, the three main components (i.e., transmitter, optical fiber, and receiver) are modeled by using Butterworth filters. The effect of each component on intersymbol interference is evaluated and plotted. The intersymbol interference is characterized by two quantities; that is, normalized maximum intersymbol interference and normalized RMS intersymbol interference. The model using Butterworth filters is compared to the model using raised cosine-rolloff filters. The advantages and disadvantages of each model are explained. The last part of this chapter evaluates the power penalty due to intersymbol interference.

Chapter 5 includes a summary of the work done, conclusions, and suggestions for future work.

2.0 Impairments in fiber optic systems

In this chapter, impairments in fiber optic systems; that is, thermal noise, shot noise, signal-dependent noise, and intersysmbol interference will be discussed. The theory and results developed from [1] to [31] are summarized. Thermal noise, which originates from random movement of the charge carriers in a conductor, is explained. The formula for thermal noise power will be given. The random nature of the electron-hole pairs generated by an incident optical signal at photodetector results in a fluctuation to the photocurrent. This fluctuation causes a noise called shot noise. The characteristics of shot noise will be discussed. Next, signal-dependent noise will be explained. Signal-dependent noise in fiber optic systems can be categorized into three types; that is, modal noise, mode-partition noise, and relative intensity noise. Characteristics of each will be discussed. Finally, intersymbol interference, which is induced by the pulse broadening, will be explained.

2.1 Thermal noise

An important source of noise in optical receivers is thermal noise. This type of noise originates from the random movement of the charge carriers in a conductor [4]. This random motion introduces a current fluctuation in a resistor; thus, thermal noise. The thermal noise current is modeled as a stationary Gaussian random process with a spectral density that can be considered to be white up to the frequency of 1 THz [1]. The thermal noise mean square current of an optical receiver is given by [2]

$$\left\langle i_{th}^2 \right\rangle = \frac{4k_B T \Delta f}{R_L} \qquad (2.1.1)$$

where i_{th} is the current induced by thermal noise

k_B is the Boltzmann constant (=1.38*10^{-23} J/K)

T is the absolute temperature

Δf is the effective noise bandwidth of the receiver

R_L is the effective noise resistance.

From equation (2.1.1), the variance of thermal noise current depends on three parameters, i.e., the absolute temperature, the noise bandwidth of the receiver, and the effective noise resistance. This equation is based on the assumption that the frequency range over which the power spectral density of thermal noise is white is larger than the effective bandwidth of the receiver. In practice, the current generated from a photodetector will be amplified by a preamplifier. There are many designs for this preamplifier. One important design is a transimpedance amplifier. In this design the load resistor is connected as a feedback resistor around an inverting amplifier [1]. The effective noise resistance of a transimpedance receiver can be approximated by this feed back load resistance. The effective noise bandwidth of this receiver is given by

$$\Delta f = \frac{1}{2\pi R_L C_e} \qquad (2.1.2)$$

where C_e is the effective noise capacitance of the transimpedance preamplifier.

For a transimpedance amplifier C_e may be smaller than the photodiode capacitance, and is determined by parasitic capacitances in the amplifier. Good receivers have $C_e \approx 0.1$ pF [5].

From equation (2.1.1), if the effective noise resistance is increased, the variance of thermal noise is decreased. However, the effective noise bandwidth of the receiver will be smaller as shown from equation (2.1.2). This small receiver bandwidth can lead to intersymbol interference if the bit rate of the data is higher than the receiver bandwidth.

Substituting equation (2.1.2) into equation (2.1.1), the variance of thermal noise can be rewritten as

$$\left\langle i_{th}^2 \right\rangle = 8\pi q V_T C_e (\Delta f)^2 \qquad (2.1.3)$$

where q is the charge of an electron (= $1.6*10^{-19}$ C)

$$V_T = \frac{k_B T}{q} = 0.025 \text{ V} \quad \text{at } T = 290 \text{ K} .$$

The variance of thermal noise in equation (2.1.3) will be used in the next chapter, which will discuss the effects of impairments on the system performance.

2.2 Shot noise

In the detection process of an optical transmission system, the photocurrent of a photodetector is generated by the incident photons at the end face of the fiber. The average photocurrent is given by [7]

$$I_p = \frac{\eta q}{h\nu} P_{in} \qquad (2.2.1)$$

where η is the quantum efficiency

q is the charge of an electron (=1.6*10^{-19} C)

h is Planck' s constant (=6.6256*10^{-34} J-s)

ν is the optical signal frequency

P_{in} is the incident optical power.

From equation (2.2.1) the average photocurrent depends on three parameters; that is, the quantum efficiency, the optical signal frequency, and the incident optical power. If the incident optical power fluctuates, it can surely cause noise in the receiver. Such noise will be discussed later. However, if the incident light power is constant, a fluctuation in the photocurrent still occurs. This fluctuation is from the nature of the discreteness and randomness of the electrons generated in the photodetector [7]. The optical energy transmitted by a beam of light is proportional to the number of photons incident on the photodetector, which is a discrete number. The arrival times of photons from a transmitter to a photodetector are governed by Poisson statistics [6]. These incident photons generate the electrons at the photodetector randomly; therefore, the photocurrent fluctuates. This fluctuation causes a noise called shot noise. Shot noise in an optical fiber system is also called quantum noise since it comes from the quantum nature of light [6]. The power of the shot noise is given by [1]

$$\sigma_s^2 = 2qI_p\Delta f \qquad (2.2.2)$$

where Δf is the effective noise bandwidth of the receiver.

From equation (2.2.2), the shot noise power depends on the photocurrent due to the incident optical power and the effective noise bandwidth of the receiver. However, the dark current, I_d, also generates shot noise in the photodetecter. This dark current is caused by the thermal generation of electron-hole pairs, which occurs in all photodiodes [8]. If the dark current is considered to be one of the source of shot noise, the power of shot noise in equation (2.2.2) will be changed to be [1]

$$\sigma_s^2 = 2q(I_p + I_d)\Delta f \qquad (2.2.3)$$

In general, the value of the dark current in high bandwidth optical communication system is very small compared to the average photocurrent due to the incident optical power, and may be neglected. Thus, equation (2.2.2) is still useful for the receiver noise calculation in communication systems.

In [7], shot-noise voltage is measured as follows. A laser beam of power P is split at a beam splitter and launched onto two photodetectors. An adjustable attenuator is placed in front of a photodetector to balance the two laser beam intensities; thus, the laser-intensity fluctuations are suppressed. The difference between the photocurrents produced by these photodetectors is sent to a transimpedance amplifier. This current includes a fluctuation from shot noise corresponding to the total photocurrent I_p. At the transimpedance amplifier, the input current is converted to a voltage signal, and a fluctuation from thermal noise is added to the voltage signal. To get shot noise power, this voltage signal is fed into a squarer producing an output voltage. Then, this output voltage is further fed into a lock-in amplifier, which will produce the difference of the squared noise signals when the laser beam is ON or OFF. The output voltage of the lock-in amplifier is called the lock-in amplifier input voltage, which is proportional to the mean-square shot-noise voltage; that is, shot noise power. The result, shown in Figure 2.1, indicates that the lock-in amplifier input voltage varies linearly with the laser power from 3 mW down to 1 μW. Consequently, shot noise power is also proportional to the laser power. This result agrees with equation (2.2.1) and equation (2.2.2).

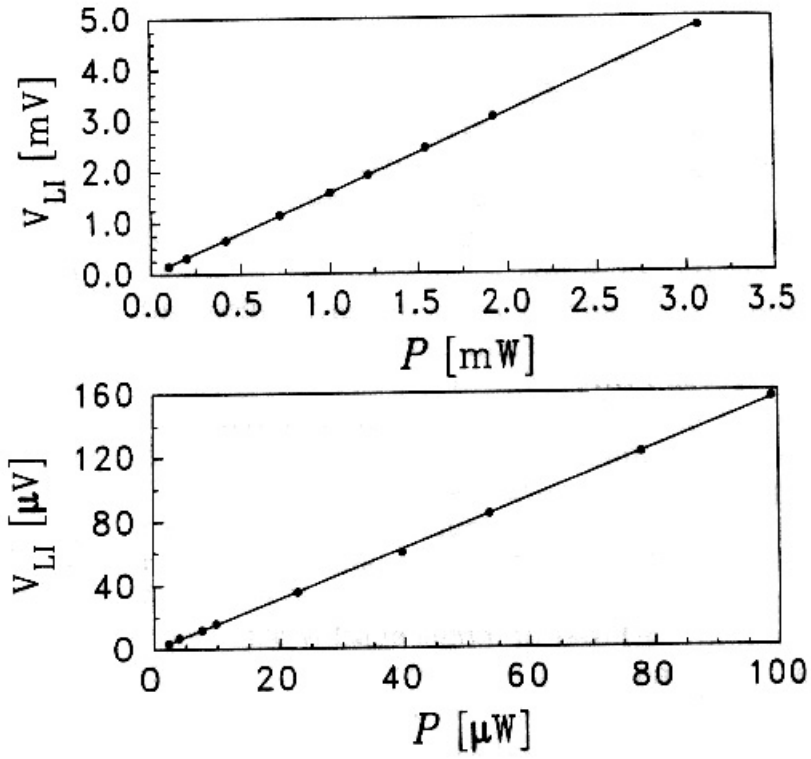

Figure 2.1 The lock-in amplifier input voltage as a function of incident laser power [7].

The effect of shot noise also changes as the type of photodetector changes. An avalanche photodetector (APD) is one type of photodetector that can increase the photocurrent from equation (2.2.1) by a factor of M. The multiplication factor (M) is from a phenomenon called impact ionization in the APD [1]. The impact ionization process will generate additional electron-hole pairs at random times. These electron-holes pairs will increase the achievable photocurrent but also add some additional fluctuations to the photocurrent because of their randomness. Therefore, shot noise in an APD become more significant compared to shot noise in a p-i-n photodetector. The effect of shot noise on the receiver performance will be discussed in the next chapter.

2.3 Signal-dependent noise

2.3.1 Modal Noise

In multimode fiber transmission systems, there are many guided modes supported by the fiber. These guided modes can randomly interfere with one another as they travel along the fiber path since their propagating velocities are different. This modal interference causes a type of noise called modal noise [9]. The interference among the various propagating modes in the multimode fiber generates a speckle pattern at the end face of the fiber [1]. When this speckle pattern varies with time, a fluctuation of the optical signal at the receiver occurs; that is, the modal noise. This noise seriously impairs transmission performance in both analog and digital multimode fiber systems [14]. This leads both to a power penalty and bit-error-rate floor as shown in [15]. There are many factors that lead to modal noise; for example, the narrow source linewidth, the fiber imperfections, the connection points along the fiber, and so forth. In [16], modal noise is categorized into two frequency components. Low frequency modal noise is caused by the physical distortion, microbending, mode coupling, and variations in the magnitude of spatial filtering. This type of modal noise refers to the slow changes in the speckle pattern. In high frequency modal noise, on the other hand, the change in the speckle pattern is fast. The cause is from the frequency fluctuation in the emitted source spectrum.

The source linewidth ($\Delta\nu$) is one main factor for generating the modal noise. The reciprocal of this parameter is the coherence time ($T_{coh} = 1/\Delta\nu$), which is the time duration that the phase remains relatively stable. Mode interference occurs if the coherence time is longer than the intermodal delay time, which is caused by the fiber dispersion. Thus, when a highly coherent source (a narrow source linewidth) is used in a multimode fiber system, modal noise is easily introduced to the system. At this point, we can see that a low coherence source or incoherent source is preferred (from the standpoint of modal noise) since their coherence time is short; resulting in low modal noise.

The fiber imperfections that affect the system in terms of modal noise are elliptic deformation and microbending [13]. The effect of microbending on the modal noise has been studied in [10] and [13]. It was shown in [13] that the mode-mode interference causes the temporal fluctuations, which give rise to the modal noise. For a given

microbending loss, many microbends, which have small amplitude, cause much less modal noise than a few microbends with large amplitude. The effect of the longitudinal gap between two multimode fibers on the modal noise is shown in [12]. The modal noise and distortion can be caused by the gap between the fibers. For a given gap width, Das *et al.* in [12] have shown that the use of index matching can lessen the modal noise and distortion caused by the longitudinal gap. However, for a given loss, the index matching does not improve anything. Connecting points along a fiber path also lead to the modal noise as shown in [11]. At the connecting point, the optical power fluctuates and causes the modal noise. This fluctuation depends on the total loss due to the fiber misalignment at the connecting point. That is, if the total loss is decreased, the modal noise power is lowered.

There are many ways to reduce the modal noise in the system. From the factors mentioned above, modal noise reduction methods are listed:

- Use of a low coherence source or an incoherent source. A multimode laser or a light emitting diode (LED) should be used if the system operates with a multimode fiber. For multimode lasers, gain-guided lasers are shown in [15] to give less modal noise than index-guided lasers since gain-guided lasers can excite more transverse modes than index-guided lasers do.
- Using a fiber with a large numerical aperture. This increases the number of modes, which makes large fluctuation less likely [2].
- Using a single mode fiber is the way to avoid modal noise since it supports only one mode; that is, there is no mode-mode interference. However, the length between pairs of fiber connections should be large enough to prevent the effect of the power from fundamental mode (LP_{01} mode) coupling to the first higher-order mode (LP_{11} mode) at the first connection and converting back to the fundamental mode at the second connection, which leads to additional modal noise [2].
- It is shown in [11] that the connector and microbending loss should be minimized as much as possible to reduce modal noise. If these losses are lessened, the signal fluctuation is reduced; that is, modal noise is decreased.

- Index matching should be used to reduce the effect of the longitudinal gap on modal noise.
- The decision threshold optimization can also reduce the effect of modal noise on system performance [15]. Since modal noise is signal-dependent, the noise powers at ON and OFF stages are different. This leads to a change in the optimum decision threshold.
- The effect of signal-dependent noise on system degradation in avalanche photodetector (APD) receiver is considered in Appendix A. It is shown that the effects of signal-dependent noise on power penalty in the shot noise limit (for APDs) and the thermal noise limit (for PINs) are the same.

2.3.2 Mode partition noise

In a semiconductor laser, the intensity in each longitudinal mode fluctuates randomly even though the total optical output is constant. This fluctuation takes place both within a pulse and from pulse to pulse. Even if a single-mode laser is used, the intensity fluctuation still occurs if the side modes are not sufficiently suppressed. The fluctuation results from the intrinsic fluctuation caused by the laser operation and the influence of the reflected feedback light from the fiber end faces and connectors [17]. Along the dispersive fiber, each longitudinal mode travels with a different velocity and reaches the receiver at a different time. The optimum sampling time at the receiver is shifted; therefore, timing jitter results. The combination of the intensity fluctuation among longitudinal modes and the time delay of each mode, caused by the fiber dispersion, results in a degradation of the bit error rate performance of the fiber optic system. The signal-to-noise ratio due to the mode partition noise is independent of signal power since the noise power is proportional to the signal power and the intensity distribution among the longitudinal modes. Mode partition noise introduces a lower bound for the achievable bit error rate for the system; that is, even if the launched power into the fiber increases, the achieved bit error rate cannot be improved further. At a higher bit rate, the side-mode transient occupies a larger fraction of the data pulse duration and the increased rate of increase of injected electrons causes a larger growth of the side mode on the initial transient [21]. Therefore, mode partition noise becomes more serious as the bit rate increases.

Assuming that the total laser output power is constant and the partition probability function is based on the Gaussian time averaged spectrum, Ogawa [18] shows that the signal-to-noise ratio due to the mode partition noise is estimated by

$$SNR = \frac{1}{\sigma_{pc}^{\,2}} \tag{2.3.2.1}$$

where

$$\sigma_{pc}^{\,2} = \frac{1}{2}(\pi B)^4 \left[A_1^{\,4}\sigma^4 + 48A_2^{\,4}\sigma^8 + 42A_1^{\,2}\sigma^6 \right] \tag{2.3.2.2}$$

$$A_1 = \frac{2\pi c}{\lambda_c^2}\beta_2 z = -Dz \tag{2.3.2.3}$$

$$A_2 = \left(\frac{2\pi c}{\lambda_c^2} \right)^2 \beta_3 z \approx Sz \qquad (2.3.2.4)$$

σ_{pc}^2 is the noise power due to the mode partition noise

B is the bit rate

c is the light velocity in vacuum

λ_c is the center wavelength of the laser

β_2 is the second derivative of β respect to λ_i at λ_c

β_3 is the third derivative of β respect to λ_i at λ_c

β is the propagation constant

z is the fiber length

σ is the half width of the laser diode spectrum (in nm)

D is the dispersion parameter (ps/km-nm)

S is the dispersion slope (ps/km-nm^2)

From equation (2.3.2.1) and (2.3.2.2), it is seen that the signal-to-noise ratio due to the mode partition noise depends on the half width of the laser diode spectrum, the fiber dispersion, and the bit rate. It does not depend on the signal power. A_1 is the product of dispersion parameter and fiber length, and A_2 is the product of dispersion slope and fiber length. These two parameters depend on the fiber dispersion. A_1 will be much higher than A_2 if the center wavelength (λ_c) is far from the zero dispersion wavelength. However, if λ_c is near the zero dispersion wavelength, A_2 will become more important. The power penalty due to the mode partition noise is determined by

$$\text{PowerPenalty(in dB)} = -5\log(1 - Q^2 \sigma_{pc}^{\ 2} k^2) \qquad (2.3.2.5)$$

where Q is the parameter related to the required bit error rate in the Gaussian approximation. For the bit error rate of 10^{-9}, Q is equal to 6.

k is the mode partition coefficient which lies between 0 to 1.

The mode partition coefficient, k, indicates the mode partition characteristic of a laser diode. For a larger k, the mode partition noise is higher. This coefficient can be measured by two simple methods; that is, the low-pass filter method and the sampling method; which are given in [19]. For different operating conditions, the value of k varies

between 0.14-0.7. When the pulse width increases, *k* decreases; that is, at a lower data rate, the mode partition noise becomes smaller. In a single-mode fiber system, *k* is between 0.4 and 0.7. Unless narrow linewidth single longitudinal mode lasers are used, mode partition noise is a dominant limitation is single mode fiber systems.

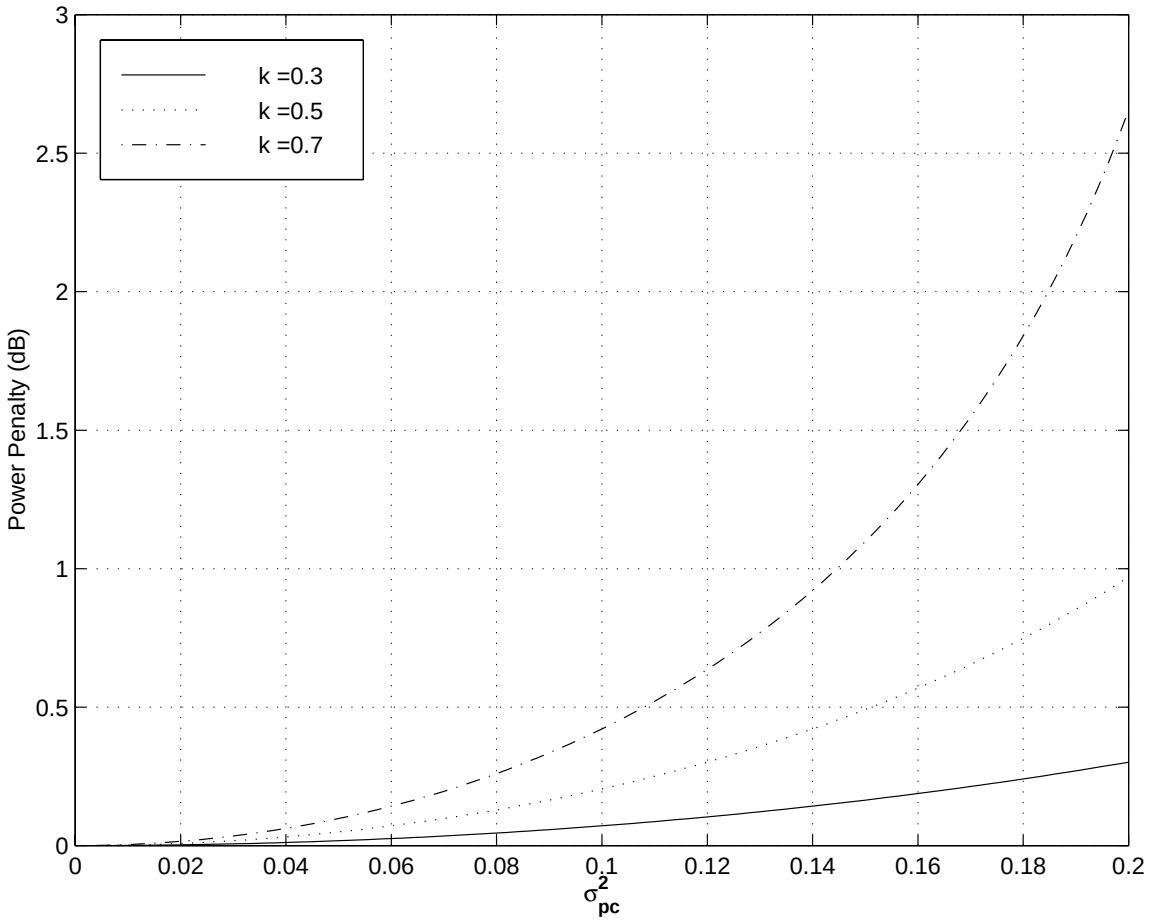

Figure 2.2 Power penalties versus the mode partition noise power: for mode partition coefficients of 0.3, 0.5, and 0.7.

The power penalty due to the mode partition noise is shown in Figure 2.2. This plot is for the bit error rate of 10^{-9}. For a higher mode partition coefficient, the mode partition noise becomes larger and introduces more power penalty; for example, for σ_{pc}^2 = 0.18, the power penalties are 0.24, 0.75, and 1.84 dB for the mode partition coefficient of 0.3, 0.5, and 0.7 respectively. From equation (2.3.2.3), the noise due to the mode partition can be reduced if the bit error rate is lowered and/or the operating wavelength is at the zero dispersion wavelength. High bit rate and low noise is important for fiber optic communication systems. Therefore, there should be some approaches to minimize the mode partition effect at high bit rate. Even if a distributed-feedback (DFB) laser is used to solve the dispersion problem at a wavelength far from the zero dispersion wavelength, the mode partition noise may still cause a system problem [22]. The reason is that the main mode of the DFB laser is accompanied by many smaller amplitude side modes. These side modes can cause the mode fluctuations that cause the mode partition noise.

It has been suggested that setting the quiescent bias point of the laser above the threshold can increase side mode suppression and consequently reduce the error from mode partition noise. Nevertheless, the power extinction ratio and large thermal effects likely counteract this improvement. Thus, this method is not a good way to reduce the mode partition noise. To reduce the effect of the mode partition noise, Miller in [21] found that the differential loss between the main mode and side modes internal to the laser must be larger. The larger differential loss will reduce the incidence of the side-mode turn on and the duration of power in the side mode in a given pulse.

2.3.3 Relative intensity noise

By setting the bias current to the laser diode to be constant, there will still be some fluctuations in terms of intensity, phase, and frequency at the optical output [1]. These fluctuations are mainly caused by intrinsic characteristics of the laser; that is, the spontaneous emission in the laser. This emission results in noise at the optical output. The spontaneous photons can randomly interrupt the amplitude and the phase of the coherent photons occurring by the stimulated emission. This leads to the intensity fluctuation; thus, the relative intensity noise (RIN). The power spectral density of the relative intensity noise is determined by [1]

$$RIN(\omega) = \int_{-\infty}^{\infty} C_{pp}(\tau) \cdot e^{-i\omega t} dt \qquad (2.3.3.1)$$

where

$$C_{pp} = \frac{\langle \delta P(t) \cdot \delta P(t+\tau) \rangle}{\overline{P}^2}. \qquad (2.3.3.2)$$

$\delta P(t)$ is the fluctuation in number of photons at time t,

$\delta P(t) = P(t) - \overline{P}$.

$\overline{P}$ is the average number of photons

From equation (2.3.3.1) and (2.3.3.2), we can see that the power spectral density of RIN is the Fourier transform of the normalized photon-fluctuation autocorrelation. If the output photons fluctuate strongly, the RIN will be very high.

Apart from the intrinsic characteristic of the lasers that introduces relative intensity noise (RIN) into the system, any optical feedback from reflections from outside of the lasers can also enhance RIN. The optical feedback is mainly caused by the refractive index discontinuities in the optical fiber systems. These discontinuities are from the structure of the laser itself and the index discontinuities along the fiber path. The refractive index discontinuities along a fiber transmission line are caused by many components; for example, connectors, splices, fiber end faces, and so on. RIN enhancement from the optical feedback induced by these index discontinuities can be categorized into two types; that is, RIN enhancement from the optical feedback into the semiconductor lasers and RIN enhancement from the phase-to-intensity noise conversion. When the optical signal is reflected back into lasers, it can perturb the radiation characteristics of lasers; thus, RIN enhancement. To solve this problem, an optical

isolator should be placed between the transmitter and the optical fiber. Nonetheless, another type of RIN enhancement is still a problem. The optical feedback from multiple reflections along the fiber introduces RIN enhancement resulting from the phase-to-intensity noise conversion. RIN can severely degrade the system performance and introduce a bit-error-rate floor [26]. The effect of RIN is lessened in multimode optical transmission systems since other effects such as mode partition noise are generally more serious. However, single-mode optical systems are attractive because they can give a higher bit rate-distant product compared to the multimode optical systems.

There are many types of lasers that can give a single longitudinal mode; for example, the distributed-feedback and the coupled-cavity semiconductor lasers. In these lasers, optical feedback is a factor that can increase RIN. There has been considerable research on this subject [23], [24], [25], and [27]. In the external cavity coupled semiconductor lasers, it has been shown in [23] that if the amount of optical feedback that is fed back into a laser cavity is fixed, the increase of RIN depends on the phase of optical feedback. If the phase difference between optical fields in the laser cavity and that of feedback light changes with time, the amplification of optical fields in the laser will change with time; consequently, the intensity fluctuation is increased. The power spectral density of RIN can be divided into two ranges: the low-frequency fluctuations (LFF) and the high-frequency fluctuations (HFF) [23]. Both of them change with the change of the multi-external cavity oscillation depending on the length of the external cavity and the injection current to the laser. As the length of the external cavity changes, the phase of the optical feedback also changes. This phase change can change the amount of RIN. As shown in Figure 2.3 [24], if the length of the external cavity is decreased in small steps and the injection current is held constant, the spectral density of RIN (both LFF and HFF) is decreased and totally disappears with decreasing cavity length. Then, it suddenly reappears with a strong peak again and remains at that value even as the cavity length is further decreased. The injection current to the laser is also a factor that can control the power spectral density of RIN. From Figure 2.4 [24], increasing the injection current from 28 mA to 39 mA increases the half-width and the center frequency of the LFF and HFF components of RIN. This means that the specral density of RIN can be controlled by using these two parameters. To reduce the RIN for this case, thus, the cavity length and

the injection current must be adjusted appropriately so that the laser operates at the single-external mode oscillation [23].

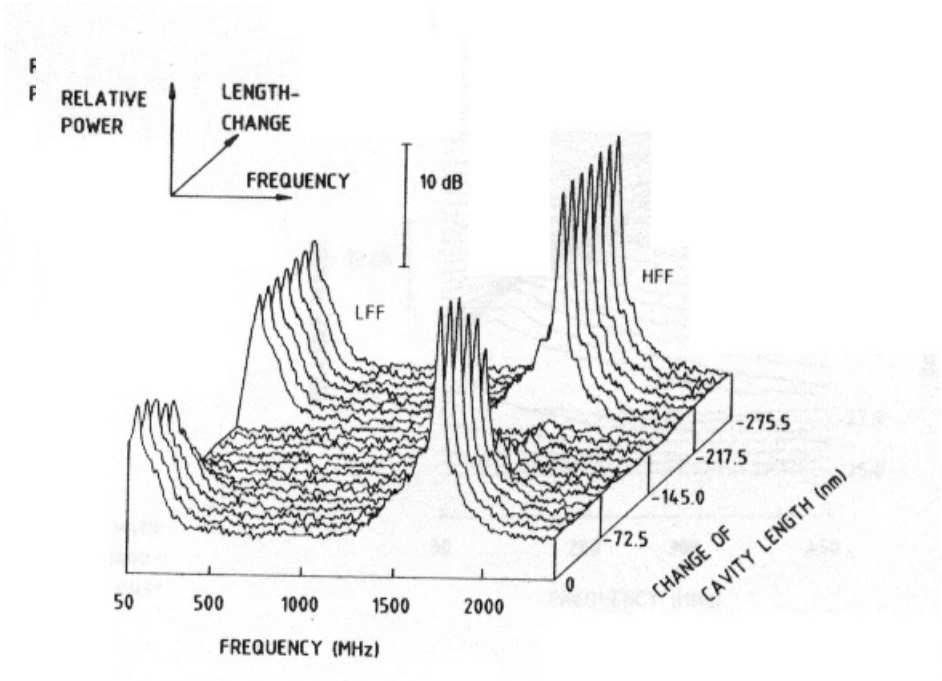

Figure 2.3 The power spectral density of RIN vs the change of cavity length for a constant injection current of 27.4 mA [24].

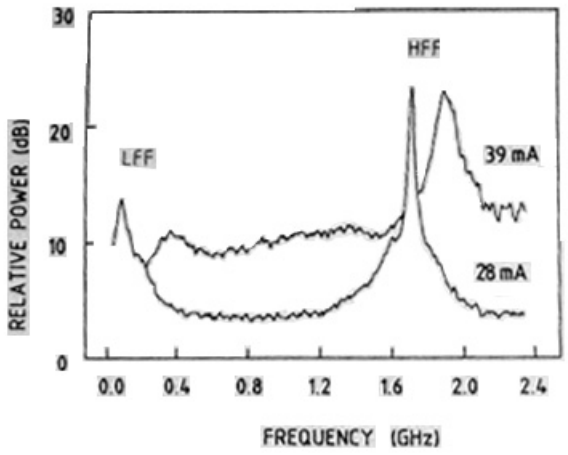

Figure 2.4 The power spectral density of RIN for different injection currents [24].

When an optical isolator is placed between the laser and the optical fiber, the optical feedback caused by the refractive index discontinuities along the fiber path cannot travel back to the laser. However, this optical feedback can still enhance the RIN and cause degradation to the system. The effect of this optical feedback can be thought of as the interferometric conversion of laser phase noise to intensity noise resulting from multiple reflections along the optical fiber path [26]. In [26], [28], and [29], the effect of these index discontinuities was studied. The diagram for multiple reflection along the optical transmission line shown in Figure 2.5 [26].

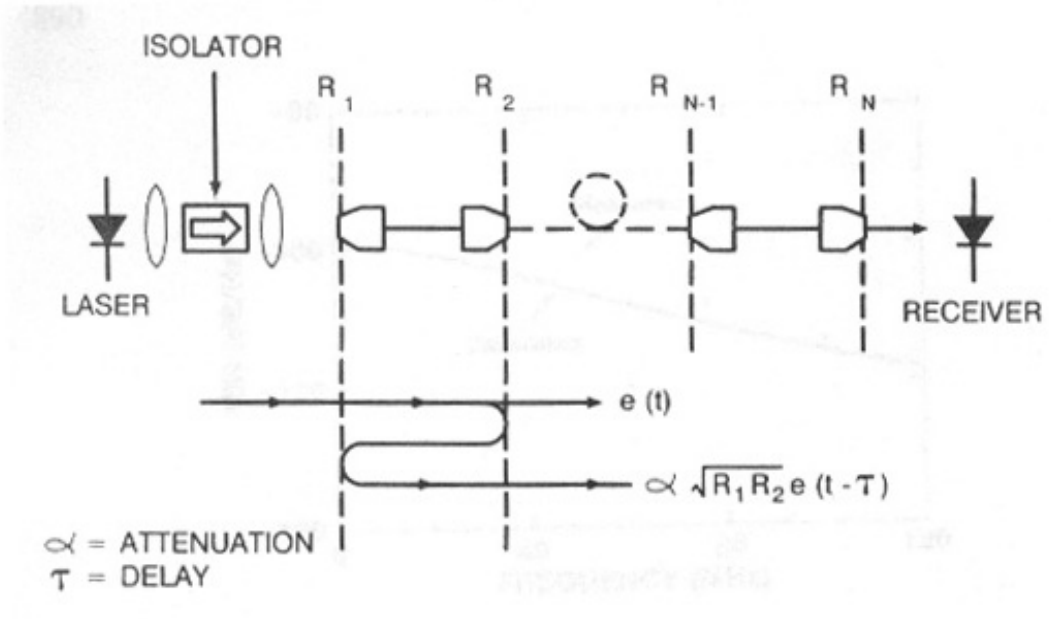

Figure 2.5 Diagram of a fiber transmission system with multiple reflection points after an optical isolator [26].

From the diagram, e(t) is the input optical field. Each reflection point has its own reflection coefficient; for example, R_1, R_2, and so on. The single pass intensity transmittance is denoted by α. The length between each pair of reflection points leads to the time delay ($\tau/2$). For this case, if the reflection coefficients are assumed to be sufficiently small, higher order terms in R_iR_j are negligible. Therefore, more than double reflections of the optical field may be neglected. Gimlett and Cheung in [26] have shown that RIN enhancement from these multiple reflections depends on the linewidth (Δv) of the source, the number of reflections, and the reflection coefficients. With a large

linewidth, the RIN is enhanced substantially. To reduce this effect, the source linewidth must be reduced so that the power spectral density of RIN is decreased; thus, small RIN. However, if the term $2\pi(\Delta\nu)\tau$ is much greater than 1, the spectral density of RIN is given by [26]

$$RIN(f) \approx \frac{4}{\pi}\left[\frac{(\Delta\nu)}{f^2+(\Delta\nu)^2}\right]\sum_{i=2}^{N}\sum_{j=1}^{i-1}R_{ij}^2 \qquad (2.3.3.3)$$

where N is the number of discontinuities

R_{ij} is a generalized relfection coefficient defined by

$$R_{ij} = \alpha_{ij}\sqrt{R_i R_j}\,\vec{p}(t)\cdot\vec{p}_{ij}(t-\tau_{ij}) \qquad (2.3.3.4)$$

α_{ij} is the transmittance between two discontinuities

$\vec{p}(t)$ is the unit magnitude polarization vector of the direct optical field

$\vec{p_{ij}}(t)$ is the unit magnitude polarization vector of the $(ij)^{\text{th}}$ component of the delayed optical field

τ_{ij} is the round trip path delay between i^{th} and j^{th} discontinuities.

From equation (2.3.3.3), it is seen that if the source linewidth is very large, the power spectral density of RIN is small. Consequently, for very wide linewidth sources such as LEDs, the effect of multiple reflections on RIN enhancement is negligible. The number of reflections and the reflection coefficients also affect the power spectral density of RIN as seen in equation (2.3.3.3) and (2.3.3.4). RIN increases as the number of reflections or the reflection coefficients increase. It has been shown in [28] that a small number of reflections with a reflection coefficient of a few percent can significantly increase the level of RIN to the system. For the case of many reflections, even each with the reflection coefficient of 1 percent, the effect of phase-to-intensity noise conversion can introduce considerable additional RIN to the system [29].

To reduce the effect of RIN from the multiple reflections along the fiber path, the source linewidth should be as narrow as possible for the case of a laser diode. The number of reflections must be minimized and the reflection coefficients must be reduced substantially.

The effect of the RIN on the system performance, such as receiver sensitivity and power penalty, will be discussed in the next chapter.

2.4 Intersymbol Interference (ISI)

When the signal waveform goes through a communication system, its shape will be broadened in time because the bandwidth of the system is limited. If the bandwidth of the system is much higher than the data rate, this broadening will be insignificant but receiver noise will be a problem. From both noise and implementation considerations it is desirable to narrow the system bandwidth as much as possible. Consequently, the effect of pulse broadening becomes significant. The pulse of each symbol will spread in time and overlap to the adjacent symbols. This overlap causes intersymbol interference. An example of intersymbol interference is shown in Figure 2.6 [30] below.

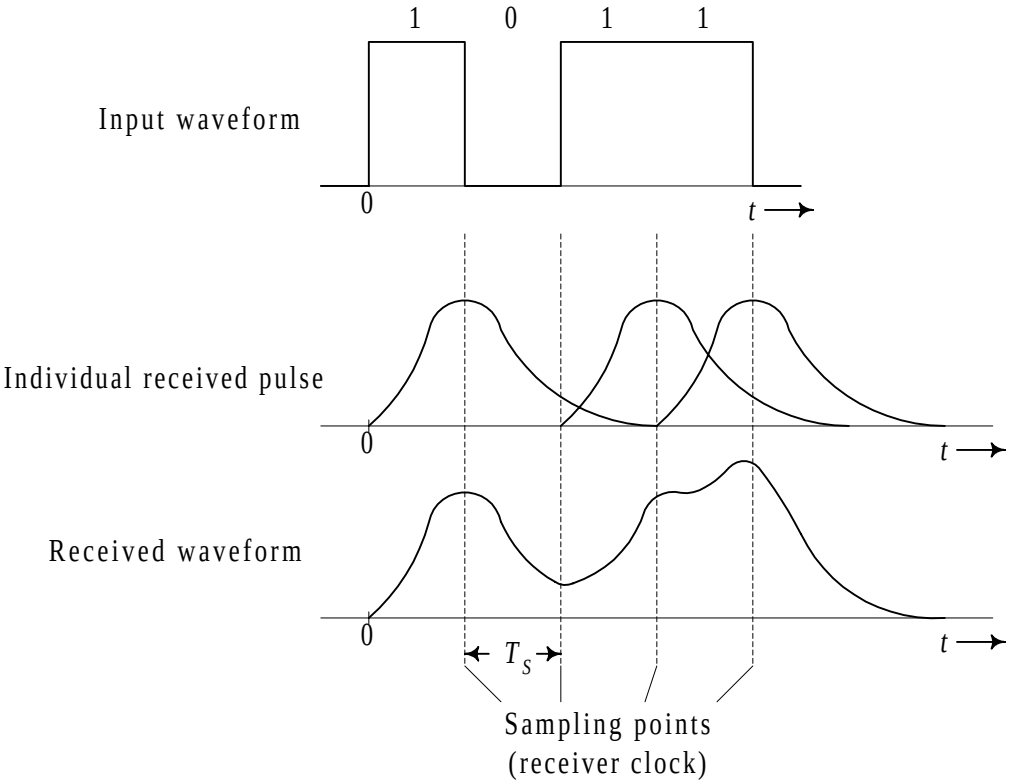

Figure 2.6 Examples of ISI on received pulses in a binary communication system [30].

Bandwidth limitations in the transmitter, fiber, or receiver cause the pulses to spread out in time. Each pulse will overlap to the adjacent pulses. The amplitude of each pulse at the sampling point is changed because of intersymbol interference. The change in amplitude may lead to the wrong decision in the decision circuit; thus, increasing the bit-

error-rate. For example, at the second bit, the transmitted bit was 0, but the amplitude of the received pulse for this bit at the sampling point is not zero because of the effect of pulse broadening from the first bit. And this may cause the wrong decision on this bit.

In an optical communication system, intersymbol interference is potentially a problem since the system bandwidth is not infinite. Pulse broadening in optical communication systems is mainly caused by fiber dispersion and the receiver bandwidth if the bandwidth of the transmitter is assumed to be very large. When the optical signal travels along the fiber, each spectral component of the signal travels with a particular propagation velocity, which is different from those of other spectral components. Consequently, each spectral component will reach the receiver at a different time. This causes the pulse spreading at the receiver end. The effect of fiber dispersion limits the bit rate-distance product that can be achieved [1]. The receiver bandwidth can also introduce intersymbol interference in the received signal [2]. As mentioned in the previous section, the noise depends on the effective receiver bandwidth; thus, to reduce the noise at the receiver the effective receiver bandwidth should be small. This small effective receiver bandwidth will result in the pulse broadening of the signal. However, in the absence of fiber dispersion, transmitter and receiver bandwidths should be matched and a proper spectral shape should be chosen such that intersymbol interference is negligibly small.

To reduce the intersymbol interference, an equalizer is required at the receiver. This component is usually placed before the decision circuit. In [31], Liu et al. have calculated the bit-error-rate from three types of equalizers for different amounts of intersymbol interference. They found that the use of proper equalizer can significantly improve the bit-error-rate performance and the best choice of an equalizer depends on the input waveform, amount of intersymbol interference, and the APD gain. The effect of optical system bandwidth on the intersymbol interference will be simulated and shown in chapter 4.

3.0 Effect of impairments on system performance

The effects of impairments, discussed in chapter 2, on system performance will be considered in this chapter. An additional impairment, extinction ratio, will also be included. An important performance parameter for a digital communication system is bit-error-rate or error probability. The error probability calculation in this chapter will be approximated by the Guassian approximation, which will be discussed first. Other performance parameters for optical communication systems are the minimum received power and the power penalty. The minimum received power in this chapter will be expressed by the average number of photons per bit at the receiver since the received power is proportional to the number of incident photons. The formula for these parameters will be given. Also, some plots of these parameters will be shown and discussed.

3.1 Gaussian approximation for the error probability calculation

In a binary communications system, one important parameter indicating the system performance is the error probability. To compute the error probability, the probabilities of sending bit 0 and bit 1, and the probability density function of the signal at the receiver have to be known. The error probability, in general, is given by

$$P_e = \Pr[0]\Pr[\hat{s}=1 \mid s=0] + \Pr[1]\Pr[\hat{s}=0 \mid s=1] \qquad (3.1.1)$$

where Pr[0] and Pr[1] are the probabilities of sending bit 0 and bit 1 from the transmitter, respectively

$\hat{s}$ is the estimated bit from the decision circuit

s is the bit that was transmitted.

In an optical communications system, the optical signal at the receiver is converted to a current by the photodetector, and then is passed through electrical components for electrical processing; for example, amplification and filtering. Finally, the signal current is sent to the decision circuit to estimate the data bit. Many types of noise are added to the signal as mentioned in chapter 2. The more noise in the system, the more fluctuation on the input current to the decision circuit. That is, the spread of the probability density function of the signal will increase. In many cases, a good approximation of the probability density function for the input current to the decision circuit is given by the Gaussian distribution. The Gaussian probability density function is given by

$$p(x) = \frac{1}{\sigma_x \sqrt{2\pi}} e^{-\frac{(x-m_x)^2}{2\sigma_x^2}} \qquad (3.1.2)$$

where m_x is the mean of the random variable x

σ_x^2 is the variance of the random variable x.

From equation (3.1.2), only two parameters are needed to define the Gaussian probability density function; that is, mean and variance. The probability density function of the input current to the decision circuit when bit 1 and bit 0 are transmitted can be approximated using equation (3.1.2). The probability that the estimate is bit 1 when bit 0 was transmitted and the probability that the estimate is bit 0 when bit 1 was transmitted are given by

$$\Pr[\hat{s}=1 \mid s=0] = \int_{I_{th}}^{\infty} p_0(i)di = \int_{I_{th}}^{\infty} \frac{1}{\sigma_0\sqrt{2\pi}} e^{-\frac{(i-I_0)^2}{2\sigma_0^2}} di = Q\left(\frac{I_{th}-I_0}{\sigma_0}\right) \qquad (3.1.3)$$

$$\Pr[\hat{s}=0 \mid s=1] = \int_{-\infty}^{I_{th}} p_1(i)di = \int_{-\infty}^{I_{th}} \frac{1}{\sigma_1\sqrt{2\pi}} e^{-\frac{(i-I_1)^2}{2\sigma_1^2}} di = Q\left(\frac{I_1-I_{th}}{\sigma_1}\right) \qquad (3.1.4)$$

where $Q(x) = \int_{x}^{\infty} \frac{1}{\sqrt{2\pi}} e^{-\frac{y^2}{2}} dy$

$p_0(i)$ and $p_1(i)$ are the probability density functions of the input current for bit 0 and bit 1, respectively

i is the input current to the decision circuit

I_0 and I_1 are the mean of i when bit 0 and bit 1 are transmitted, respectively

σ_0^2 and σ_1^2 are the variance of i when bit 0 and bit 1 are transmitted, respectively

I_{th} is the current threshold.

Substituting equations (3.1.3) and (3.1.4) into (3.1.1), and setting Pr[0]=Pr[1]=0.5, the error probability is given by

$$P_e = 0.5\left\{Q\left(\frac{I_{th}-I_0}{\sigma_0}\right) + Q\left(\frac{I_1-I_{th}}{\sigma_1}\right)\right\} \qquad (3.1.5)$$

Equation (3.1.5) allows us to find the error probability if values of all parameters are known. To get a minimum error probability, the current threshold should be chosen such that the probability density functions of bit 0 and bit 1 are the same. This follows by differentiating equation (3.1.5) with respect to the current threshold (I_{th}). However, setting $\Pr[\hat{s}=1 \mid s=0] = \Pr[\hat{s}=0 \mid s=1]$ is generally a good approximation of choosing the optimum threshold. That is, setting

$$Q\left(\frac{I_{th}-I_0}{\sigma_0}\right) = Q\left(\frac{I_1-I_{th}}{\sigma_1}\right) \qquad (3.1.6)$$

$$\Rightarrow \quad \frac{I_{th}-I_0}{\sigma_0} = \frac{I_1-I_{th}}{\sigma_1} \equiv k\,. \qquad (3.1.7)$$

From equation (3.1.7), the current threshold is given by

$$I_{th} = \frac{\sigma_0 I_1 + \sigma_1 I_0}{\sigma_0 + \sigma_1} \tag{3.1.8}$$

and the minimum error probability is given by

$$P_{e,\min} = Q(k) \tag{3.1.9}$$

where

$$k = \frac{I_1 - I_0}{\sigma_0 + \sigma_1} \tag{3.1.10}$$

The minimum error probability is dependent on the parameter *k*. For good performance, the error probability of optical communications systems should be less than 10^{-9}; that is, *k* is greater than 6.

3.2 Effect of impairments for zero extinction ratio

The input current to the decision circuit combines the signal and the various sources of noise, which are added to the signal along the transmission path. The combined noise is assumed to be a zero mean Gaussian process. This assumption is good as long as the system is not in the shot noise limit. The input current to the decision circuit can be written as

$$i = I_p + i_{th} + i_{sh} + i_{rin} \tag{3.2.1}$$

where I_p is the mean of the input current i for bit 0 or bit 1

i_{th} is the current induced by thermal noise

i_{sh} is the current induced by shot noise

i_{rin} is the current induced by relative intensity noise (RIN).

The average input current for each bit is given by

$$\langle i_0 \rangle = I_0 = \varepsilon I_1 \tag{3.2.2}$$

and

$$\langle i_1 \rangle = I_1 \tag{3.2.3}$$

where ε is the extinction ratio = I_0/I_1

From equation (2.2.1), (3.2.2) and (3.2.3), the average received power and the average photons per bit are given by

$$\overline{P}_R = \frac{h\nu}{\eta q}\frac{(I_1 + I_0)}{2} = \frac{h\nu I_1(1+\varepsilon)}{2\eta q} \tag{3.2.4}$$

$$\overline{N}_p = \frac{\overline{P}_R}{h\nu B} = \frac{I_1(1+\varepsilon)}{2\eta q B} \tag{3.2.5}$$

where B is bit rate

The variance of input current is needed to calculate the minimum error probability. The variance of input current for each bit (bit 0 or bit 1) is just the sum of variances of the currents induced by each source of noise since the various noise sources are assumed to be independent. Therefore, the variance of input current is given by

$$\sigma^2 = \sigma_{th}^2 + \sigma_{sh}^2 + \sigma_{rin}^2 \tag{3.2.6}$$

From chapter 2, the variances of thermal noise and shot noise are given by

$$\sigma_{th}^2 = \langle i_{th}^2 \rangle = 8\pi q V_T C_e (\Delta f)^2 \tag{3.2.7}$$

$$\sigma_{sh}^2 = \left\langle i_{sh}^2 \right\rangle = 2qI_p(\Delta f) \tag{3.2.8}$$

The variance of the relative intensity noise is given by [1]

$$\sigma_{rin}^2 = \left\langle i_{rin}^2 \right\rangle = r_I^2 I_p^2 \tag{3.2.9}$$

where $$r_I^2 = \frac{1}{2\pi}\int_{-\infty}^{\infty} RIN(\omega)d\omega \tag{3.2.10}$$

$RIN(\omega)$ is the power spectral density of relative intensity noise given in equation (2.3.3.1)

If the bandwidth of the power spectral density of RIN is much greater than the bandwidth of the receiver, the term r_I^2 in equation(3.2.10) can be approximated by

$$r_I^2 = RIN(0)\cdot\Delta f \tag{3.2.11}$$

where $RIN(0)$ is the relative intensity noise at ω=0.

3.2.1Effect of thermal noise and shot noise

If only thermal noise and shot noise are included in the signal current, the input current to the decision circuit is given by

$$i = I_p + i_{th} + i_{sh}\,. \tag{3.2.12}$$

Since we are considering the case of zero extinction ratio (ε=0), the average input current for bit 0 is equal to zero and the average input current for bit 1 is I_1. And the variances of input current for bit 0 and bit 1 are given by

$$\sigma_0^2 = 8\pi q V_T C_e (\Delta f)^2$$

$$\sigma_1^2 = 8\pi q V_T C_e (\Delta f)^2 + 2qI_1(\Delta f)$$

Substituting the average input currents and their variances into equation (3.1.10), the parameter k is given

$$k = \frac{I_1 - I_0}{\sigma_0 + \sigma_1}$$

$$= \frac{I_1}{\sqrt{8\pi q V_T C_e (\Delta f)^2} + \sqrt{8\pi q V_T C_e (\Delta f)^2 + 2qI_1(\Delta f)}} \tag{3.2.13}$$

Substituting I_1 in equation (3.2.13) by equation (3.2.5) with zero extinction ratio, k will be given by

$$k = \frac{B}{\Delta f} \cdot \frac{\eta q \overline{N}_p}{\sqrt{2\pi q V_T C_e} + \sqrt{2\pi q V_T C_e + q^2 \eta \overline{N}_p \frac{B}{\Delta f}}} \qquad (3.2.14)$$

From equation (3.2.14), the average number of photons per bit is given by

$$\overline{N}_p = \left(\frac{k^2}{\eta}\right)\left(\frac{\Delta f}{B}\right)\left(1 + \frac{1}{k}\sqrt{\frac{8\pi V_T C_e}{q}}\right) \qquad (3.2.15)$$

From equation (3.2.15), it is assumed that the receiver bandwidth only affects the noise. For a matched filter receiver, sensitivity or the average number of photons per bit depends on signal energy; therefore, nonreturn-to-zero (NRZ) or return-to-zero (RZ) line codings have the same theoretical sensitivity with a matched filter receiver.

In equation (3.2.15), for a p-i-n photodetector, the thermal noise is dominant, the average number of photons per bit will be given by

$$\overline{N}\,p = \left(\frac{k}{\eta}\right)\left(\frac{\Delta f}{B}\right)\sqrt{\frac{8\pi V_T C_e}{q}} \qquad (3.2.16)$$

The minimum error probability can be calculated by using k in equation (3.2.14) with equation (3.1.9). Figure 3.1 shows the minimum error probability versus the average number of photons per bit for different ratios of [$\Delta f/B$]. The effective capacitance is 1 pF and the quantum efficiency is 0.8. As the number of photons increases, the minimum error probability decreases. As the ratio of the receiver bandwidth to bit rate, [$\Delta f/B$], increases, the minimum error probability for a given number of photons per bit increases. For example, at $\overline{N}_p$=10,000 photons, the minimum error probability for [$\Delta f/B$] of 0.7, 0.9, and 1.1 are $5.2*10^{-9}$, $4.2*10^{-6}$, and $1.3*10^{-4}$, respectively. The reason is when the ratio [$\Delta f/B$] increases, the effective noise bandwidth of the receiver increases; thus, there is more noise in the input current to the decision circuit. Consequently, the minimum error probability with a high [$\Delta f/B$] is poorer than the minimum error probability with a low [$\Delta f/B$].

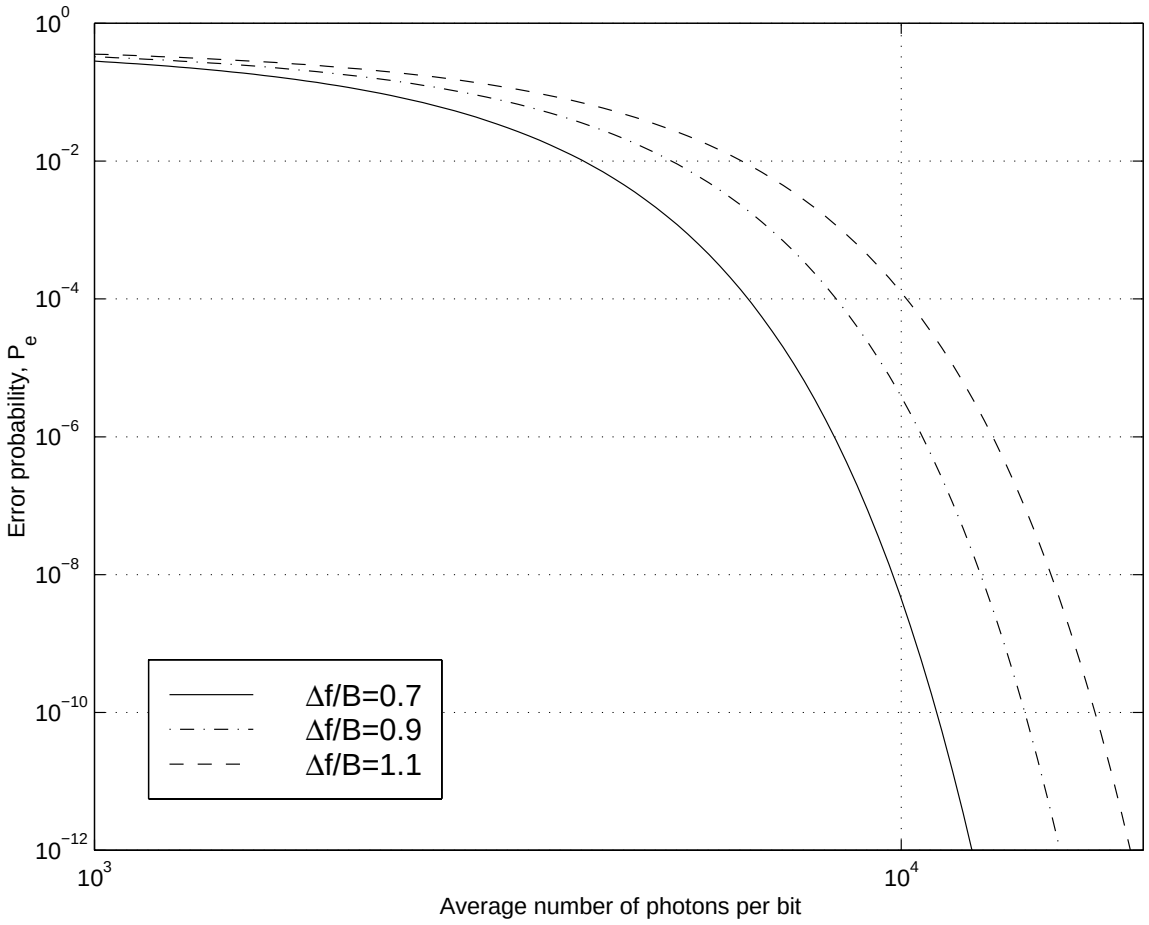

Figure 3.1 The minimum error probability vs the average number of photons per bit for different ratio of $\Delta f/B$.

3.2.2 Effect of relative intensity noise (RIN)

If the relative intensity noise (RIN) effect is included to the input current to the decision circuit, the input current to the decision circuit is given by

$$i = I_p + i_{th} + i_{sh} + i_{rin}. \tag{3.2.17}$$

The average input currents for bit 0 and bit 1 are the same as in the previous section; that is, for bit 0, the average input current is zero, and, for bit 1, the average input current is I_1. Moreover, the variance for the input current for bit 0 is from the thermal noise only since the variance from RIN depends on the average input current as shown in equation (3.2.9). For bit 1, the variance of the input current is the sum of variances from the currents induced by thermal noise, shot noise, and relative intensity noise. That is,

$$\sigma_1^2 = 8\pi q V_T C_e (\Delta f)^2 + 2qI_1(\Delta f) + RIN(0)(\Delta f) I_1^2 \tag{3.2.18}$$

Substituting the average input currents and their variances into equation (3.1.10), parameter k is given by

$$k = \frac{I_1}{\sqrt{8\pi q V_T C_e (\Delta f)^2} + \sqrt{8\pi q V_T C_e (\Delta f)^2 + 2qI_1(\Delta f) + RIN(0)(\Delta f) I_1^2}} \tag{3.2.19}$$

Expressing I_1 in terms of $\overline{N}_p$ (using equation (3.2.5) with zero-extinction ratio), k is then

$$k = \frac{B}{\Delta f} \cdot \frac{\eta q \overline{N}_p}{\sqrt{2\pi q V_T C_e} + \sqrt{2\pi q V_T C_e + q^2 \eta \overline{N}_p \frac{B}{\Delta f} + RIN(0) \cdot \eta^2 q^2 B \frac{B}{\Delta f} (\overline{N}_p)^2}} \tag{3.2.20}$$

From equation (3.2.20), the average number of photons per bit is given by

$$\overline{N}_p = \left(\frac{1}{1 - RIN(0) \cdot (\Delta f) k^2} \right) \left(\frac{k^2}{\eta} \right) \left(\frac{\Delta f}{B} \right) \left(1 + \frac{1}{k} \sqrt{\frac{8\pi V_T C_e}{q}} \right) \tag{3.2.21}$$

Comparing equation (3.2.21) with equation (3.2.15), it is seen that the effect of relative intensity noise is to multiply $\overline{N}_p$ by the first factor in equation (3.2.21).

The minimum error probability versus the average number of photons per bit for different values of RIN(0) is plotted in Figure 3.2. In this Figure, the effective capacitance is 1 pF, the quantum efficiency is 0.8, and the bit rate is 200 Mbps. As the value of RIN(0) increases, the minimum error probability increases. For example, at the average number of photons per bit of 10,000, the minimum error probabilities for zero

RIN, -97 dB/Hz RIN, and – 94 dB/Hz RIN are $4.4*10^{-9}$, $1.4*10^{-4}$, and $1.6*10^{-3}$ respectively. Furthermore, there is a minimum error probability (error floor) resulting from the RIN.

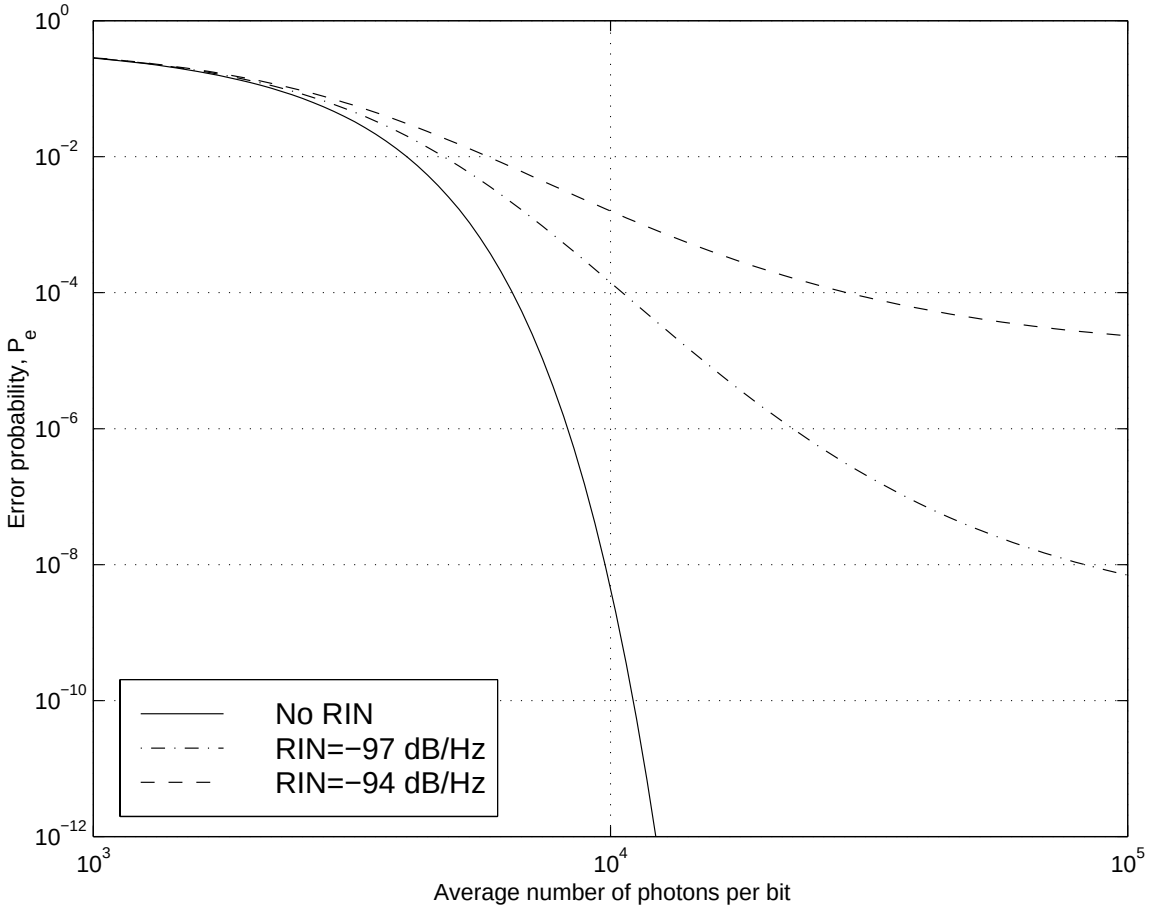

Figure 3.2 The error probability versus the average number of photons per bit for different values of RIN with zero-extinction ratio.

The power penalty from the relative intensity noise relative to that from thermal noise and shot noise alone is given by

$$\delta_{RIN}(dB) = 10\log_{10}\left(\frac{\overline{P}_{R,RIN}}{\overline{P}_R}\right) \tag{3.2.22}$$

where $\overline{P}_R$ is the average received power without RIN

$\overline{P}_{R,RIN}$ is the average received power with RIN.

In general, the average received power can be written in terms of the average number of photons per bit as shown below.

$$\overline{P}_R = \overline{N}_p h\nu B \tag{3.2.23}$$

Substituting equation (3.2.23) into equation (3.2.22), the power penalty from relative intensity noise is given by

$$\delta_{RIN}(dB) = 10\log_{10}\left(\frac{\overline{N}_{p,RIN}}{\overline{N}_p}\right) \tag{3.2.24}$$

Substituting the average number of photons per bit from equation (3.2.21) and (3.2.15) into equation (3.2.24), the power penalty from relative intensity is given by

$$\delta_{RIN}(dB) = 10\log_{10}\left(\frac{1}{1 - RIN(0)\cdot\Delta f\cdot k^2}\right) \tag{3.2.25}$$

From equation (3.2.25), the power penalty due to RIN depends on RIN(0), Δf, and k. The effective noise bandwidth of the receiver (Δf) should be increased as the increase of bit rate (B) to get an appropriate ratio between Δf and B. It is seen that for a given $[RIN(0)\cdot\Delta f]$, there exists a maximum value of k. This means that there is a lower bound to the error probability that can be achieved even though the input optical power is increased. The maximum value of k is given by

$$k_{\max} = \frac{1}{\sqrt{RIN(0)\cdot\Delta f}} \tag{3.2.26}$$

and the lower bound of the error probability is given by

$$P_{e,lower} = Q(k_{\max}) \tag{3.2.27}$$

The power penalty from the relative intensity noise in equation (3.2.25) is shown in Figure 3.3. The power penalty is plotted versus $[RIN(0)\cdot\Delta f]$ for k = 6. As $[RIN(0)\cdot\Delta f]$

increases, the power penalty increases substantially and approaches infinity. The lowest error probability from equation (3.2.27) is plotted versus [$RIN(0)\cdot\Delta f$] in Figure 3.4. From this figure, we can see that the error probability of 10^{-9} cannot be achieved if [$RIN(0)\cdot\Delta f$] is greater than 0.0278.

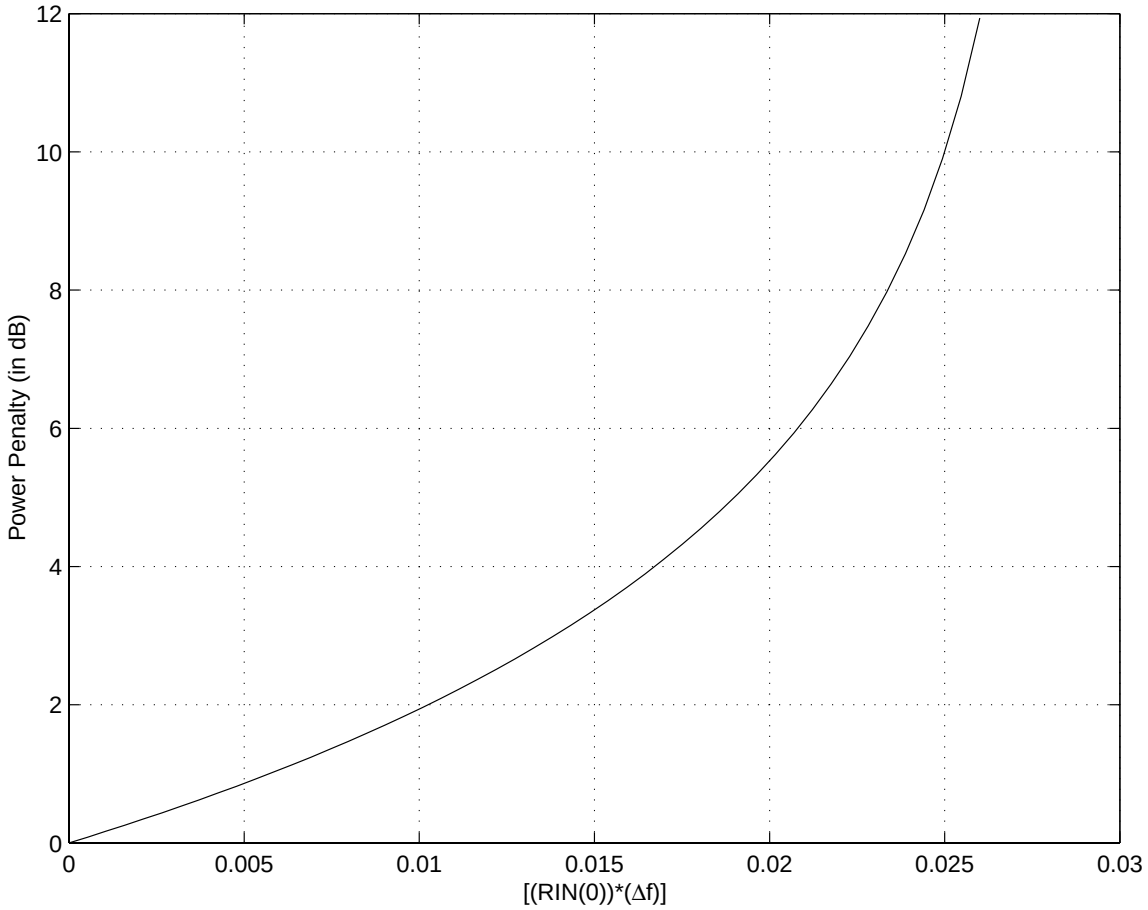

Figure 3.3 The power penalty (in dB) versus [$RIN(0)\cdot\Delta f$] for zero-extinction ratio.

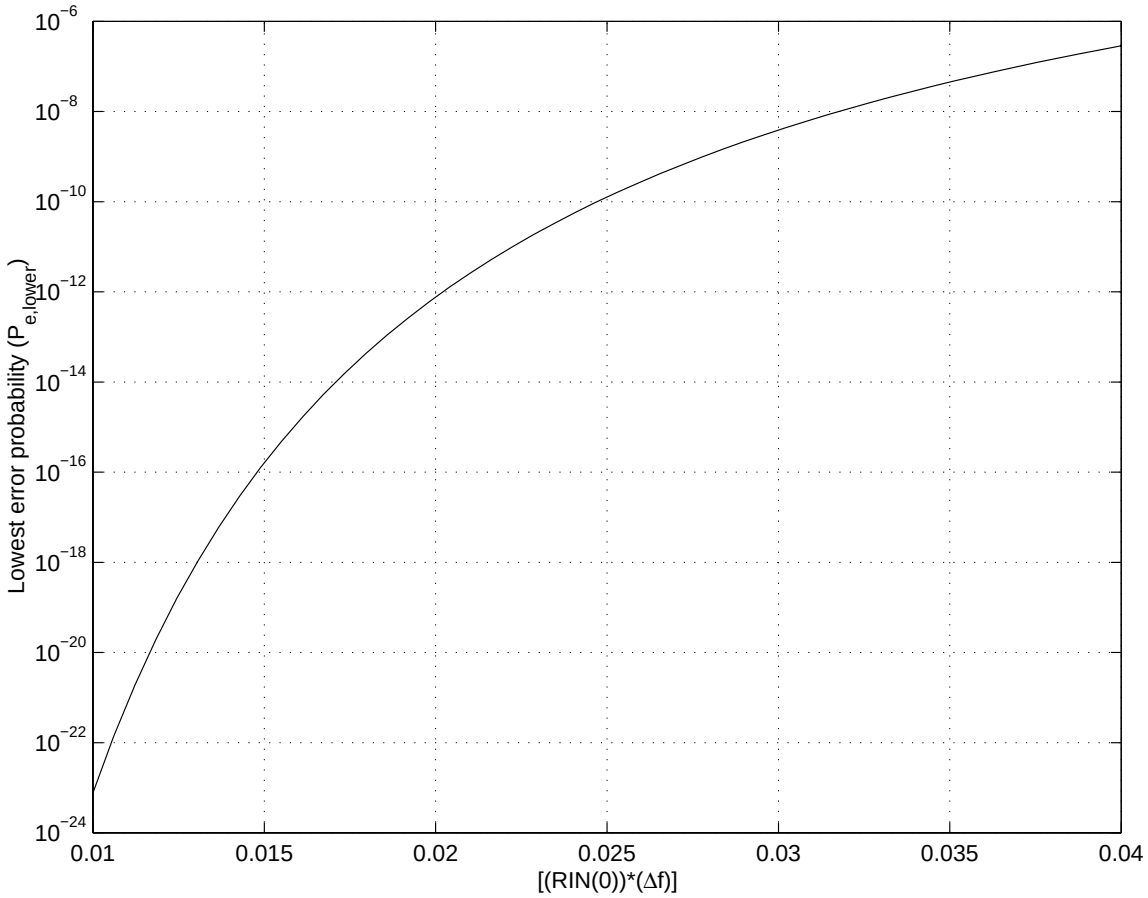

Figure 3.4 The lowest error probability versus [$RIN(0)\cdot\Delta f$] for zero-extinction ratio.

3.3 Effect of impairments for nonzero extinction ratio

For the nonzero extinction ratio case, the signal energy that was sent from the transmitter for bit 0 is not completely zero. There is some energy sent out into the fiber. This energy makes the average current for bit 0 at the decision circuit to be nonzero. The average input current to the decision circuit was shown in equation (3.2.2); that is,

$$\langle i_0 \rangle = I_0 = \varepsilon I_1 \tag{3.3.1}$$

where ε is the extinction ratio.

3.3.1 Effect of thermal noise and shot noise

Similar to the case of a zero extinction ratio in section 3.2.1, all parameters are almost the same except the average input current for bit 0 and it' s variance. The average input currents for bit 0 and bit 1 are εI_1 and I_1, respectively. The variances of the input current for bit 0 and bit 1 are given by

$$\begin{aligned}\sigma_0^2 &= 8\pi q V_T C_e (\Delta f)^2 + 2qI_0(\Delta f) \\ &= 8\pi q V_T C_e (\Delta f)^2 + 2q\varepsilon I_1(\Delta f)\end{aligned} \tag{3.3.2}$$

$$\sigma_1^2 = 8\pi q V_T C_e (\Delta f)^2 + 2qI_1(\Delta f) \tag{3.3.3}$$

From equation (3.3.2), the variance of the input current to the decision circuit for bit 0 also includes the effect of shot noise because of the nonzero extinction ratio. The variance for bit 1 is identical to the case of a zero extinction ratio. Substituting the average input currents and their variances into the parameter *k* in equation (3.1.10), we get

$$k = \frac{(1-\varepsilon) I_1}{\sqrt{8\pi q V_T C_e (\Delta f)^2 + 2q\varepsilon I_1(\Delta f)} + \sqrt{8\pi q V_T C_e (\Delta f)^2 + 2qI_1(\Delta f)}} \tag{3.3.4}$$

Substituting I_1 in equation (3.3.4) by equation (3.2.5) with an extinction ratio of ε, *k* will be

$$k = \frac{(1-\varepsilon)\dfrac{2\eta q B \overline{N}_p}{1+\varepsilon}}{\sqrt{8\pi q V_T C_e (\Delta f)^2 + 2q\dfrac{\varepsilon 2\eta q B \overline{N}_p}{(1+\varepsilon)}(\Delta f)} + \sqrt{8\pi q V_T C_e (\Delta f)^2 + 2q\dfrac{2\eta q B \overline{N}_p}{(1+\varepsilon)}(\Delta f)}}$$

$$k = \frac{\left(\frac{1-\varepsilon}{1+\varepsilon}\right)\left(\frac{B}{\Delta f}\right)\eta q\overline{N}_p}{\sqrt{2\pi q V_T C_e + \frac{\varepsilon}{(1+\varepsilon)}\eta q^2 \overline{N}_p\left(\frac{B}{\Delta f}\right)} + \sqrt{2\pi q V_T C_e + \frac{1}{(1+\varepsilon)}\eta q^2 \overline{N}_p\left(\frac{B}{\Delta f}\right)}} \qquad (3.3.5)$$

Using the parameter *k* in equation (3.3.5) with equation (3.1.9), we can find the error probability versus the average number of photons per bit for different values of extinction ratios. This plot is shown in Figure 3.5.

For a p-i-n photodetector, the thermal noise dominates especially for bit 0. Therefore, from equation (3.3.5), if the effect of shot noise in bit 0 is neglected the average number of photons per bit is given by

$$\overline{N}_p = \left(\frac{k^2}{\eta}\right)\left(\frac{\Delta f}{B}\right)\left(\frac{1+\varepsilon}{(1-\varepsilon)^2} + \left(\frac{1+\varepsilon}{1-\varepsilon}\right)\left(\frac{1}{k}\right)\sqrt{\frac{8\pi V_T C_e}{q}}\right) \qquad (3.3.6)$$

From equation (3.3.6), if the thermal noise is the dominant noise in both bit 0 and bit 1, the effect of shot noise can be neglected and the average number of photons per bit will be

$$\overline{N}_p = \left(\frac{1+\varepsilon}{1-\varepsilon}\right)\left(\frac{k^2}{\eta}\right)\left(\frac{\Delta f}{B}\right)\sqrt{\frac{8\pi V_T C_e}{q}} \qquad (3.3.7)$$

Comparing equation (3.3.7) to equation (3.2.16), we can find the power penalty due to the extinction ratio. Similar to equation (3.2.24), the power penalty due to the extinction ratio is

$$\delta_\varepsilon(dB) = 10\log_{10}\left(\frac{\overline{N}_{p,extinction}}{\overline{N}_p}\right) \qquad (3.3.8)$$

Substituting the average number of photons per bit from equation (3.3.7) and (3.2.16) into equation (3.3.8), the power penalty due to a nonzero extinction ratio is given by

$$\delta_\varepsilon(dB) = 10\log_{10}\left(\frac{1+\varepsilon}{1-\varepsilon}\right) \qquad (3.3.9)$$

From equation (3.3.9), it is shown that as the extinction ratio increases the power penalty will increase. The plot of power penalty due to the extinction ratio is shown in Figure 3.6.

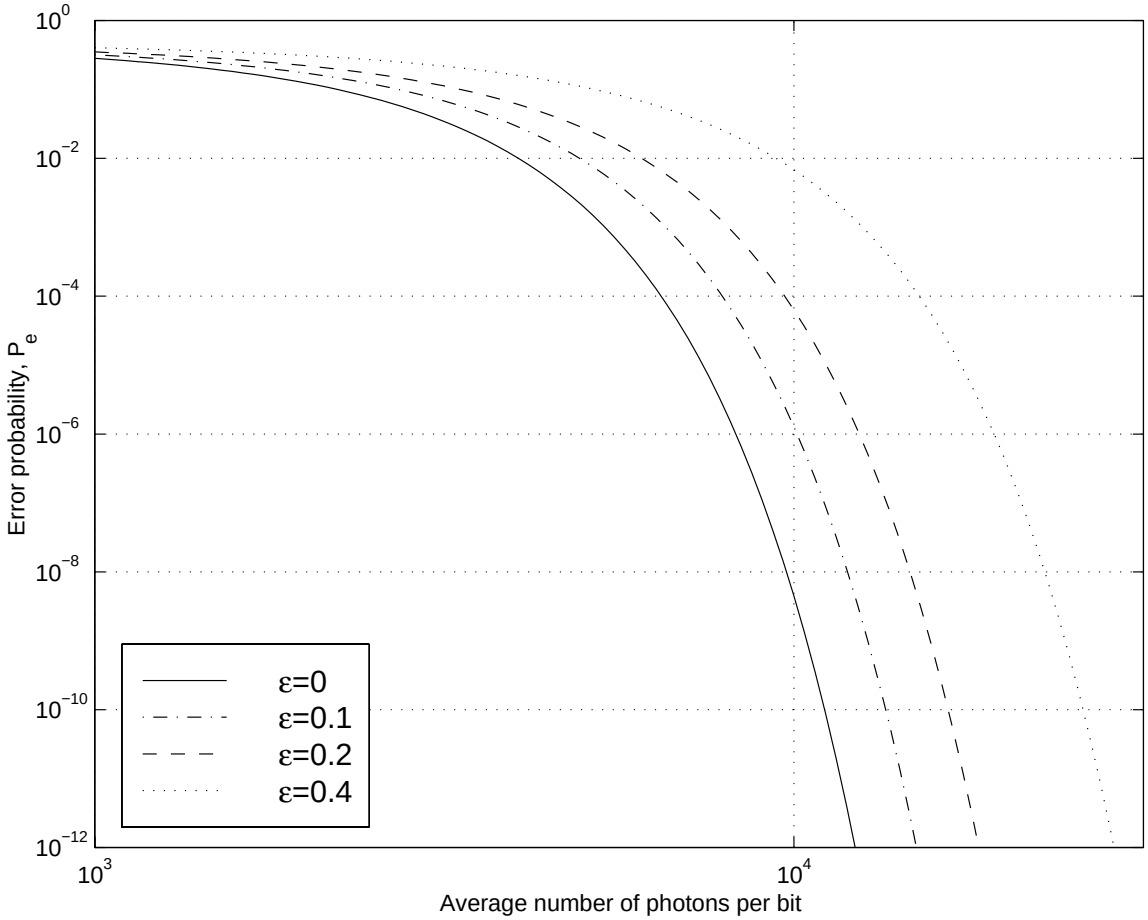

Figure 3.5 The error probability versus the average number of photons per bit for different extinction ratios.

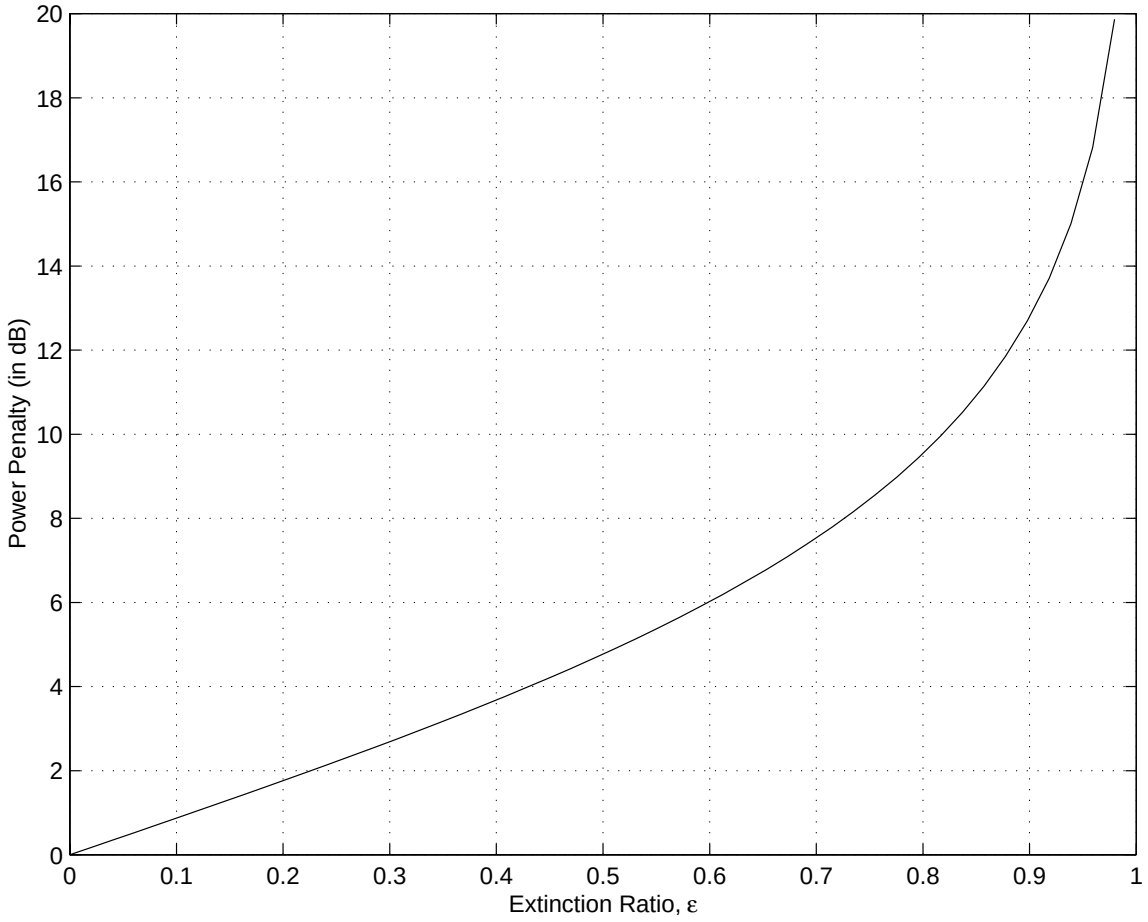

Figure 3.6 The power penalty (in dB) versus the extinction ratio, ε.

Using equation (3.3.5), the plot of the error probability versus the average number of photons per bit is shown in Figure 3.5. The effective capacitance is 1 pF and the quantum efficiency is 0.8. There are four values of extinction ratios; that is, 0, 0.1, 0.2, and 0.4. The error probability decreases as the average number of photons per bit increases. The best error probability is for the case of zero-extinction ratio. From the figure, it is seen that as the extinction ratio increases, the error probability increases; for example, at $\overline{N}_p$ =10,000 photons/bit, the error probabilities for the extinction ratios of 0, 0.1, 0.2, and 0.4 are $4.4*10^{-9}$, $1.3*10^{-6}$, $6.3*10^{-5}$, and $6.9*10^{-3}$, respectively. However, if the extinction ratio is kept less than 1.0, the effect of nonzero-extinction ratio will not introduce an error floor as the effect of RIN does. This means that the error probability can be reduced if the average number of photons per bit increases; thus, more power is required.

The additional required power can be interpreted in terms of power penalty, which was shown in equation (3.3.9). In Figure 3.6, the power penalty due to the extinction ratio with k=6 (i.e., $P_e=10^{-9}$) is plotted. The power penalty increases as the extinction ratio increases. It is seen that the power penalty is lower than 1 dB if the extinction ratio is less than 0.12. From this figure, it is also seen that the degradation due to the extinction ratio does not give an error floor as long as the extinction ratio less than 1, which is reasonable in practice.

3.3.2 Effect of relative intensity noise (RIN)

In this section, the effect of RIN is included to the calculation with a nonzero-extinction ratio. As mentioned previously, the average input current for bit 0 is not zero because of a nonzero-extinction ratio; thus, RIN will affect the signal at bit 0 also. From equation (3.2.9) and (3.2.11), the variances of the current induced by RIN for bit 0 and bit 1 are determined by

$$\sigma_{0,RIN}^2 = [(RIN(0)) \cdot (\Delta f)] I_0^2$$

$$= [(RIN(0)) \cdot (\Delta f)] (\varepsilon I_1)^2 \qquad (3.3.10)$$

$$\sigma_{1,RIN}^2 = [(RIN(0)) \cdot (\Delta f)] I_1^2 \qquad (3.3.11)$$

Adding $\sigma_{0,RIN}^2$ and $\sigma_{1,RIN}^2$ to σ_0^2 in equation (3.3.2) and σ_1^2 in equation (3.3.3), the variances of the input current for bit 0 and bit 1 will be

$$\sigma_0^2 = 8\pi q V_T C_e (\Delta f)^2 + 2q\varepsilon I_1 (\Delta f) + [(RIN(0)) \cdot (\Delta f)](\varepsilon I_1)^2 \qquad (3.3.12)$$

$$\sigma_1^2 = 8\pi q V_T C_e (\Delta f)^2 + 2q I_1 (\Delta f) + [(RIN(0)) \cdot (\Delta f)] I_1^2 \qquad (3.3.13)$$

Substituting the average input currents and their variances into equation (3.1.10), *k* will be

$$k = \frac{(1-\varepsilon) I_1}{\sqrt{\sigma_{th}^2 + 2q\varepsilon I_1 (\Delta f) + r_I^2 (\varepsilon I_1)^2} + \sqrt{\sigma_{th}^2 + 2q I_1 (\Delta f) + r_I^2 I_1^2}} \qquad (3.3.14)$$

where $\sigma_{th}^2 = 8\pi q V_T C_e (\Delta f)^2$

$r_I^2 = [(RIN(0)) \cdot (\Delta f)]$.

Substituting I_1 in equation (3.3.14) by equation (3.2.5) with an extinction ratio, ε, *k* will be

$$k = \frac{\left(\frac{1-\varepsilon}{1+\varepsilon}\right)\left(\frac{B}{\Delta f}\right)\eta \overline{N}_p}{\sqrt{A_1 + A_2 A_3 + [RIN(0)] A_2^2 A_4} + \sqrt{A_1 + A_5 A_3 + [RIN(0)] A_5^2 A_4}} \qquad (3.3.15)$$

where $A_1 = \frac{2\pi V_T C_e}{q}$, $A_2 = \frac{\varepsilon}{1+\varepsilon}$, $A_3 = \eta \overline{N}_p \left(\frac{B}{\Delta f}\right)$,

$A_4 = B\left(\frac{B}{\Delta f}\right)(\eta \overline{N}_p)^2$, $A_5 = \frac{1}{1+\varepsilon}$.

For a p-i-n photodetector, the effect of shot noise and RIN for bit 0 can be neglected since the thermal noise is dominant. Consequently, from equation (3.3.15), the average number of photons per bit is given by

$$\overline{N}_p = \frac{\left(\frac{k^2}{\eta}\right)\left(\frac{\Delta f}{B}\right)\left((1+\varepsilon)+\frac{(1-\varepsilon^2)}{k}\sqrt{\frac{8\pi V_T C_e}{q}}\right)}{(1-\varepsilon)^2 - k^2[RIN(0)](\Delta f)} \tag{3.3.16}$$

If the effect of shot noise in bit 1 is also neglected, the average number of photons per bit in equation (3.3.16) will be

$$\overline{N}_p = \frac{(1-\varepsilon^2)\left(\frac{k}{\eta}\right)\left(\frac{\Delta f}{B}\right)\sqrt{\frac{8\pi V_T C_e}{q}}}{(1-\varepsilon)^2 - k^2[RIN(0)](\Delta f)} \tag{3.3.17}$$

The average number of photons per bit in equation (3.3.17) is for the case that thermal noise dominates and RIN affects only bit 1. Comparing equation (3.3.17) to equation (3.2.16), we can find the power penalty of RIN in the case of nonzero-extinction ratio. The power penalty is given by

$$\delta_{\varepsilon,RIN} = 10\log_{10}\left(\frac{(1-\varepsilon^2)}{(1-\varepsilon)^2 - k^2[RIN(0)](\Delta f)}\right) \tag{3.3.18}$$

From equation (3.3.18), it follows that for a given $[RIN(0)](\Delta f)$ and ε, there is a maximum value of k that can be achieved. This maximum k leads to the lower bound of the minimum error probability that we can get from the system. The maximum value of k is given by

$$k_{\max} = \frac{(1-\varepsilon)}{\sqrt{[RIN(0)](\Delta f)}} \tag{3.3.19}$$

and the lower bound on the minimum error probability is given by

$$P_{e,lower} = Q(k_{\max}) \tag{3.3.20}$$

Using equation (3.3.15) with equation (3.1.9), the error probability versus the average number of photons per bit is plotted in Figure 3.7. The effective capacitance is 1 pF and the quantum efficiency is 0.8. The bit rate is 200 Mbps. In this figure, the extinction ratio and $RIN(0)$ are varied. The error probability for zero-extinction ratio and no RIN is the best. For the zero-extinction ratio, if $RIN(0)$ increases, the error probability increases. The effect of RIN will give a lower bound on the error probability as shown in

the figure. This lower bound will increase if the value of *RIN*(0) increases. This effect was mentioned previously in section 3.2.2. However, here, the effect of a nonzero-extinction ratio is included in the calculation. From the figure, it is shown that as the extinction ratio changes from zero to 0.1, the error probabilities for both values of *RIN*(0) increase. And the lower bound for the error probability increases, as well.

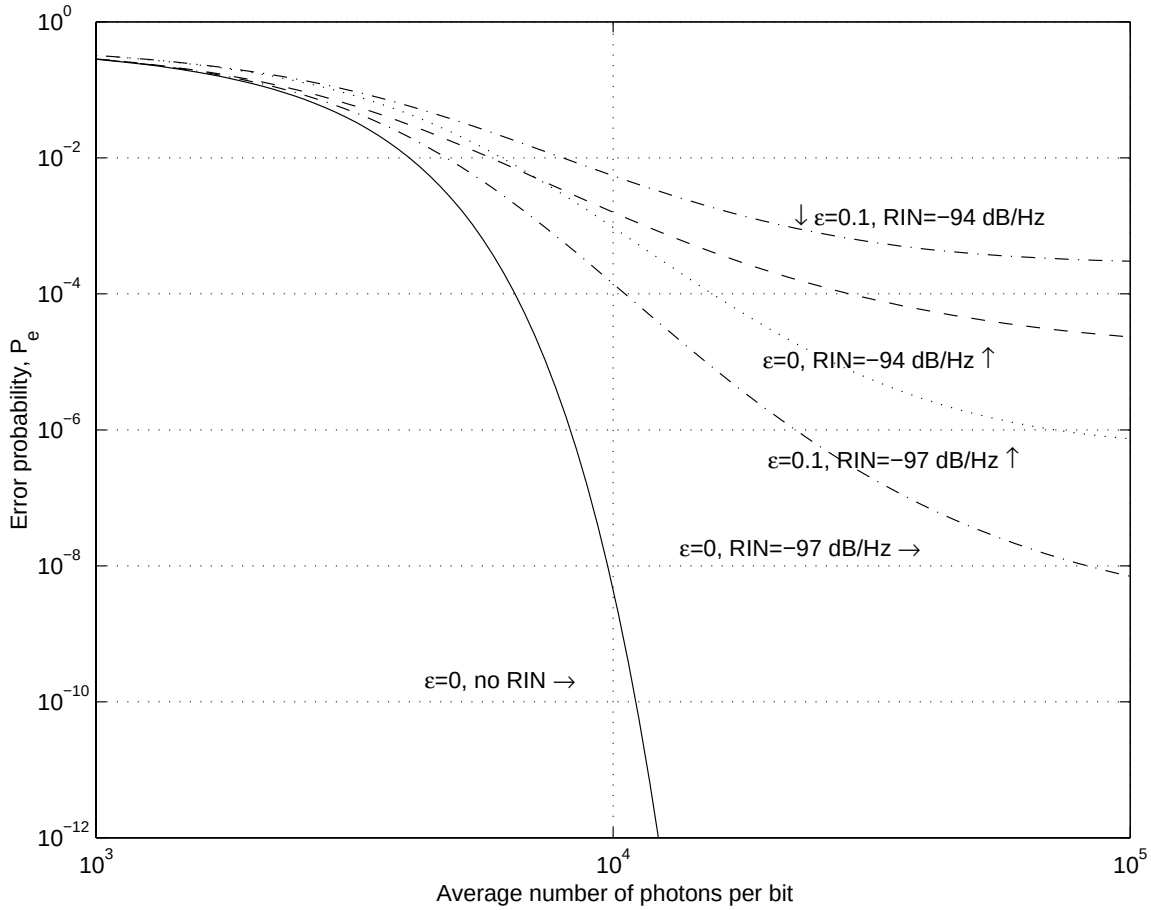

Figure 3.7 The error probability versus the average number of photons per bit for different extinction ratios and RINs.

The power penalties for different extinction ratios and $[(RIN(0))\cdot(\Delta f)]$ are plotted in Figure 3.8 and 3.9. The power penalty versus $[(RIN(0))\cdot(\Delta f)]$ for different values of extinction ratio is shown in Figure 3.9. The power penalty increases as $[(RIN(0))\cdot(\Delta f)]$ increases. And, if the extinction ratio is increased, the power penalty will increase as shown in the Figure The power penalty is also plotted versus the extinction ratio. This plot is shown in Figure 3.8. The power penalty increases as the extinction ratio increases, with the effect being more pronounced when $[(RIN(0))\cdot(\Delta f)]$ is high. From these two figures, an important result should be pointed out. That is, the power penalty for the case of nonzero-extinction ratio and nonzero RIN is not just the linear combination of the individual power penalties. For example, at $[(RIN(0))\cdot(\Delta f)]=0.01$ with zero-extinction ratio, power penalty is 2 dB; and , at an extinction ratio of 0.2 with zero RIN, the power penalty is 1.8 dB. However, from Figure 3.8, we can see that at $[(RIN(0))\cdot(\Delta f)]=0.01$ and the extinction ratio of 0.2, the power penalty is 5.4. This example shows that the effect for the case of a nonzero-extinction ratio with a nonzero RIN can degrade the system performance considerably. And, from both plots, if the value of $[(RIN(0))\cdot(\Delta f)]$ or extinction ratio reaches some particular values the power penalty will approach infinity; that is, a lower bound on the error probability (an error floor) will occur. This effect will be plotted on the next two figures.

The lower bound on the error probability is shown in Figure 3.10 and 3.11. These figures are plotted from the relationship in equation (3.3.19) and (3.3.20). In Figure 3.10, the lowest error probability for different values of $[(RIN(0))\cdot(\Delta f)]$ is plotted versus the extinction ratio. It is shown that as the extinction ratio increases the lowest error probability increases; i.e., the system performance is degraded. Also, in Figure 3.11, the lowest error probability for different extinction ratios is plotted versus $[(RIN(0))\cdot(\Delta f)]$. The results indicate that a higher extinction ratio will give a greater lower bound on the error probability.

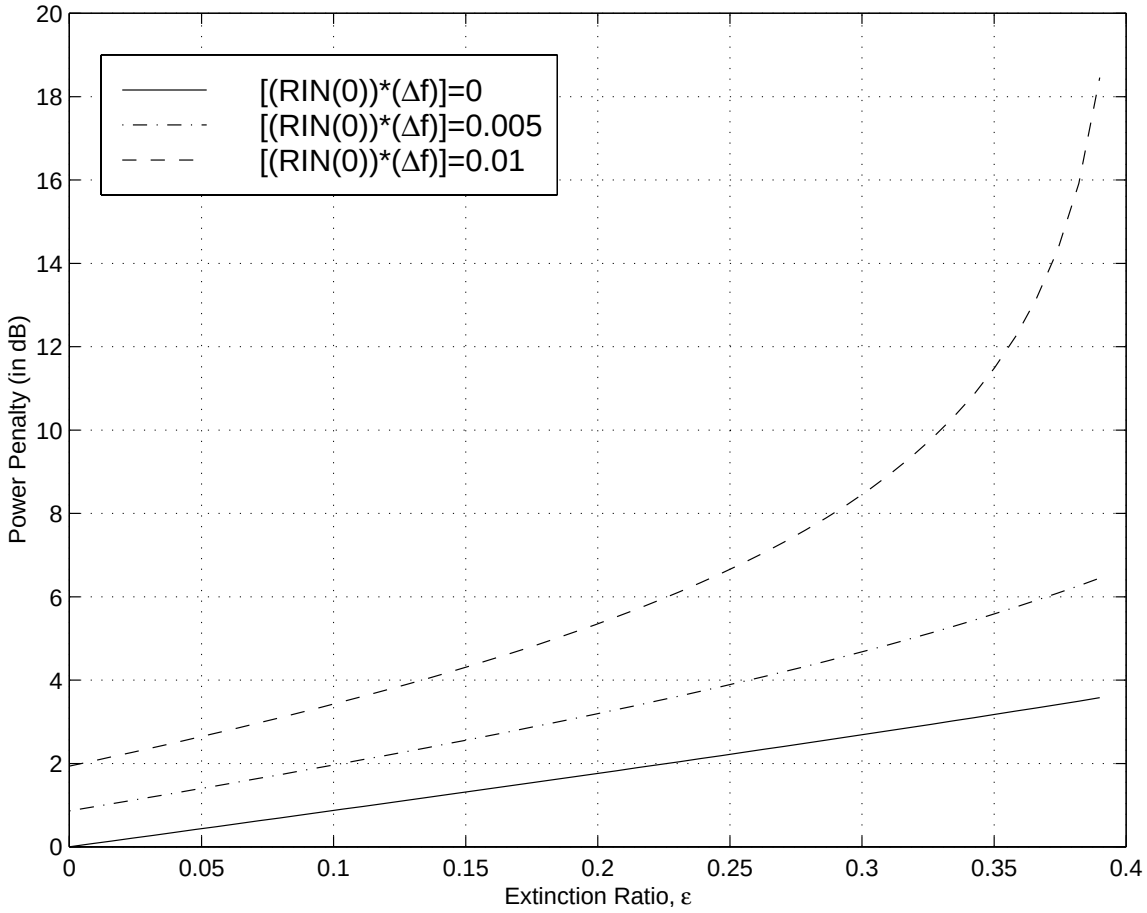

Figure 3.8 The power penalty versus the extinction ratio: for different values of $[(RIN(0))\cdot(\Delta f)]$.

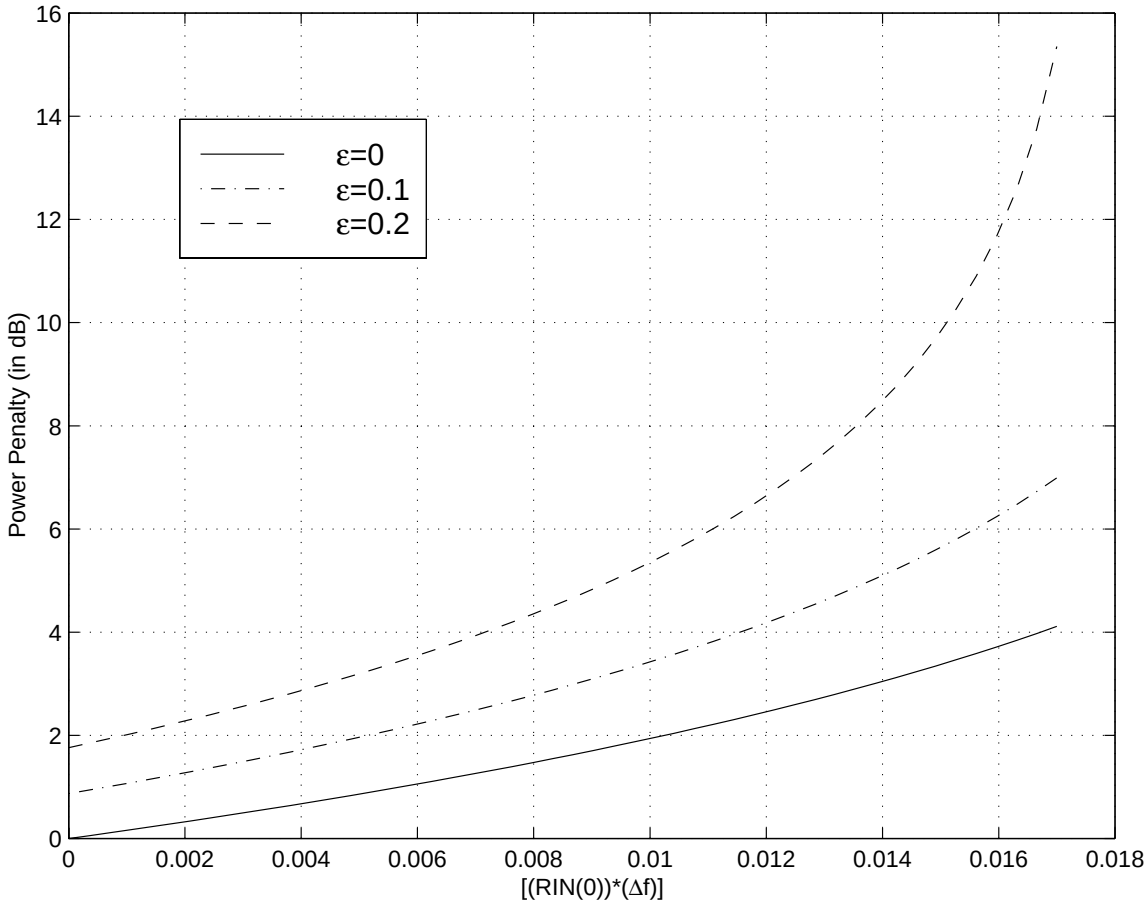

Figure 3.9 The power penalty versus $[(RIN(0))\cdot(\Delta f)]$: for different values of extinction ratio.

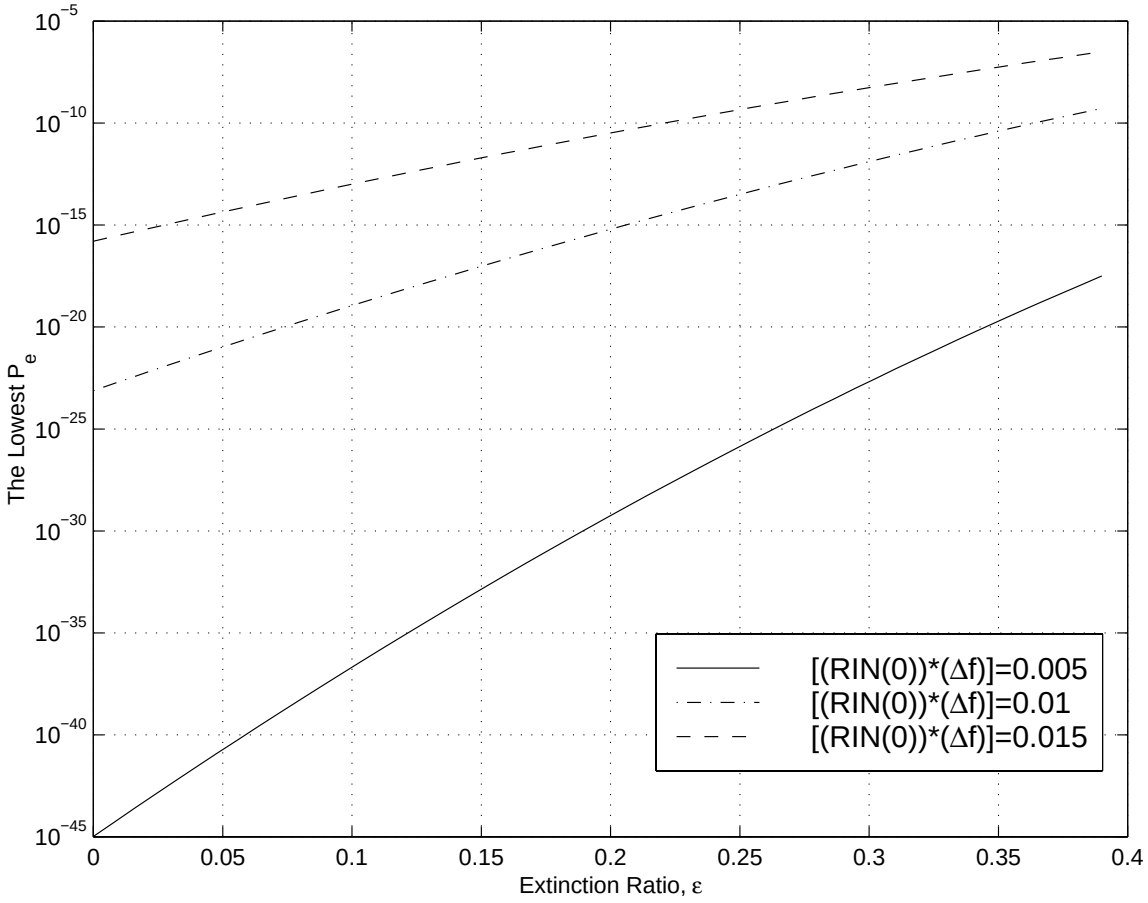

Figure 3.10 The lowest error probability versus the extinction ratio for different values of [(*RIN*(0))·(Δ*f*)].

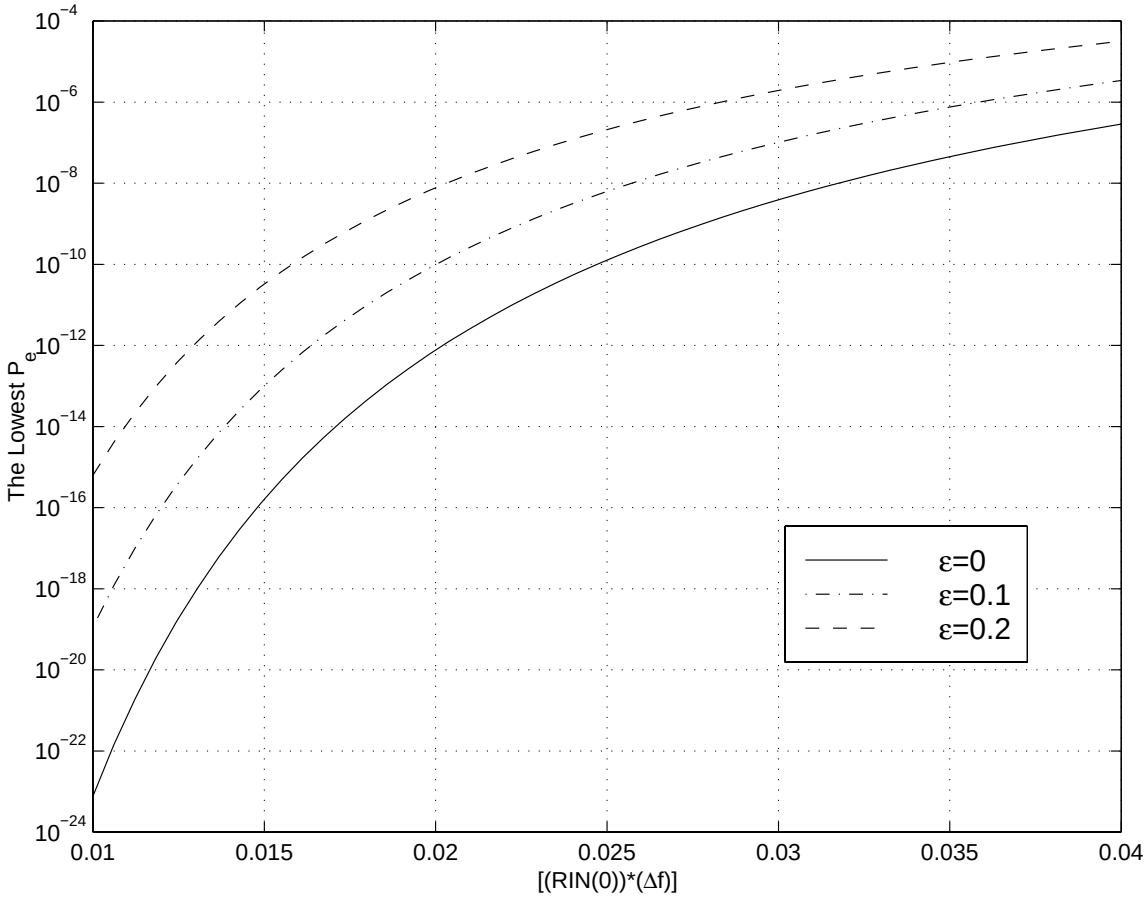

Figure 3.11 The lowest error probability versus [(*RIN*(0))·(Δ*f*)] for different extinction ratios.

3.4 Effect of vertical offset from the optimal threshold

From section 3.1, the error probability of an optical communication system is calculated by a Gaussian approximation. The error probability from this approximation will be optimal if the current threshold is set appropriately; that is,

$$I_{th} = \frac{\sigma_0 I_1 + \sigma_1 I_0}{\sigma_0 + \sigma_1} \qquad (3.4.1)$$

In this section, the power penalty resulting from a vertical offset from the optimum threshold will be evaluated. Considering an optical detector, a simple diagram of this detector is shown below.

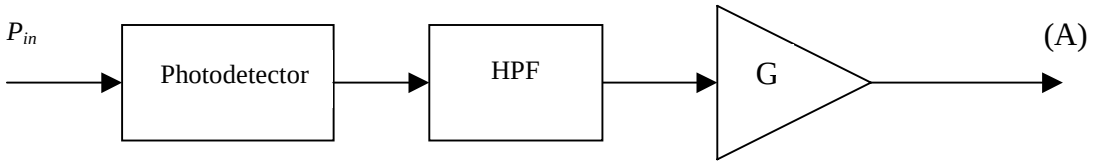

Figure 3.12 Block diagram of an optical detector

The optical signal, which has a power of P_{in}, is incident onto a photodectector. This photodetector will convert the optical signal into an electrical signal and sends this electrical signal into a high-pass filter. This filter will remove the dc component from the input electrical signal and gives a balanced signal.The balanced current signal will be amplified and sent to the decision circuit at point (A). This amplifier has a gain of G. This gain is varied to maintain the eye opening at the decision circuit; that is, if the average optical current from the photodetector is high, the gain G will be decreased. But if the average optical current from the photodectetor is low, the gain G will be increased. The change of G depends on the average input power (P_{in}). The effect of gain G will not affect the input current to the decision circuit since the eye opening is fixed but it will affect the variance of the input current to the decision circuit. The input current at point (A) for bit 1 and bit 0 will be symmetrically displaced from the zero-current line since the detector is a balanced detector. Here the input current to the decision circuit for bit 1 and bit 0 are denoted by I_{on} and I_{off}, which are given by

$$I_{on} = I_1 - \bar{I} \qquad (3.4.2)$$

$$I_{off} = I_0 - \bar{I} \qquad (3.4.3)$$

where $\bar{I}$ is the average optical current from the photodetector, $\bar{I} = \left(\frac{1+\varepsilon}{2}\right) I_1$

ε is the extinction ratio.

I_{on} and I_{off} from equation (3.4.2) and (3.4.3) can be rewritten as

$$I_{on} = aI_1 \tag{3.4.4}$$

$$I_{off} = -aI_1 \tag{3.4.5}$$

where $a = \frac{1-\varepsilon}{2}$.

From the input currents in equation (3.4.4) and (3.4.5), the current threshold for the decision circuit (referenced to the amplifier input) is given by

$$I_{th} = \frac{\sigma_0 I_{on} + \sigma_1 I_{off}}{\sigma_0 + \sigma_1} \tag{3.4.6}$$

Substituting these input currents to I_1 and I_0 in equation (3.1.5), and multiplying σ_0 and σ_1 by g, the minimum error probability will be given by

$$P_e = 0.5\left\{Q\left(\frac{I_{th} - I_{off}}{g\sigma_0}\right) + Q\left(\frac{I_{on} - I_{th}}{g\sigma_1}\right)\right\} \tag{3.4.7}$$

where $$g = \frac{G}{G_0} \tag{3.4.8}$$

G is the amplifier gain when there is a vertical offset from the optimum threshold

G_0 is the amplifier gain when there is no vertical offset.

Since the amplifier gain (G) in Figure 3.12 is inversely proportional to the input optical power, the parameter g in equation (3.4.8) gives the ratio between the optical powers without and with a vertical offset. If a vertical offset from the current threshold occurs (i.e., I_{th} in equation (3.4.7) is substituted by I_{th}+offset), the input optical power (P_{in}) needs to be increased to maintain the value of P_e. The average optical current from the photodetector will be increased. Then, the gain G will be reduced to keep the eye size constant. Consequently, g is reduced or more optical power is needed.

It follows from the above discussion that the parameter g is the inverse of the power penalty. The power penalty from the vertical offset is then given by

$$\delta_{offset}(\text{in dB}) = -10\log_{10}(g) \qquad (3.4.9)$$

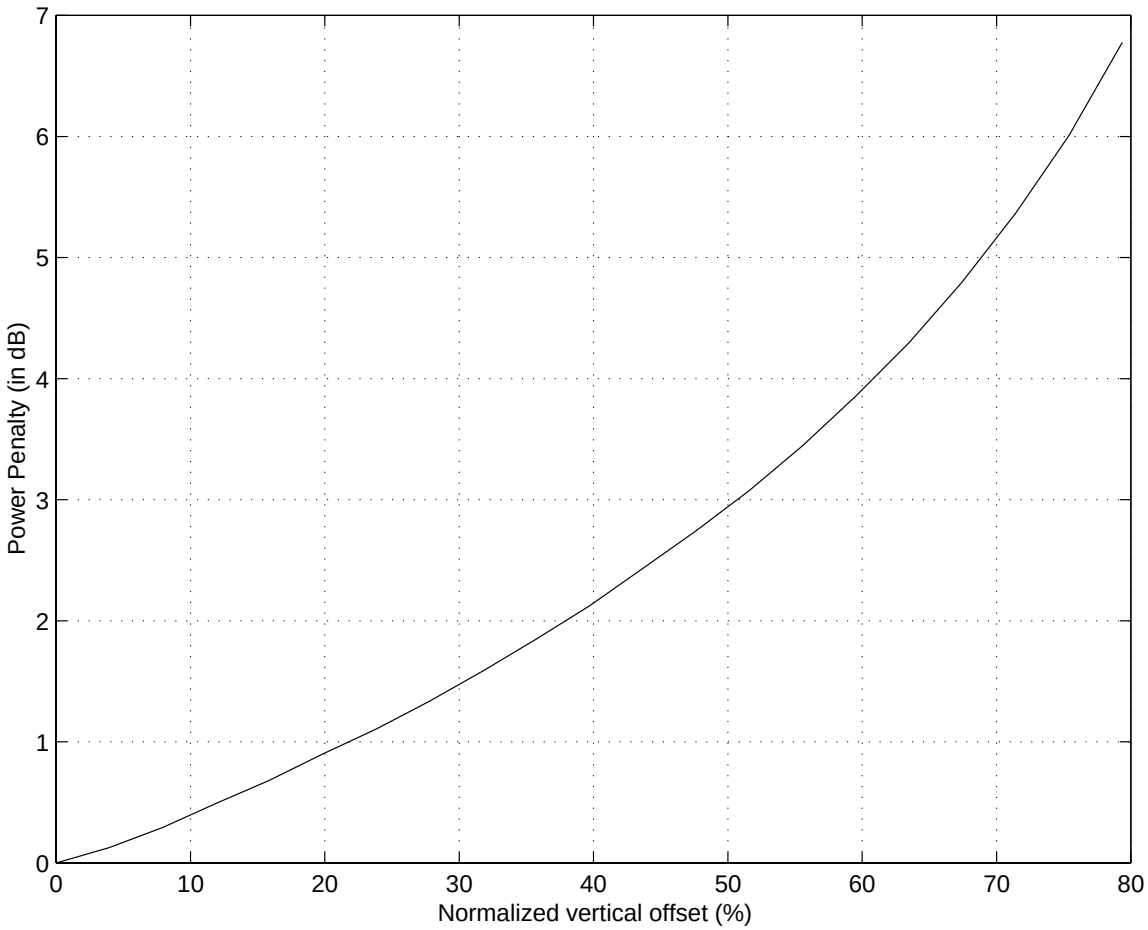

Figure 3.13 The power penalty (in dB) due to the vertical offset from the optimal current threshold.

Assuming that thermal noise dominates for bit 1 and bit 0, the variances of optical currents for bit 1 and bit 0 are identical. Using this assumption and equation (3.4.7), (3.4.8), and (3.4.9) with $P_e = 10^{-9}$, the power penalty due to the vertical offset is shown in Figure 3.13. The vertical offset is normalized by the half of the height of the eye diagram. From the figure, if the vertical offset increases, the power penalty increases; that is, more optical power is needed.

4.0 Effect of system bandwidth on intersymbol interference

The three main components of optical communication systems are the optical source, the optical detector and the optical fiber. Each of these components has its own transfer function that will be combined to be the system transfer function. In this chapter, the transfer function and the impulse response of each component will be discussed. These transfer functions will be approximated by Butterworth filters. The order of each Butterworth filter will be determined appropriately for each component. These Butterworth filters will be combined to form the system transfer function. The bandwidth of each component will be varied, and the intersymbol interference (ISI) will be determined by computer simulation. The power penalty due to the ISI will also be discussed.

4.1 Modeling of fiber optic system using Butterworth filters

As mentioned, there are three main components in the optical systems. Each of them will be considered and approximated by a Butterworth filter.

-Fiber

If the source spectral width is much larger than the signal spectral width, the optical fiber can be assumed to behave as a linear low pass filter operating on the optical power. The transfer function of the fiber can be assumed to be a Gaussian spectrum, which is given by [1]

$$H(f) = \frac{1}{(1+ jf / f_2)^{1/2}} e^{\frac{-1}{2}\left(\frac{(f/f_1)^2}{1+jf/f_2}\right)} \qquad (4.1.1)$$

where $f_1 = (2\pi |D| L\sigma_\lambda)^{-1}$ (4.1.2)

$$f_2 = \left[2\pi (S + 2|D|/\lambda) L\sigma_\lambda{}^2\right]^{-1} \qquad (4.1.3)$$

σ_λ is the rms source spectral width in wavelength units

λ is the center wavelength of the optical signal

D is the fiber dispersion at λ

S is the dispersion slope at λ

L is the fiber length.

The impulse response of $H(f)$ in equation (4.1.1) has a Gaussian shape with a peak at time t=0 as shown in Figure 4.2. This impulse response is non-causal since it is not zero at negative time. Letting $f_1 << f_2$ (when the operating wavelength is far from the zero-dispersion wavelength), and plotting the frequency responses of $H(f)$ in equation (4.1.1) and different orders of Butterworth filters, it is found that the second order Butterworth filter can be used to approximate $H(f)$ in equation (4.1.1). The impulse response of the second order Butterworth filter is causal as shown in Figure 4.2.

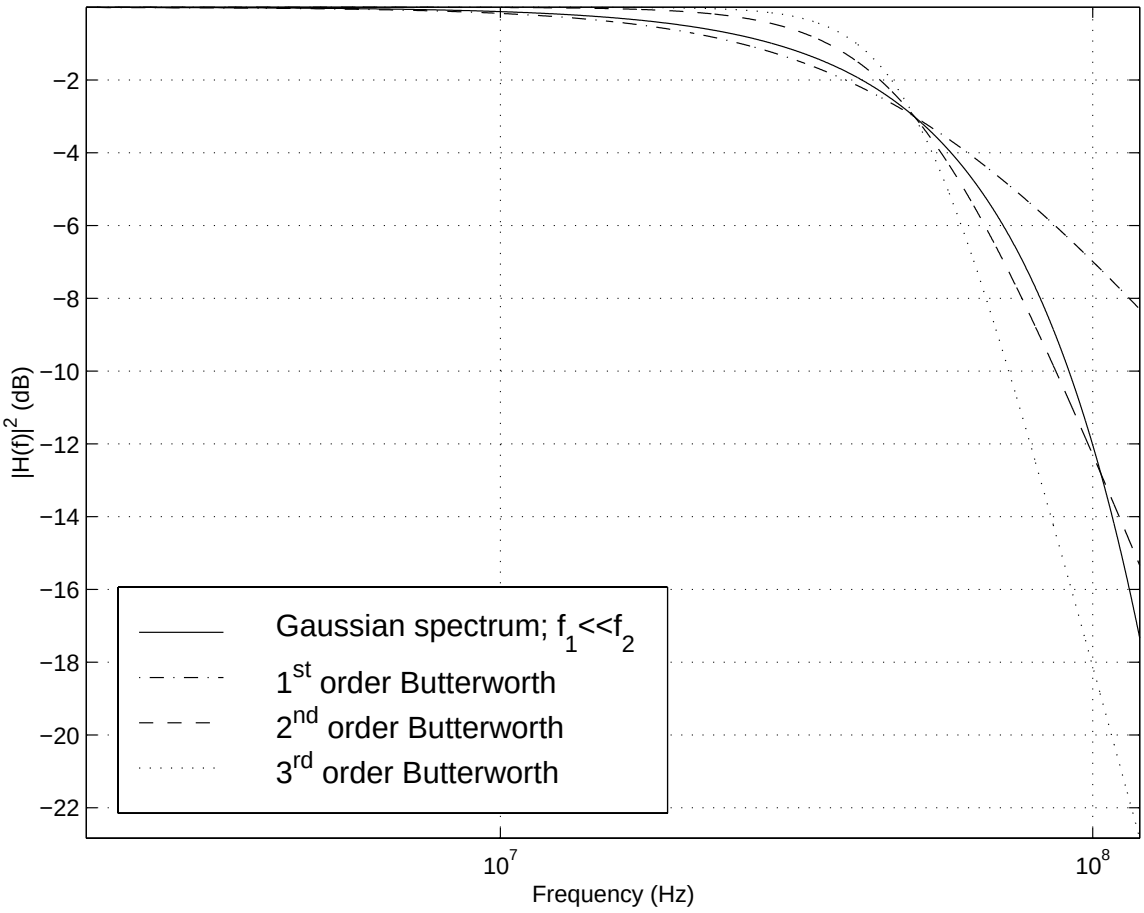

Figure 4.1 The frequency responses of the optical fibers (from equation (4.1.1.)) and the Butterworth filters with different orders: Bandwidth=50MHz.

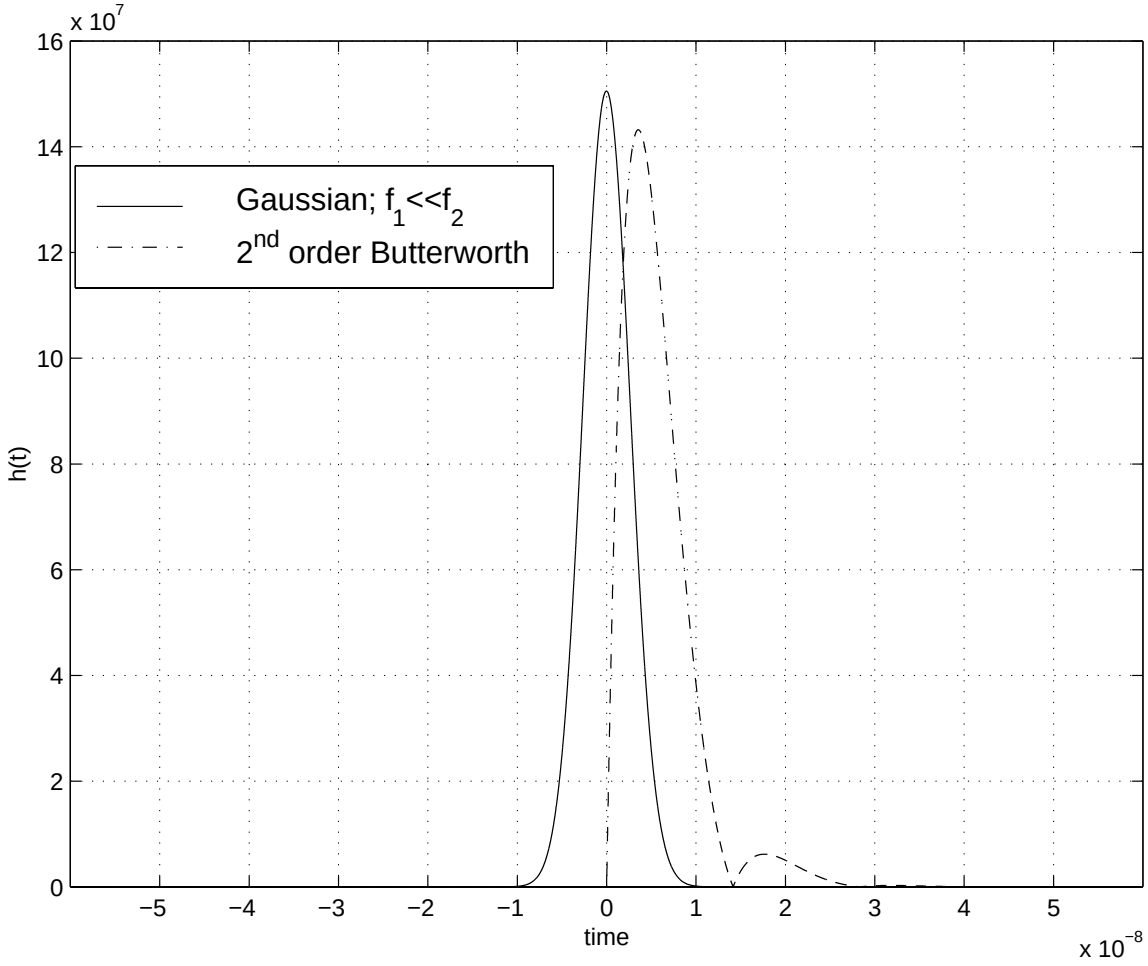

Figure 4.2 The impulse responses of the optical fiber with a Gaussian spectrum and 2^{nd} order Butterworth filter.

From Figure 4.1, we assume that f_1 is much less than f_2 and the bandwidth of the fiber in equation (4.1.1) is 50 MHz. Plotting the frequency response of a Gaussian spectrum in equation (4.1.1) and different orders of Butterworth filter with 50 MHz bandwidth each, we see that the frequency response of the second order Butterworth filter is approximately the same as the frequency response from the Gaussian spectrum in equation (4.1.1) in the range of 0 to 100 MHz. Thus, we choose this second order Butterworth filter to approximate the fiber transfer function. The impulse response of the Guassian spectrum and the second order Butterworth filter are shown in Figure 4.2. Both have almost the same profile. The main difference between them is that the impulse response of the Gaussian spectrum is non-causal but the impulse response of the second order Butterworth filter is causal.

-Optical Transmitter and Receiver

In this section, the transfer functions of the transmitter and receiver will be considered. Assuming that an LED transmitter and a transimpedance receiver are chosen, their transfer functions are given by [1]

For LED , $$H(\omega_m) = \frac{1}{1 + j\omega_m \tau_c} \qquad (4.1.4)$$

where ω_m is the modulation frequency

τ_c is the carrier lifetime

For the optical detector with the transimpedance amplifier,

$$H(f) = \frac{1}{1 + j2\pi RCf / A} \qquad (4.1.5)$$

where R is the effective noise resistance of the transimpedance amplifier

C is the effective noise capacitance of the transimpedance amplifier

A is the frequency-independent gain of the amplifier.

The transfer functions in equation (4.1.4) and (4.1.5) are ideal lowpass filters. Similar to the transfer function of the fiber, these transfer functions are compared to different orders of Butterworth filter. It is seen that these transfer functions are first-order

Butterworth. Now all main components are approximated by the Butterworth filters with different orders.

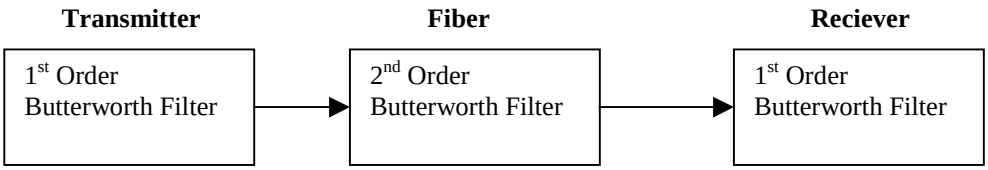

Figure 4.3 Three main components of the optical communications system

-System

The transfer functions for the fiber, transmitter and receiver, which are the Butterworth filters with different orders, are cascaded to be the system as shown in Figure 4.3. Letting the bandwidths of the transmitter, receiver, and fiber be 100, 10, and 150 MHz, respectively, and the bit rate to be 10 Mbps, the frequency response and the impulse response of the system are plotted in Figures 4.4 and 4.5. The system frequency response has smaller bandwidth than that of each component. The impulse response of the system in Figure 4.5 is causal since it is from the combination of three causal impulse responses.

In the next section, the cascaded version of Butterworth filters with orders of 1, 2, and 1 will be used for the system transfer function. The bandwidth of each component will be varied and the intersymbol interference from this varying bandwidth will be studied.

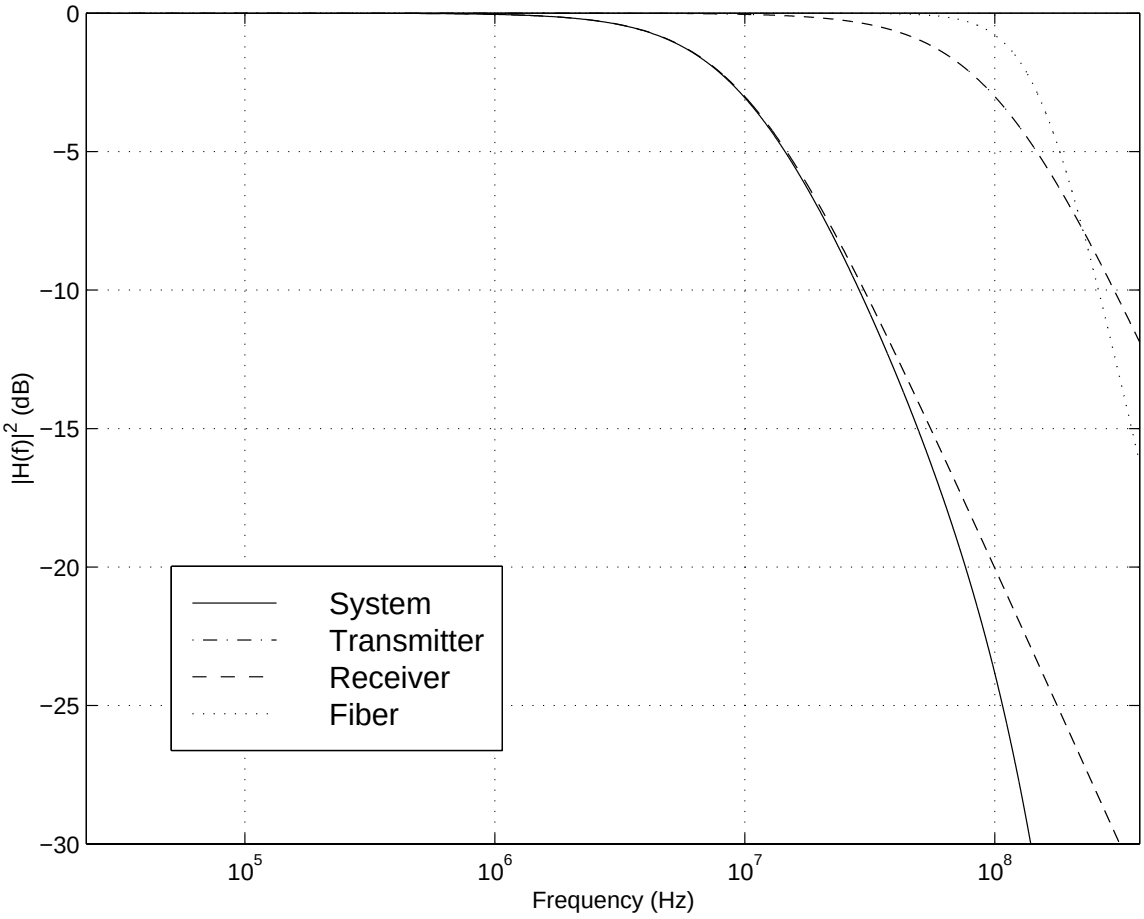

Figure 4.4 The frequency responses of transmitter, receiver, fiber, and system.

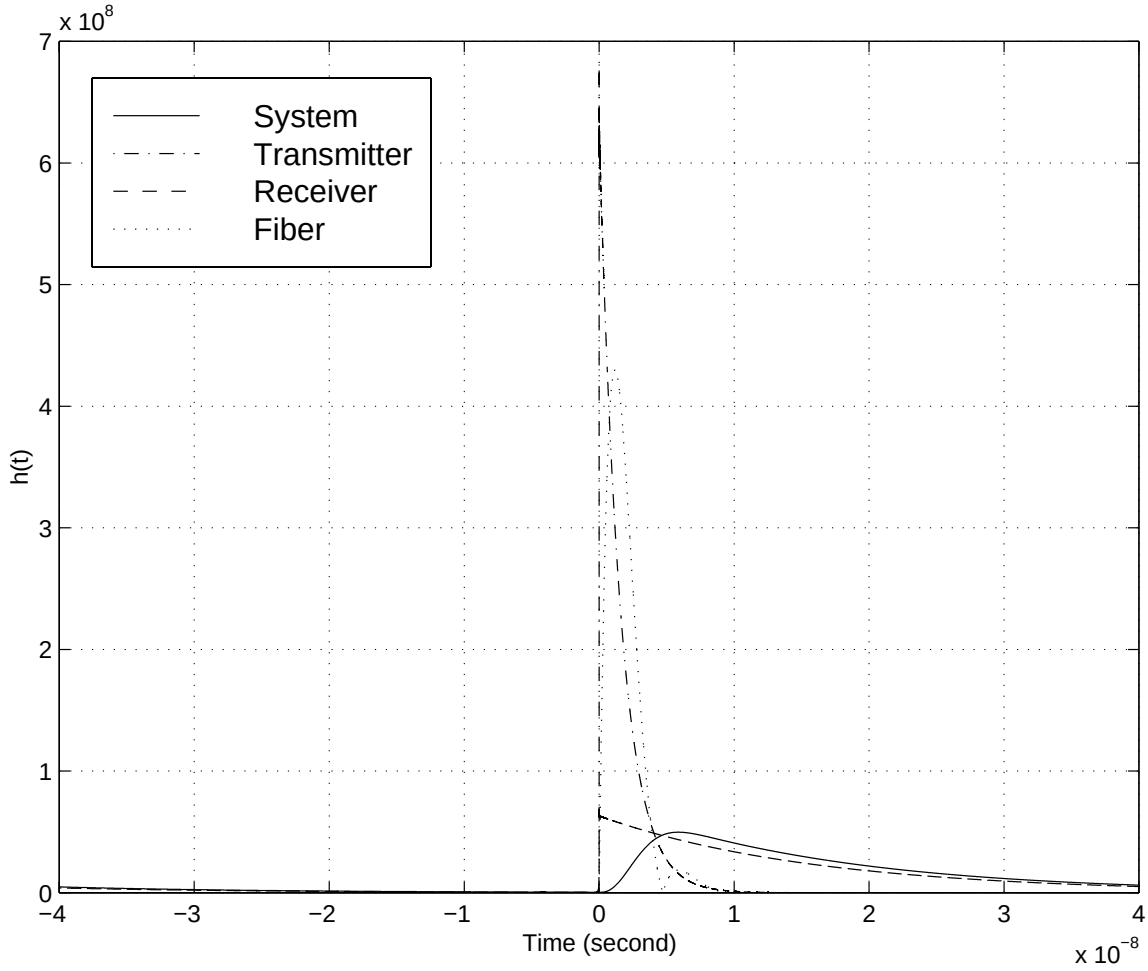

Figure 4.5 The impulse responses of transmitter, receiver, fiber, and system.

4.2 Intersymbol interference simulation

The intersymbol interference (ISI) that was discussed in chapter 2 will be simulated in this section. The normalized maximum ISI and normalized RMS ISI are given by

$$ISI_{\max,normalized} = \frac{\sum_{n=-\infty,n\neq 0}^{\infty}\left|h(nT_b)\right|}{h(0)} \approx \frac{\sum_{n=-N/2,n\neq 0}^{N/2}\left|h(nT_b)\right|}{h(0)} \tag{4.2.1}$$

$$ISI_{rms,normalized} = \frac{\sqrt{\sum_{n=-\infty,n\neq 0}^{\infty}\left|h(nT_b)\right|^2}}{h(0)} \approx \frac{\sqrt{\sum_{n=-N/2,n\neq 0}^{N/2}\left|h(nT_b)\right|^2}}{h(0)} \tag{4.2.2}$$

where N is the number of bits that interfere with the bit at time t=0

T_b is the bit period, which is equal to 1/B

B is bit rate.

$h(t)$ is the impulse response of the system assuming that $h(0)$ is maximum of $h(t)$ for the bit at time t = 0.

From equation (4.2.1) and (4.2.2), the maximum and RMS ISIs, which are the combination of the amplitudes from all neighboring bits at time t=0,are normalized by the maximum value of the bit at time t=0. Using these two equations with an appropriate shift of sampling point correspond to the maximum of $h(t)$, the effect of the bandwidth of fiber, transmitter, and receiver on ISI will be evaluated numerically.

4.2.1 Effect of the fiber bandwidth

The bandwidths of transmitter and receiver are fixed at 100 and 10 MHz respectively, and both of them are first order Butterworth filters. The bit rate is fixed at 10 Mbps, and the fiber transfer function is a second order Butterworth filter. The effect of the fiber bandwidth on the intersymbol interference is plotted in Figure 4.6. In this figure, the number of interfering bits is 30 bits. For the fiber bandwidth range of 0 to 5.65 MHz, the normalized maximum ISI and normalized RMS ISI decreases as the bandwidth of the fiber increases as shown in Figure 4.6. Then, while the fiber bandwidth increases further, the ISIs increase and peak at a fiber bandwidth of 7.2 MHz with ISI of 0.03 approximately. After that, the ISIs decrease as the fiber bandwidth increases. After the fiber bandwidth of approximately 13 MHz, the ISIs are very small and approach zero as

the fiber bandwidth increases. The normalized maximum ISI is greater than the normalized RMS ISI, but for a large fiber bandwidth the difference between these ISIs is insignificant. The reason for this is when the fiber bandwidth becomes larger, the number of interfering bits that affect ISI computation becomes smaller; thus, the normalized maximum ISI and RMS ISI move closer and finally merge.

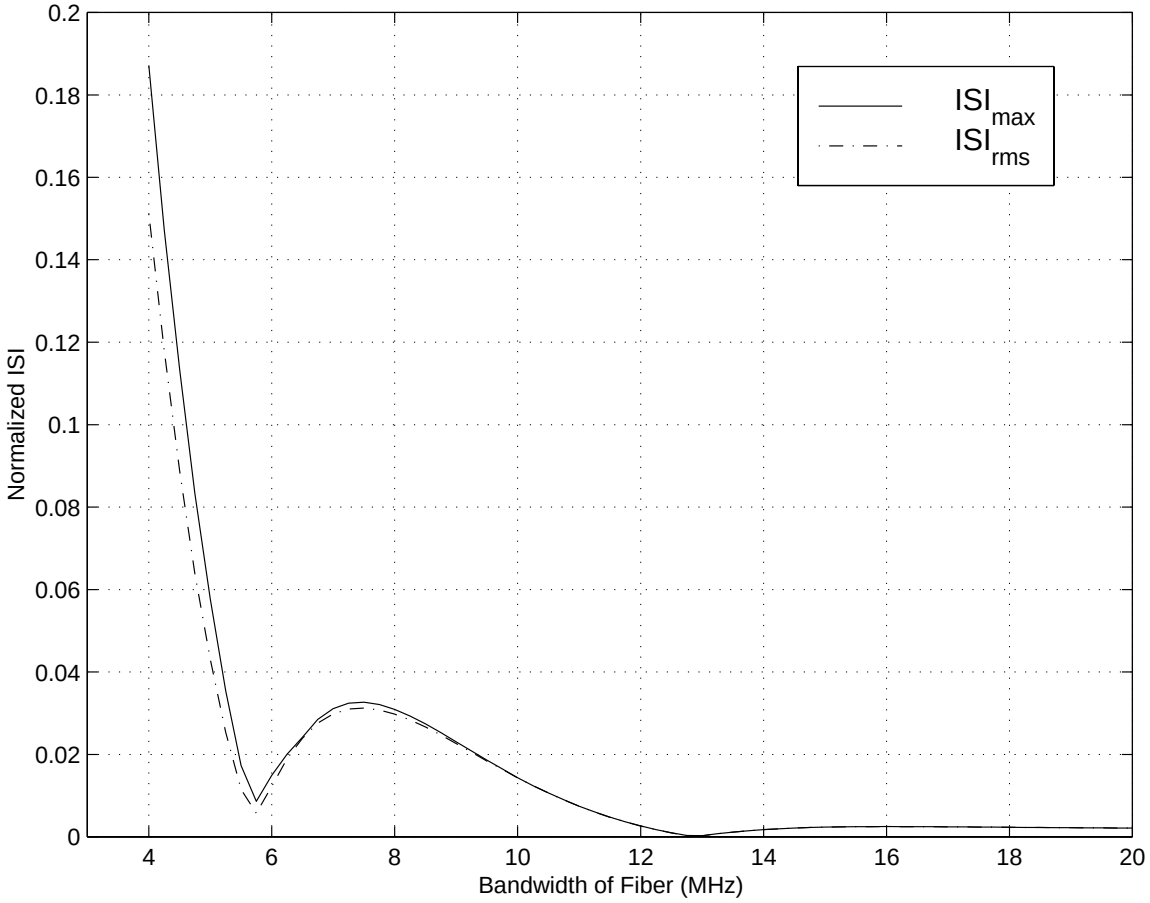

Figure 4.6 The normalized maximum ISI and normalized RMS ISI versus the fiber bandwidth.

4.2.2 Effect of transmitter and receiver bandwidths

Assuming that the bandwidth of the fiber is much larger than the bandwidths of transmitter and receiver, the bandwidth of the transmitter and receiver are identical, and the bit rate is fixed at 10 Mbps; the system transfer function is the product of the transfer functions of transmitter and receiver. Since the bit rate is 10 Mbps, the bit period, T_b, is 100 ns. By using equation (4.2.1) and (4.2.2), the normalized maximum ISI and normalized RMS ISI are plotted versus the transmitter bandwidth, as shown in Figure 4.7. From this figure, it is seen that both of the ISIs will increase as the bandwidths of the transmitter and receiver decrease; for example, at a bandwidth of 6 MHz, maximum ISI is approximately 0.1 while at a bandwidth of 4 MHz, maximum ISI is approximately 0.3. In this figure, the number of interfering bits is 30 bits.

If the bandwidth of the receiver is varied with a fixed transmitter bandwidth, the normalized maximum ISI and the normalized RMS ISI are plotted in Figures 4.8 and 4.9, respectively. The transmitter bandwidths are 50, 100, and 200 MHz. From these figures, it is seen that the normalized maximum ISI and the normalized RMS ISI decrease as the bandwidth of receiver increases. For example, at the receiver bandwidth of 6.2 MHz, both ISIs are approximately 0.02, and, at the receiver bandwidth of 7.5 MHz, the ISIs are 0.01. The normalized maximum ISI is a little bit higher than the normalized RMS ISI. Considering the fixed transmitter bandwidth, if the transmitter bandwidth is increased, both ISIs become slightly better, i.e. the ISIs are smaller. However, at a high receiver bandwidth, the effect of these transmitter bandwidths on ISI becomes less significant; that is, ISIs from all transmitter bandwidth are approximately the same.

From Figure 4.7 to 4.9, it is seen that as far as ISI is concerned, effects of transmitter and receiver bandwidths are the same; that is, ISI increases as transmitter or receiver bandwidths decrease. Even though, for a large transmitter bandwidth and a small receiver bandwidth, ISI is small as shown in Figures 4.8 and 4.9, from the performance standpoint, some signal power will be cut off at the receiver since the receiver bandwidth is much smaller than the transmitter bandwidth. This leads to a reduced signal-to-noise ratio for the received signal.

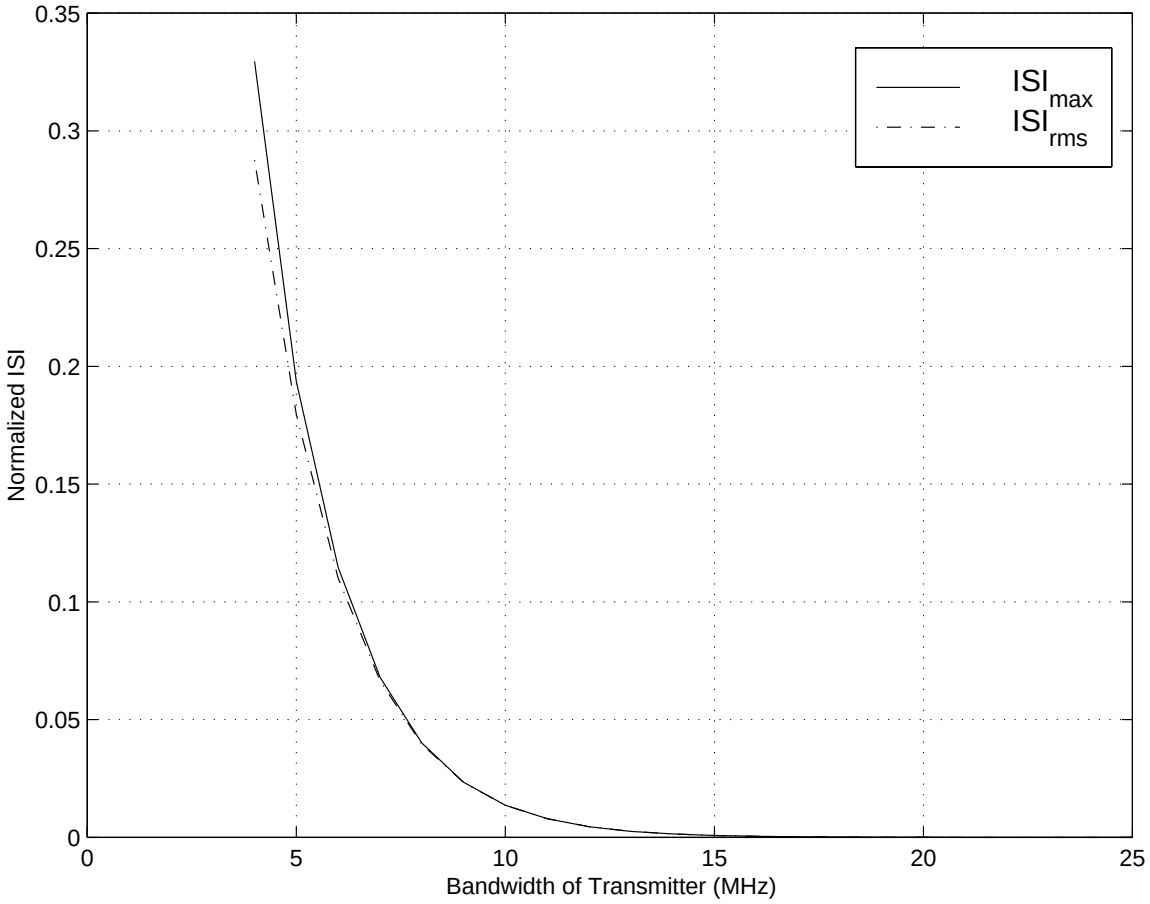

Figure 4.7 The normalized maximum ISI and normalized RMS ISI versus the transmitter bandwidth: assuming $BW_{Tx}=BW_{Rx}$.

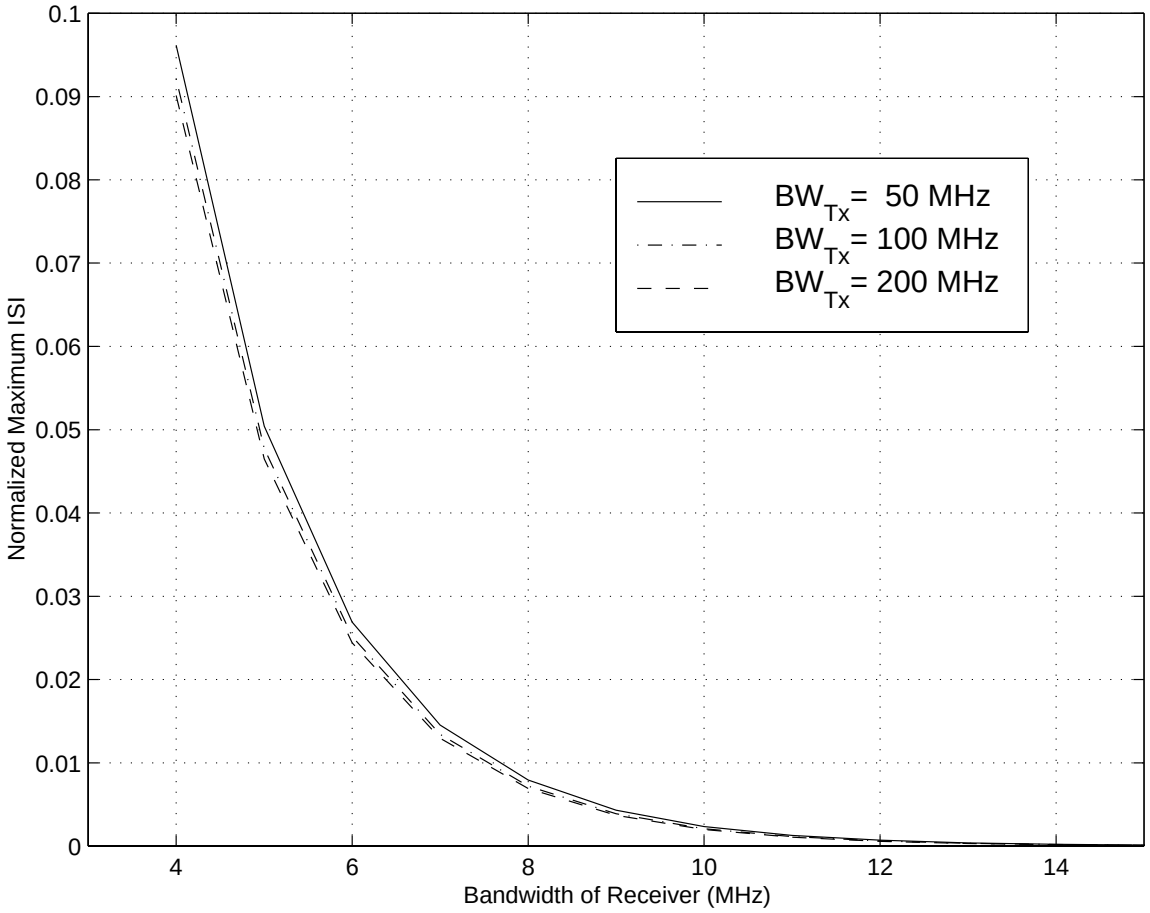

Figure 4.8 The normalized maximum ISI versus the receiver bandwidth.

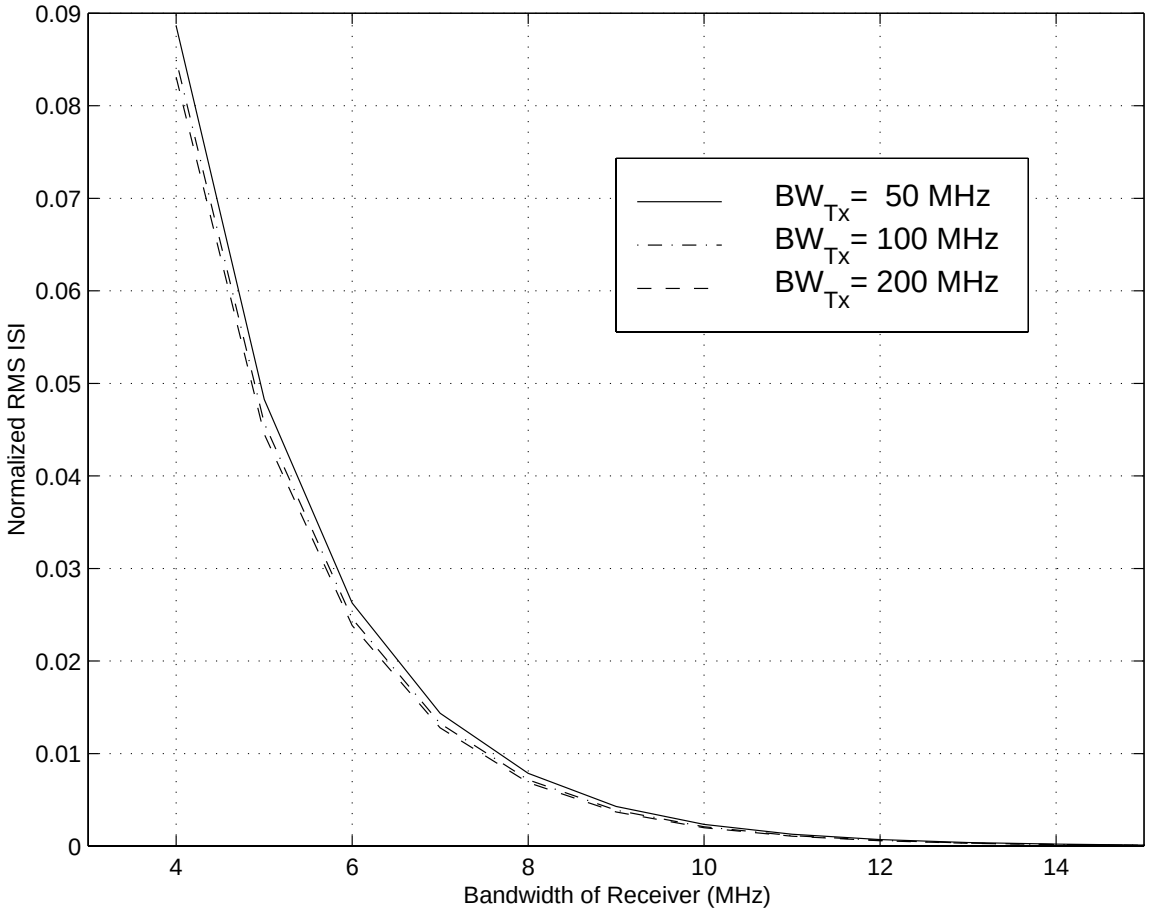

Figure 4.9 The normalized RMS ISI versus the receiver bandwidth.

In Figure 4.10, the relationship between the normalized ISIs and the ratio of transmitter bandwidth to the bit rate is plotted. The bandwidths of transmitter and receiver are assumed to be identical. The transmitter bandwidth is varied. Certainly, as the ratio of the transmitter bandwidth to the bit rate increases, the normalized maximum ISI and normalized RMS ISI decrease. It is also apparent that even though the bit rate is changed the relationship between the normalized ISIs and the ratio of transmitter bandwidth to the bit rate is the same. So, this plot can be used to find the ISIs if the ratio of transmitter bandwidth to the bit rate is given.

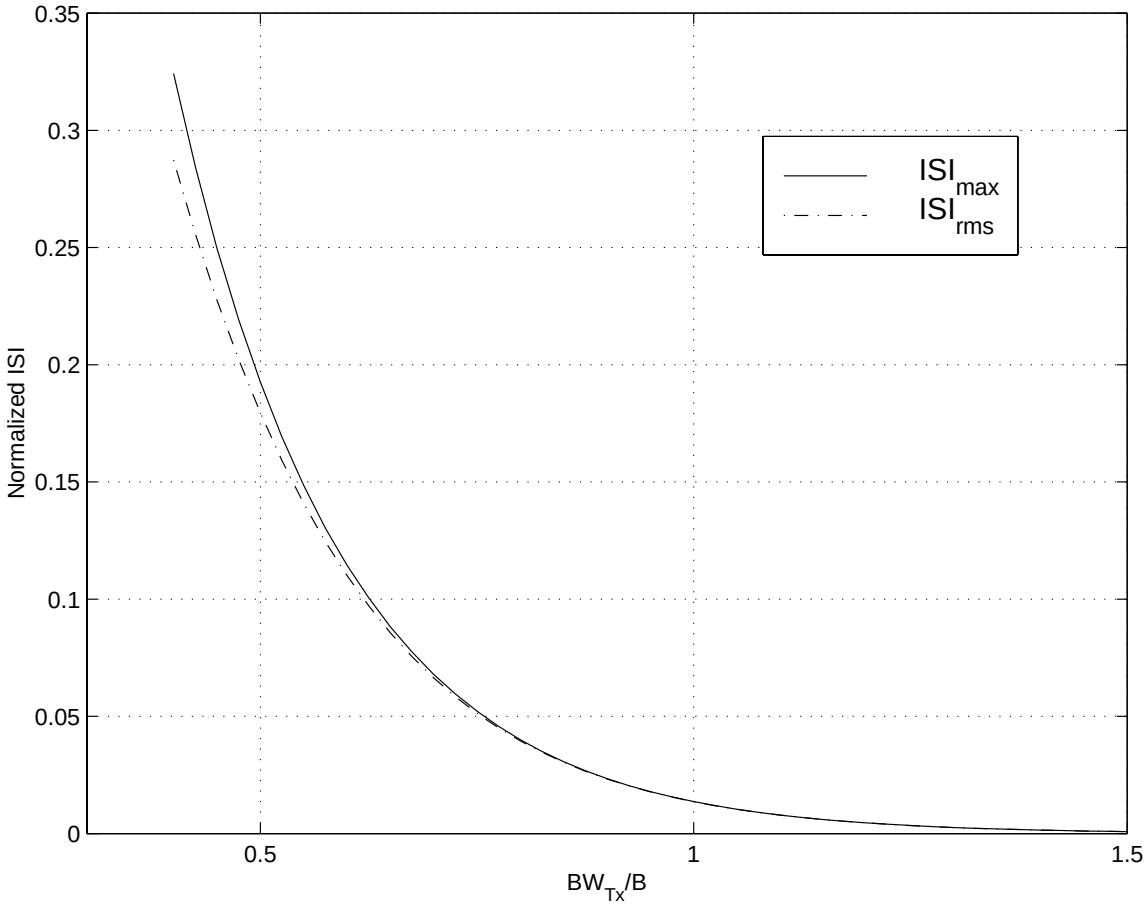

Figure 4.10 The normalized maximum ISI and normalized RMS ISI versus the ratio of transmitter bandwidth to the bit rate: asssuming $BW_{Tx}=BW_{Rx}$.

4.2.3 Effect of the number of interfering bits on ISI calculation

Assuming the bandwidth of the fiber is much higher than those of transmitter and receiver, the transfer function of the optical system is the product of the transfer functions of transmitter and receiver; that is,

$$H_{sys}(f) = H_{Tx}(f) \cdot H_{Rx}(f). \qquad (4.2.3)$$

We also assume that the transfer functions of transmitter and receiver are first order Butterworth filters, as described before. In this section, the minimum number of interfering bits (N) that are used to calculate the worst case of intersymbol interference (ISI) will be considered. Equation (4.2.1) and (4.2.2) are used to calculate the normalized maximum ISI and the normalized RMS ISI. The number of interfering bits (N) is a parameter that can be chosen. If a small N is adopted, the calculation of ISIs will become less precise. On the other hand, if a large N is adopted, the calculation of ISIs is certainly precise but it takes time. Also, in fact, the bits that influence the ISI calculation are the neighboring bits to the bit at t=0. Thus, the minimum N that gives an accurate ISI should be determined.

Setting the bit rate at 10 Mbps and assuming the bandwidth of the transmitter and receiver are identical, if the bandwidths of the transmitter and receiver increase, the achieved ISIs (both $ISI_{max,normalized}$ and $ISI_{rms,normalized}$) decrease, as shown in Figures 4.11 and 4.12. In these figures, the different numbers of interfering bits (i.e., 2, 4, and 6 bits) are used to calculate the ISIs by assuming N/2 bits from the preceding bits and another N/2 bits from the following bits. Figure 4.11 indicates that the minimum N that can give an accurate normalized maximum ISI is 4, while minimum N for the normalized RMS ISI is 2 as shown in Figure 4.12. Thus, the minimum N for ISI calculation is 4 bits.

The impulse response of the system is shown in Figure 4.13. In this figure, the bandwidths of transmitter and receiver are identical and equal to 10 MHz. The impulse response of the system is causal (i.e. zero value for negative time). The sampling points for the bit rate of 75 Mbps are shown in the figure. The signal is sampled at the time at which $h(t)$ is maximum as shown at the peak of the impulse response. Obviously, the number of interfering bits in the negative and positive time corresponding to the sampling time are not the same, since the profile of the impulse response is not symmetric. The negative time profile of the impulse response approaches zero rapidly. It is seen that the

number of interfering bits from the following bits should be less that the number of interfering bits from the preceding bits. From Figures 4.11, 4.12, and 4.13, the minimum number of interfering bits (N) that should be used to calculate ISI is 4; i.e., from 1 following bit and 3 preceding bits.

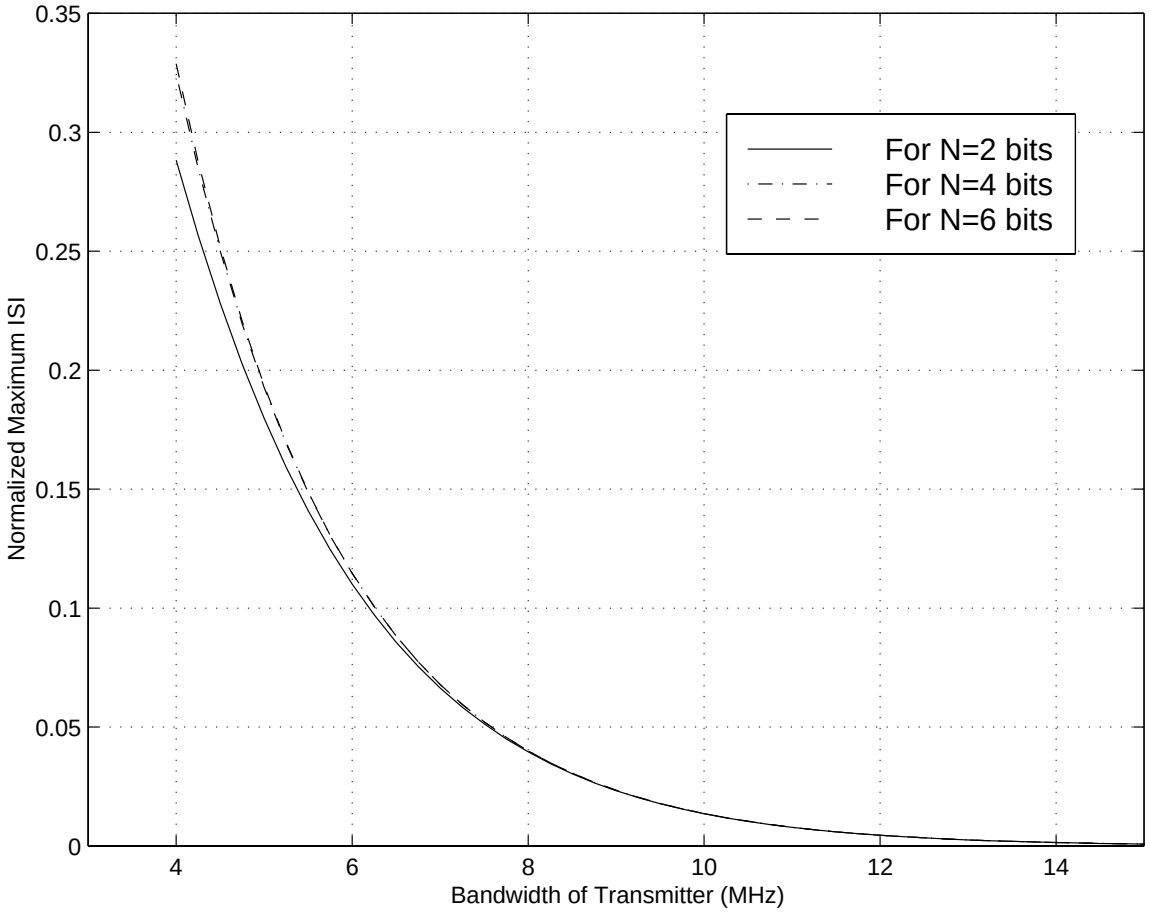

Figure 4.11 The normalized maximum ISI versus the transmitter bandwidth: for different numbers of interfering bits.

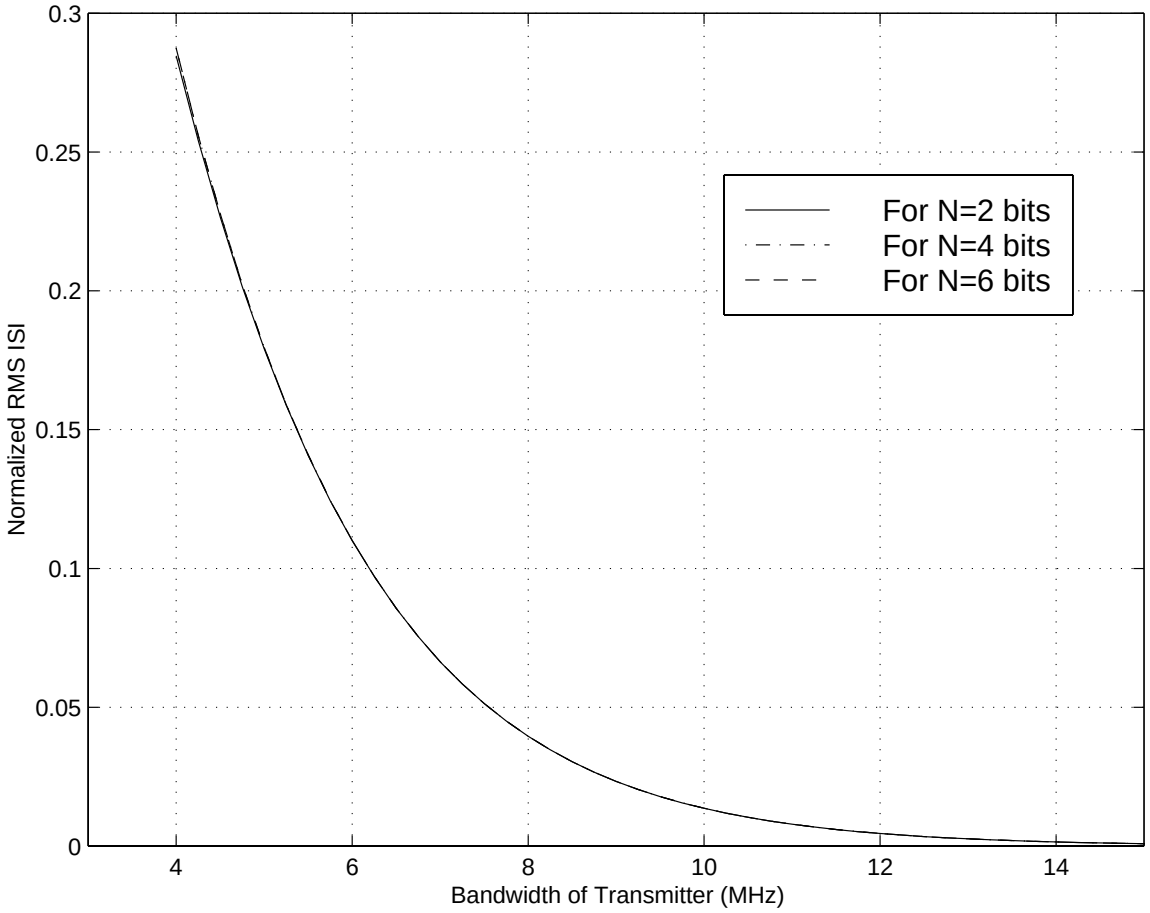

Figure 4.12 The normalized RMS ISI versus the transmitter bandwidth: for different numbers of interfering bits.

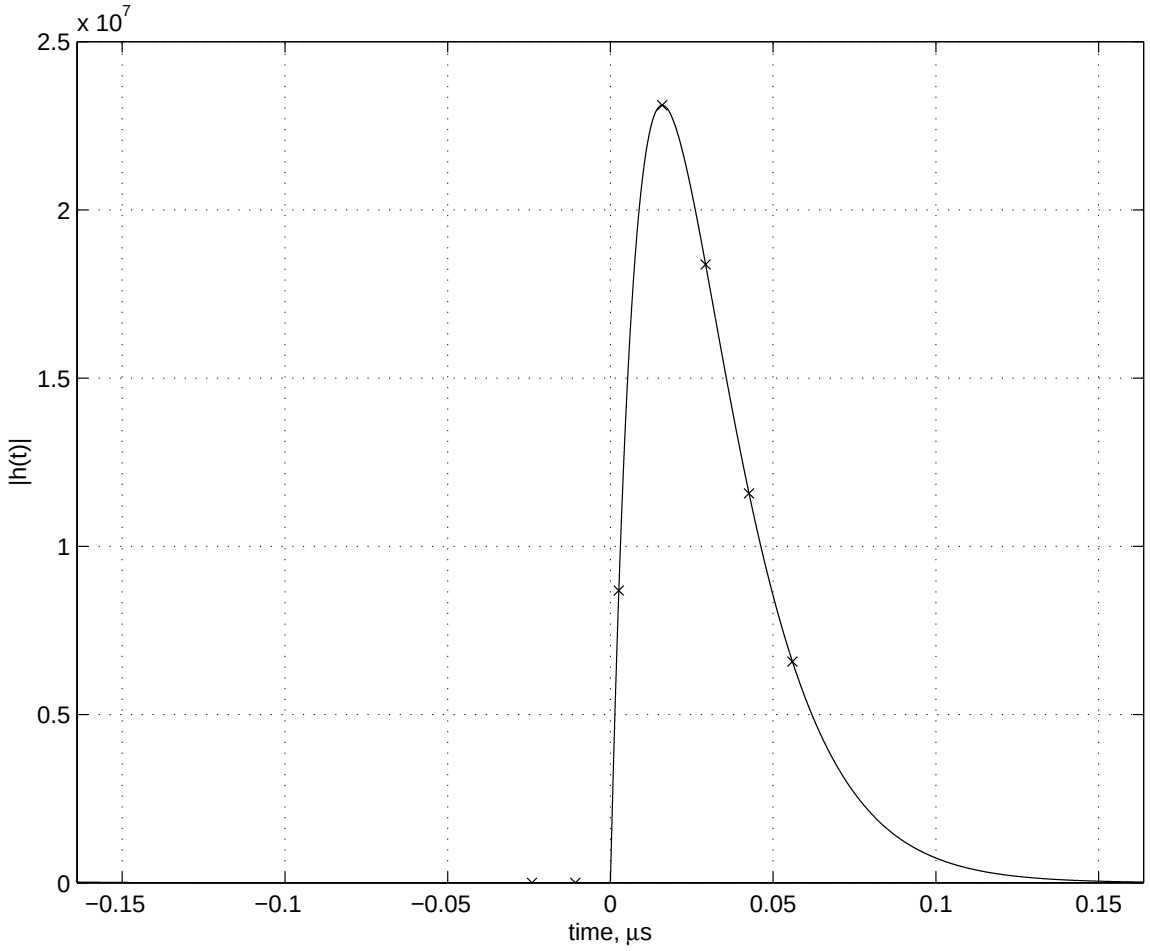

Figure 4.13 The impulse response of the system: assuming that $BW_{Tx}=BW_{Rx}=10$ MHz, and $BW_{fiber}>>BW_{Tx}$.

4.2.4 Comparison between Butterworth filters and raised cosine-rolloff filters for the transfer functions of transmitter and receiver.

A type of filter that can give zero intersymbol interference is raised cosine-rolloff filters. It is interesting to study the effect of this filter on ISI and compare the result with the result from section 4.2.2. In this section, square root raised cosine-rolloff filters with different rolloff factors (*r*) will be used to be the transmitter and receiver transfer functions. Assuming that the bandwidth of the fiber is much larger than those of transmitter and receiver, the system transfer function is given by equation (4.2.3). The intersymbol interference from this system transfer function will be compared to the system transfer function from 1st order Butterworth filters.

By setting the bit rate to be 10 Mbps and assuming that the bandwidths of the transmitter and receiver are identical, as the bandwidths of the transmitter and receiver increases, the achieved ISIs from the raised cosine-rolloff filter tend to decrease as shown in Figure 4.14. Moreover, they are zero at the bandwidths of 5, 10, 15, 20, and so on. These results come from the zero ISI condition that we can get from the raised cosine-rolloff filter. This means that we can get the best performance from using the raised cosine-rolloff filters for specific bandwidths. Considering the rolloff factor of 1, it is shown that the ISIs are zero not only at the bandwidths of multiple of 5 MHz; but at the bandwidths of 7.5, 12.5, 17.5, 22.5, and so on, as well. This results from the impulse response of the unity rolloff factor raised cosine-rolloff filter, which has twice the number of zero-crossings as from other rolloff factors. With different rolloff factors, the larger gives the better performance as seen from Figures 4.14 and 4.15. The ISIs from the rolloff factor of 1 is smaller than the ISIs from the rolloff factor of 0.9, and the ISIs from the rolloff factor of 0.9 is smaller than the ISIs from the rolloff factor of 0.5.

Comparing the raised cosine-rolloff filters to the first order Butterworth filter from Figures 4.14 and 4.15, the raised cosine-rolloff filters give much better performance than the first order Butterworth filter at the bandwidths of 5, 10, 15, and so forth. However, if the bandwidths of the transmitter and the receiver are not a multiple of 5 MHz, the achieved ISIs from the raised cosine-rolloff filters fluctuate and are higher than the achieved ISIs from the first order Butterworth filter. This means that if the bandwidth

of the raised cosine-rolloff filter is slightly changed from the multiple of 5 MHz (half the bit rate), the system ISI will increase rapidly.

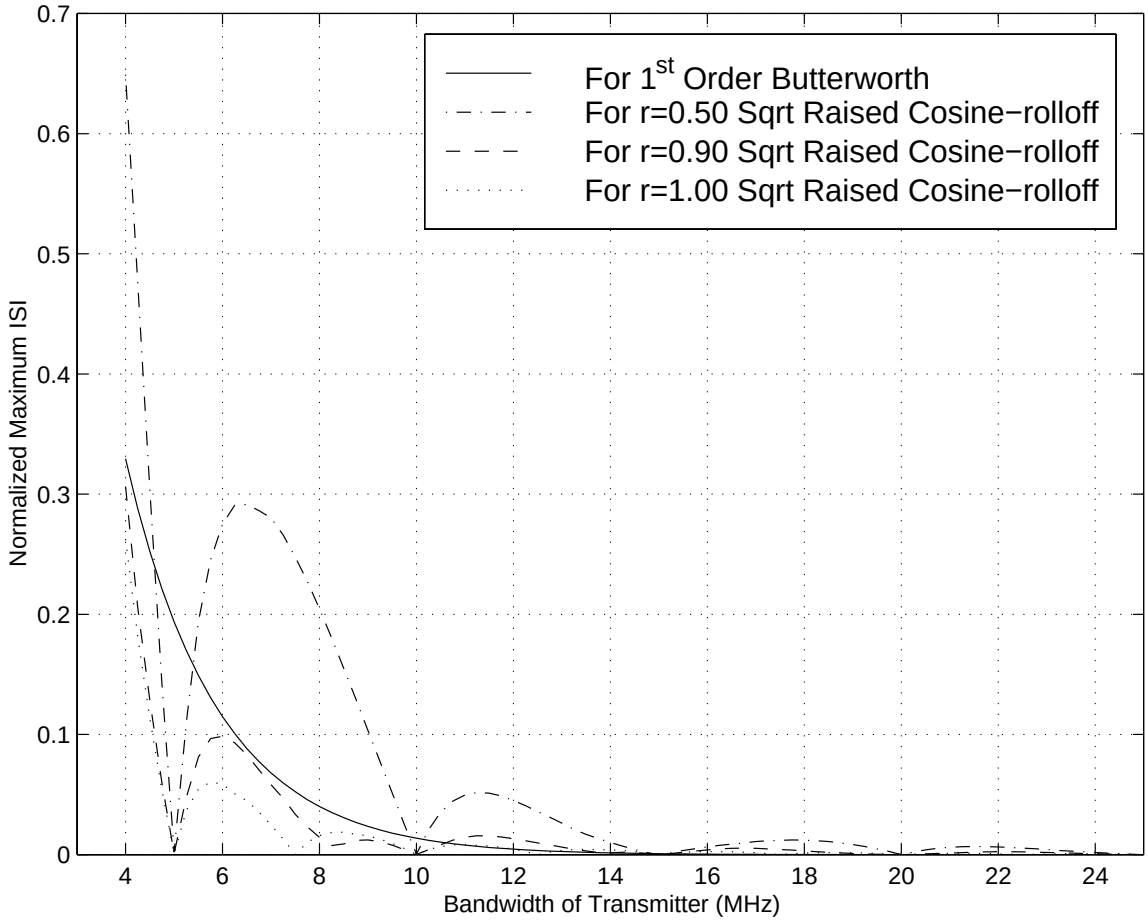

Figure 4.14 The normalized maximum ISI versus the bandwidth of transmitter: assuming that $H_{Tx}(f)=H_{Rx}(f)$, and bit rate=10 Mbps.

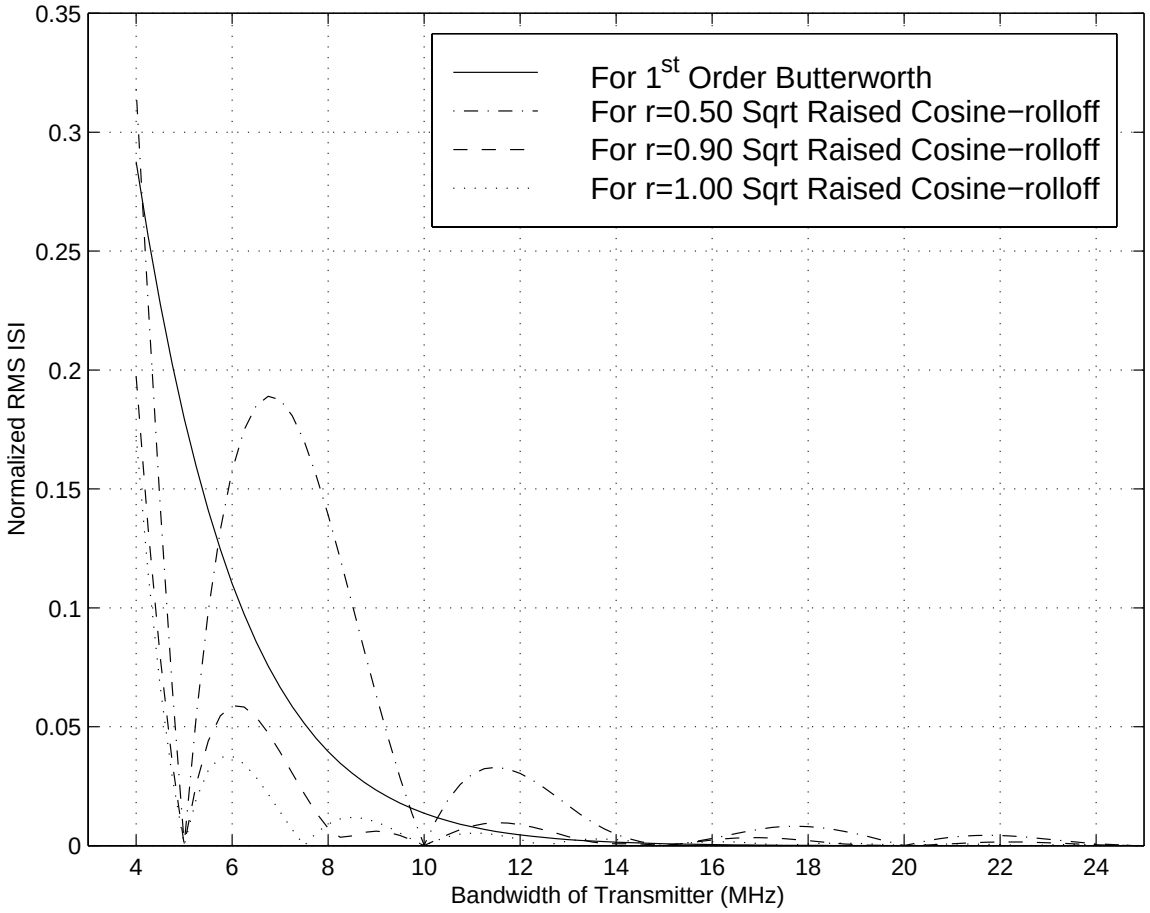

Figure 4.15 The normalized RMS ISI versus the bandwidth of transmitter: assuming that $H_{Tx}(f)=H_{Rx}(f)$, and bit rate=10 Mbps

Assuming that the bandwidth of the transmitter is fixed at 10 MHz, the bandwidth of the receiver will be varied to study the intersymbol interference. The normalized maximum ISI and the normalized RMS ISI are plotted in Figures 4.16 and 4.17, respectively. For the raised cosine-rolloff filters with the receiver bandwidth below 10 MHz, their ISIs tend to decrease as the bandwidth of the receiver increases. In this range of bandwidth, the ISIs fluctuate and become very high at a bandwidth below 3 MHz. At the receiver bandwidth of 10 MHz, the ISIs are zero because the bandwidth of the receiver matches the bandwidth of the transmitter; thus, the zero ISI condition is satisfied. For the transmitter bandwidth above 10 MHz, the ISIs increase slightly and then become constant.

Comparing the raised cosine-rolloff filters to the first order Butterworth filter from Figure 4.16 and 4.17, at the receiver bandwidth below 10 MHz, the ISIs from the first order Butterworth filter is better than the ISIs from the raised cosine-rolloff filters with 0.25 and 0.5 rolloff factors. But, for the unity rolloff factor, the ISIs from the raised cosine-rolloff filter are a little bit better than that of the first order Butterworth filter. Certainly, at the bandwidth of 10 MHz, the ISIs from the raise cosine-rolloff filters are much better because the zero ISI condition is satisfied. For the receiver bandwidth higher than 10 MHz, the ISIs from the first order Butterworth filter approach zero while those of the raised cosine-rolloff filters are constant. For example, the normalized maximum ISI for r=0.25 and 0.5 are 0.15 and 0.11, respectively, while the normalized maximum ISI of the first order Butterworth is 0.004 and approach zero as the receiver bandwidth increases.

To summarize, the raised cosine-rolloff filters can give better ISIs than the first order Butterworth filter if the bandwidths of the transmitter and receiver are identical and the bandwidths are matched to the bit rate of the signal, as shown in Figures 4.14 and 4.15. However, the achieved ISIs from the raised cosine-rolloff filters fluctuate and become much higher than the achieved ISIs from the first order Butterworth filter at a bandwidth below approximately 3 MHz. And, if the bandwidths of the transmitter and receiver are not identical, the achieved ISIs from the raised cosine-rolloff filters are almost always poorer than the ISIs from the first order Butterworth filter, except for some

cases of high rolloff factor and low receiver bandwidth; for example, at r=1 with the receiver bandwidth below 11 MHz, as shown in Figures 4.16 and 4.17.

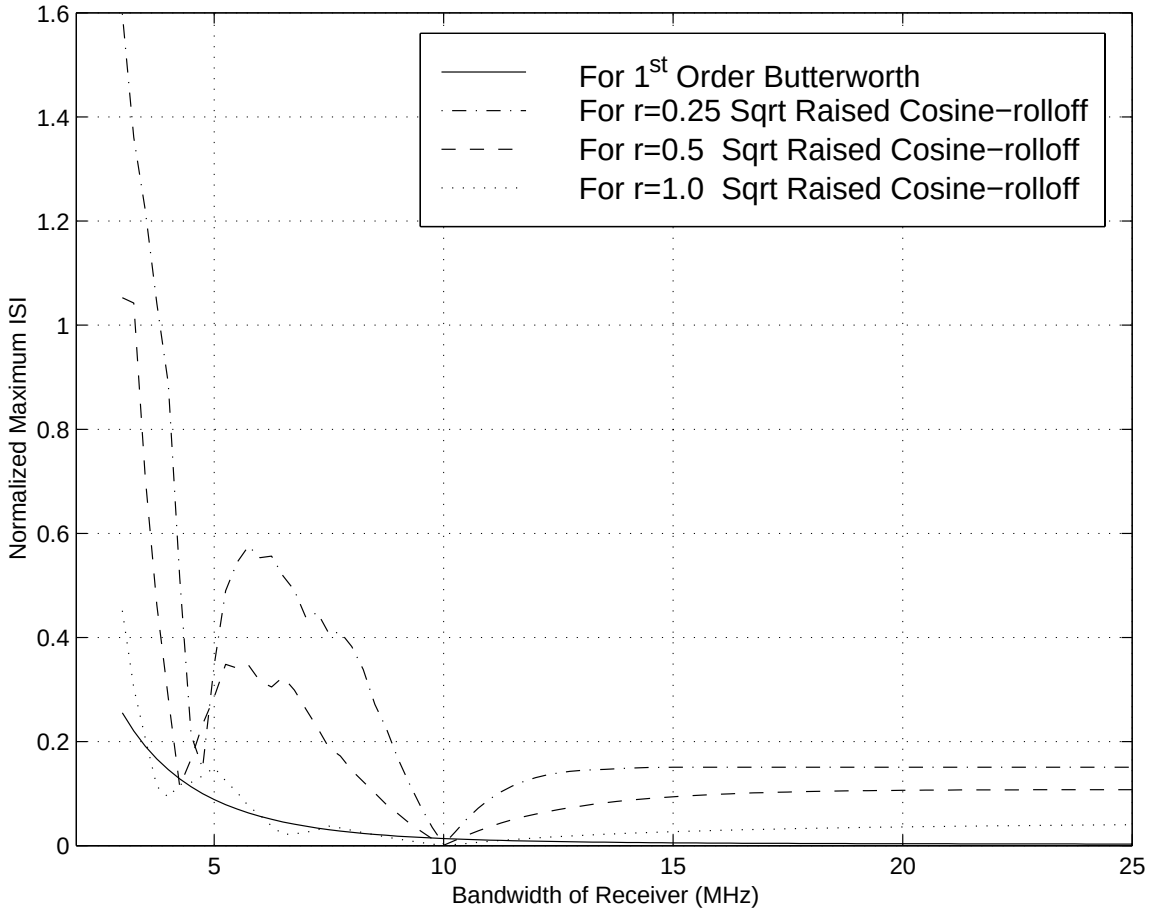

Figure 4.16 The normalized maximum ISI versus the receiver bandwidth: assuming that BW_{Tx}=10 MHz and bit rate=10 Mbps.

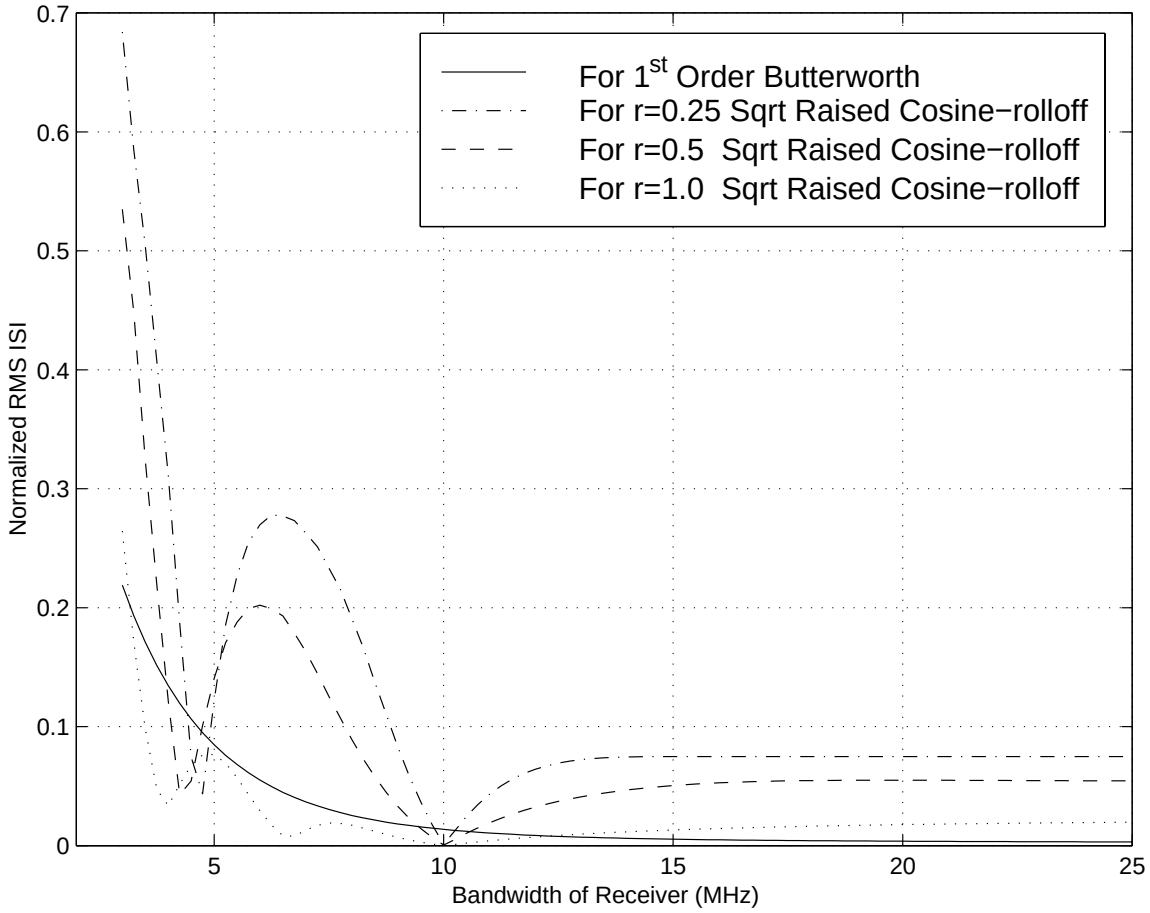

Figure 4.17 The normalized RMS ISI versus the receiver bandwidth: assuming that BW_{Tx}=10 MHz and bit rate=10 Mbps.

4.3 Power Penalty due to the intersymbol interference

In this section, the power penalty from the intersymbol interference will be discussed. From previous sections, the intersymbol interference has been categorized into two types; that is, the normalized maximum ISI and the normalized RMS ISI. The power penalty from each type will be considered.

- **Power penalty due to the normalized maximum ISI.**

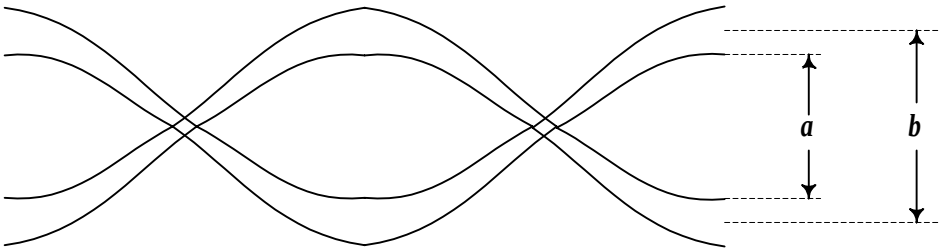

Figure 4.18 The eye diagram.

Considering the eye pattern in Figure 4.18, b is the height of the eye in the absence of ISI and a is the minimum height of the eye when the intersymbol interference occurs. The normalized maximum ISI is given by

$$ISI_{\max,normalized} = \frac{b-a}{b} \qquad (4.3.1)$$

To increase the height a (from ISI) to be the height b (in case of no ISI), the power must be increased. This increased power is the power penalty of the normalized maximum ISI, and is given by

$$\delta_{ISI,\max} = 10\log_{10}\left(\frac{b}{a}\right) \qquad (4.3.2)$$

Applying equation (4.3.1) to equation (4.3.2), the power penalty due to the normalized maximum ISI is given by

$$\delta_{ISI,\max} = -10\log_{10}\left(1 - ISI_{\max,normalized}\right) \qquad (4.3.3)$$

- **Power penalty due to the normalized RMS ISI**

Assuming that only thermal noise and intersymbol interference are impairments in the system, and the extinction ratio is zero, the input current to the decision circuit is given by

$$i = I_p + i_{th} + \chi I_p \tag{4.3.4}$$

where I_p is the mean of the input current i for bit 0 or bit 1

i_{th} is the current induced by thermal noise

χI_p is the current due to the RMS ISI

χ is the RMS ISI parameter, which is assumed to be a zero mean Gaussian random variable with a variance of σ_χ^2.

χ is assumed to be a zero mean Gaussian random variable since it is from the sum of many interfering bits, which are assumed to have the same probability density function.

Since the extinction ratio is zero, the average input currents for bit 1 and bit 0 are I_1 and 0, respectively. As mentioned in chapter 3, with the Gaussian approximation, the variance of thermal noise will be added to the variances of both bits. The intersymbol interference will also affect both bits since this interference is from the neighboring bits. Thus, the variances of bit 1 and bit 0 are the same; that is,

$$\begin{aligned}\sigma_0^2 = \sigma_1^2 &= \left\langle {i_{th}}^2 \right\rangle + \left\langle \chi^2 {I_1}^2 \right\rangle \\ &= 8\pi q V_T C_e (\Delta f)^2 + \sigma_\chi^2 I_1^2\end{aligned} \tag{4.3.5}$$

where σ_χ is the normalized RMS ISI.

Substituting the average input currents and their variances into equation (3.1.10), and substituting I_1 by equation (3.2.5) with a zero extinction ratio, the parameter k is given by

$$k = \frac{B}{\Delta f} \cdot \frac{\eta q \overline{N}_p}{\sqrt{8\pi q V_T C_e + \sigma_\chi^2 (2\eta q \overline{N}_p)^2 \left(\frac{B}{\Delta f}\right)^2}} \tag{4.3.6}$$

From equation (4.3.6), the average number of photons per bit is given by

$$\overline{N}_p = \left(\frac{1}{\sqrt{1 - 4k^2 \sigma_\chi^2}} \right) \left(\frac{k^2}{\eta} \right) \left(\frac{\Delta f}{B} \right) \sqrt{\frac{8\pi V_T C_e}{q}} \tag{4.3.7}$$

Comparing the average number of photons per bit from equation (4.3.7) to equation (3.2.16), the power penalty due to the normalized RMS ISI is given by

$$\delta_{ISI,RMS} = 10\log_{10}\left(\frac{1}{\sqrt{1-4k^2\sigma_\chi^2}}\right) \tag{4.3.8}$$

From equation (4.3.8), it is seen that for a given σ_χ, there exists a maximum value of *k*. Applying this maximum *k* into equation (3.1.9), there exists a lower bound to the error probability that can be achieved even though the input optical power is increased. The maximum value of *k* is given by

$$k_{\max} = \frac{1}{2\sigma_\chi} \tag{4.3.9}$$

In Figure 4.19, the normalized maximum ISI and RMS ISI are plotted versus the ratio of the receiver bandwidth to the bit rate. It is assumed here that the bandwidths of fiber and transmitter are much higher than the bandwidth of the receiver. Both ISIs decrease as the ratio of receiver bandwidth to bit rate increases. And, for a low [BW_{Rx}/B], the normalized RMS ISI is slightly lower than the normalized maximum ISI. Using these ISIs with equation (4.3.3) and equation (4.3.8), the power penalties from both ISIs are plotted in Figure 4.20. At a low [BW_{Rx}/B], the power penalty from the normalized RMS ISI is much higher than the power penalty from the normalized maximum ISI. If [BW_{Rx}/B] increases both power penalties will move closer and merge together at the high [BW_{Rx}/B], and finally approach zero. From this figure, for the low [BW_{Rx}/B], the power penalty of the normalized RMS ISI from equation (4.3.8) is pessimistic and may be less useful than the power penalty of the normalized maximum ISI from equation (4.3.3). The reason for this is when [BW_{Rx}/B] is small, the number of interfering bits is not high enough to assume χ to be a zero mean Gaussian random variable. The tails of the Gaussian distribution will lead to an unrealistically high power penalty. Also, as was shown in section 4.2.3 since the number of interfering bits is 4, the normalized maximum ISI is more likely to occur. The normalized maximum ISI is consequently more meaningful than the normalized RMS ISI.

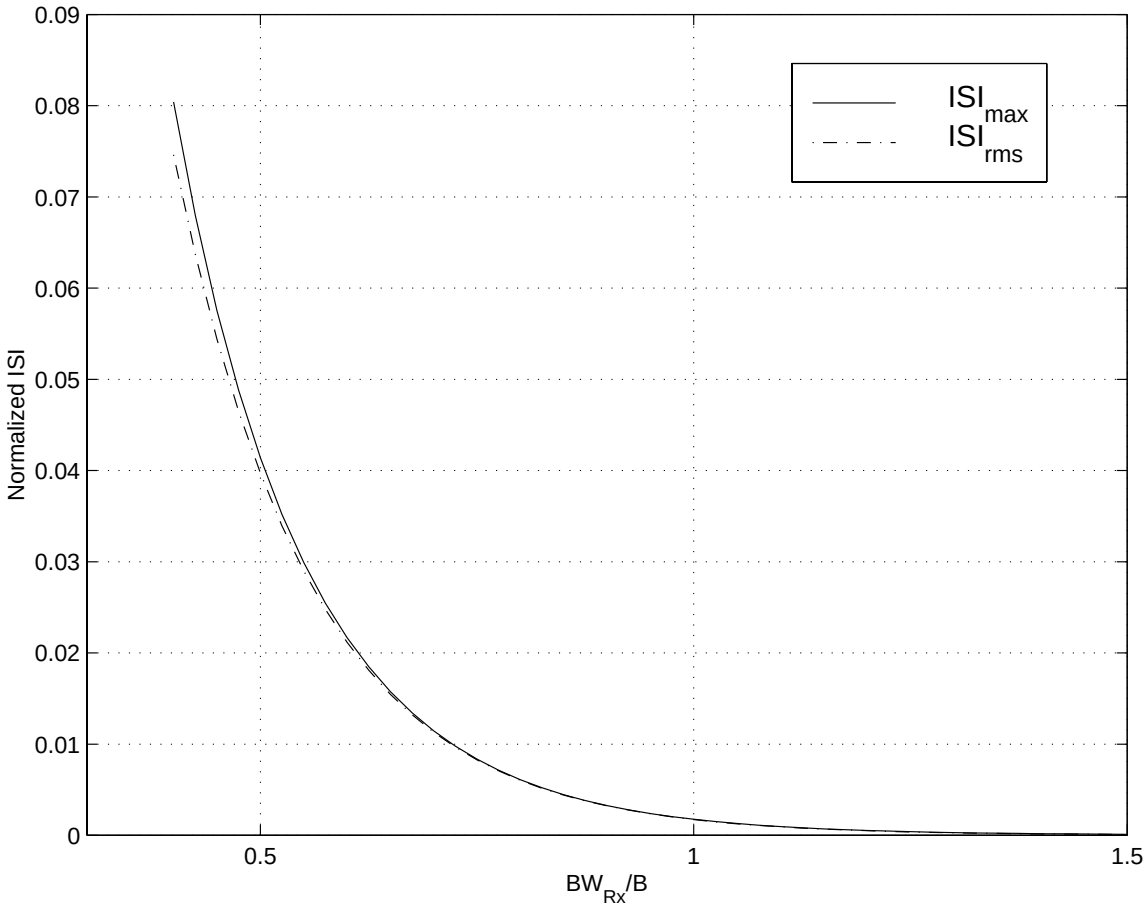

Figure 4.19 The normalized maximum ISI and normalized RMS ISI versus [BW_{Rx}/B].

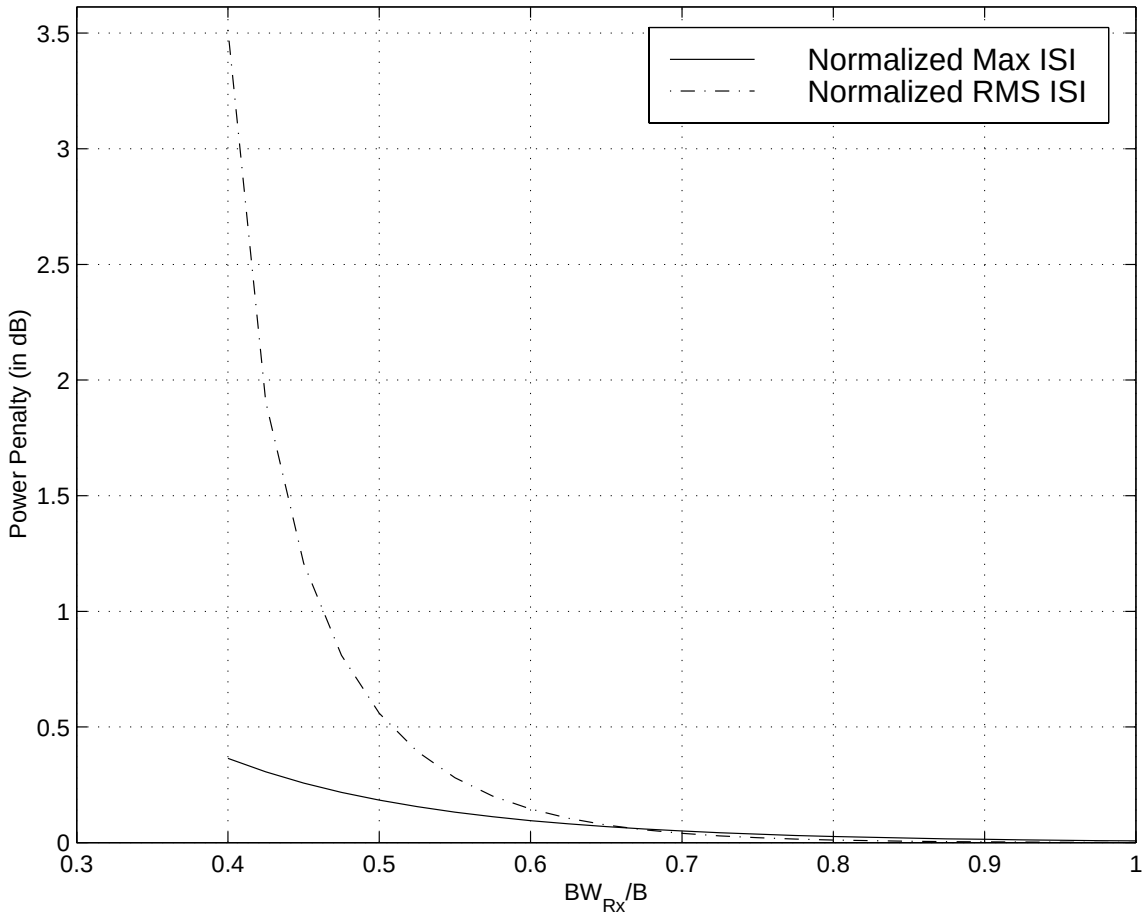

Figure 4.20 The power penalty due to the intersymbol interference versus [BW_{Rx}/B].

The normalized maximum ISI and the normalized RMS ISI are plotted versus the ratio of fiber bandwidth to bit rate (BW_{fiber}/B) in Figure 4.21. The transmitter and receiver bandwidths are fixed at 0.7 times bit rate. From the figure, it is seen that the normalized maximum ISI is slightly greater than the normalized RMS ISI. For low [BW_{fiber}/B] (e.g. [BW_{fiber}/B]=0.5), both ISIs are very high compared to those with high values of [BW_{fiber}/B]. If [BW_{fiber}/B] increases, both ISIs will decrease rapidly and get a minimum value at [BW_{fiber}/B] of 0.85. If [BW_{fiber}/B] increases further, both ISIs will slightly increase and approach ISI of 0.07 approximately. The reason for this is explained as follows. For low [BW_{fiber}/B], the effect of fiber bandwidth dominates both ISIs. The impulse response of the system for different values of [BW_{fiber}/B] is shown in Figure 4.22. It is seen that at [BW_{fiber}/B] of 0.4, the system impulse response wider than those of other values of [BW_{fiber}/B] and it is similar to the impulse response of 2^{nd} order Butterworth filter as shown in Figure 4.2. When [BW_{fiber}/B] increases from 0.4 to 0.6, the width of the impulse response is narrower and the peak of the impulse response becomes higher. This leads to a smaller ISI since the peak increases and the number of interfering bits that strongly affect ISI is small. When [BW_{fiber}/B] is 0.85, the impulse response is similar to the impulse response shown in Figure 4.13. At this [BW_{fiber}/B], the effect of interfering bits to ISI is least so there is an optimum ISI. As shown in Figure 4.21, the optimum maximum ISI and RMS ISI are 0.043 and 0.042, respectively. If [BW_{fiber}/B] increases further, the effect of transmitter and receiver bandwidths becomes more significant and finally dominates the ISI computation. As seen in Figure 4.22, the impulse response of [BW_{fiber}/B] of 1.5 is similar to that shown in Figure 4.13. Consequently, for high [BW_{fiber}/B], both ISIs will approach the values of 0.068 and 0.066 for maximum ISI and RMS ISI, respectively. These values of ISI are from [BW_{Tx}/B] of 0.7 in Figure 4.10 assuming that fiber bandwidth is much larger than transmitter and receiver bandwidths.

The power penalty due to the normalized maximum ISI is shown in Figure 4.23. It is seen that there is a minimum power penalty at [BW_{fiber}/B] of 0.85 since the normalized maximum ISI is optimal. The minimum power penalty is 0.19 dB.

From Figures 4.21 to 4.23, it is shown that if the transmitter and receiver bandwidths are fixed at 0.7, the fiber bandwidth affects ISI. For low [BW_{fiber}/B], the

effect of fiber bandwidth is dominant. On the other hand, for high [BW_{fiber}/B], the effect of transmitter and receiver bandwidths is dominant. Moreover, at [BW_{fiber}/B] of 0.85, the optimum ISI is achieved; thus, a minimum power penalty.

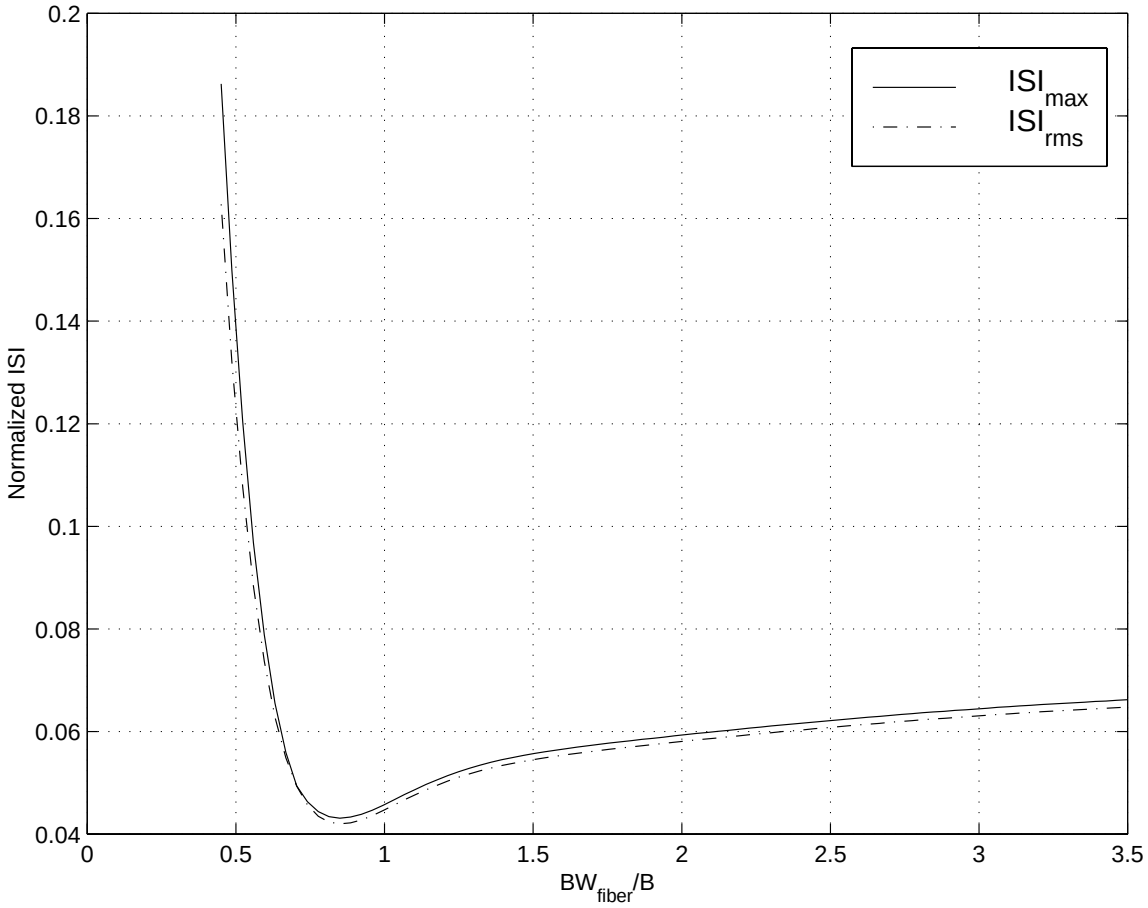

Figure 4.21 Normalized maximum ISI and normalized RMS ISI versus the ratio of fiber bandwidth (BW_{fiber}) to bit rate (B):assuming BW_{Tx}=BW_{Rx}=0.7*B.

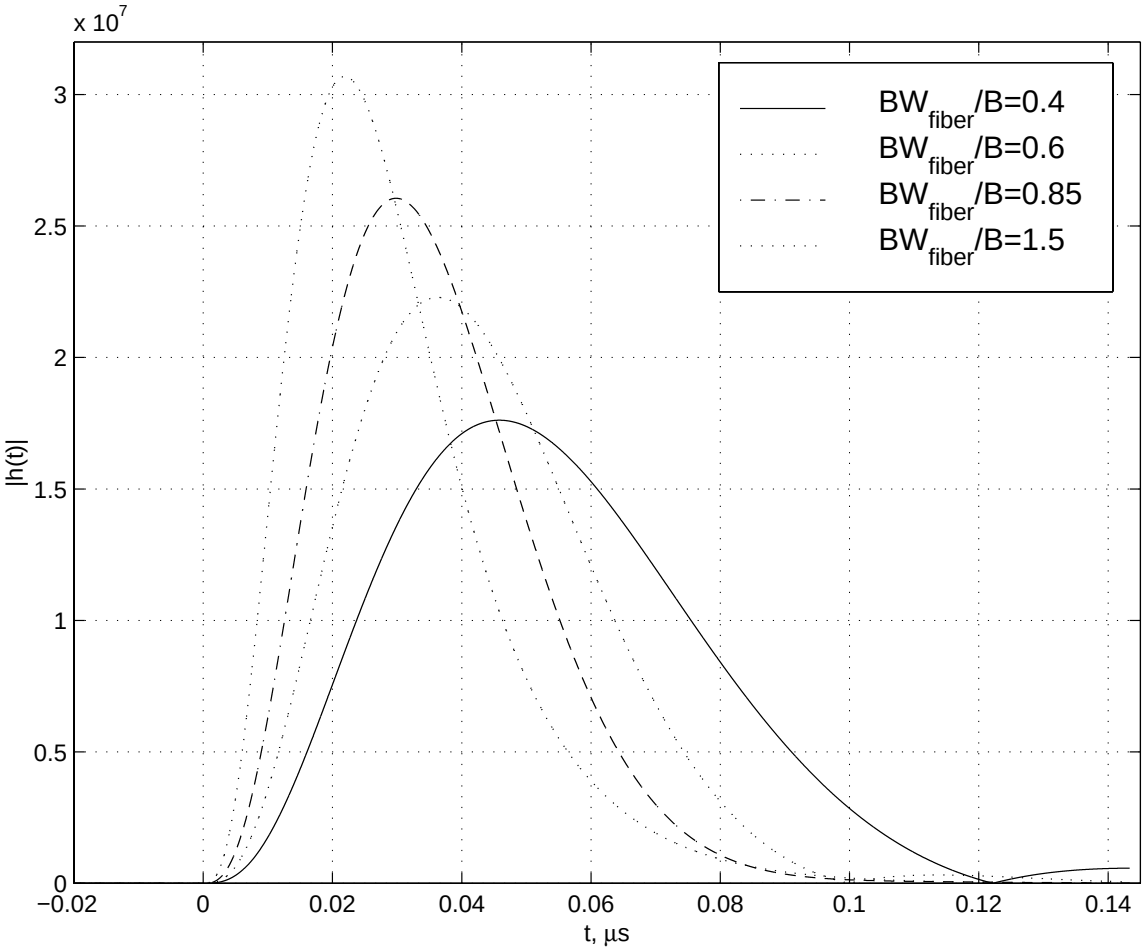

Figure 4.22 The impulse response of system for different ratios of fiber bandwidth (BW_{fiber}) to bit rate (B):assuming BW_{Tx}=BW_{Rx}=0.7*B.

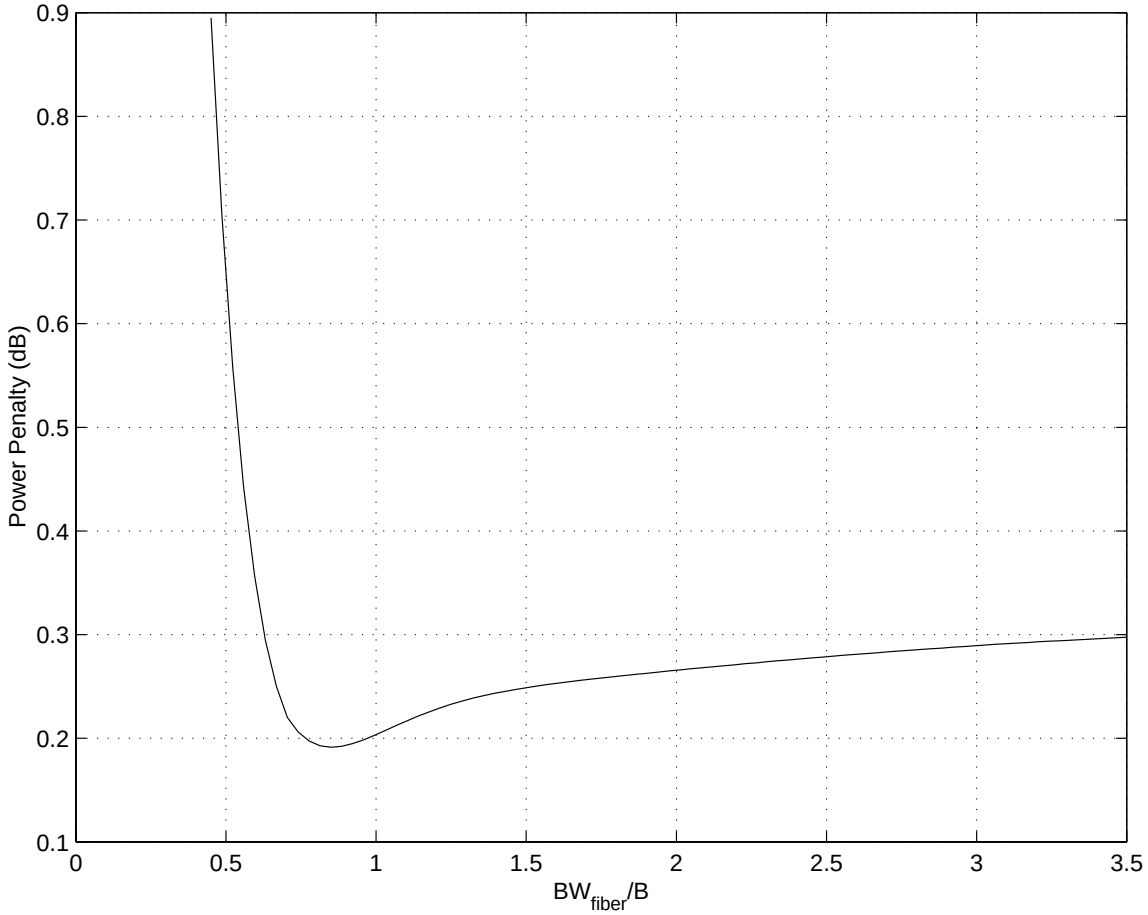

Figure 4.23 Power penalty due to the normalized maximum ISI versus the ratio of fiber bandwidth (BW_{fiber}) to bit rate (B):assuming $BW_{Tx}=BW_{Rx}=0.7*B$.

5.0 Conclusions and suggestions for future research

In optical communication systems many types of impairments are added to the signal. These impairments result in a fluctuation to the signal; therefore, they can degrade the system performance. In this thesis, the impairments have been categorized into four types; that is,

1. thermal noise
2. shot noise (quantum noise)
3. signal-dependent noise
4. intersymbol interference

Characteristics of these impairments have been discussed in chapter 2. It is indicated that thermal noise arises from the random movement of the charge carriers in electronic devices in the system. Thermal noise power does not depend on the signal power as shot noise and signal-dependent noise do. Shot noise (or quantum noise) is from the random nature of received photons that leads to a fluctuation of the photocurrent. The power of shot noise is proportional to the received optical power. For signal-dependent noise, it has been characterized into three types; that is, modal noise, mode partition noise, and relative intensity noise. The interference among the various propagating modes

in a multimode fiber results in a fluctuation of the received signal; thus, modal noise. Mode partition noise is from an intensity fluctuation among longitudinal modes of a multimode semiconductor laser and different propagating velocities caused by fiber dispersion. Relative intensity noise (RIN) originates from a fluctuation induced by the spontaneous emission in semiconductor lasers. RIN can be enhanced by optical feedback from reflection from outside of laser cavity. Even if the optical feedback is not fed back into the laser cavity, it can enhance RIN by a process called phase-to-intensity noise conversion. The last impairment is intersymbol interference (ISI). ISI is from overlapping between pulses. This overlap may result in a wrong bit decision so it can increase bit-error-rate of the system.

In chapter 3, the Gaussian approximation has been used to evaluate the system performance parameters (e.g. bit-error-rate and receiver sensitivity). The effect of thermal noise, shot noise, and signal-dependent noise are considered. The effect of nonzero-extinction ratio is also included in this chapter. It is shown in Figure 3.2 that RIN introduces an error floor to the system. In Figure 3.5, it is seen that nonzero-extinction ratios shift the bit-error-rate curve to the right. The more the extinction ratio, the more the bit-error-rate curve shifts to the right. The combined effect of RIN and nonzero-extinction ratio is shown in Figure 3.7. The left-most curve is from the presence of thermal noise and shot noise only. When RIN and nonzero-extinction ratio occur, the curve is shifted to the right and an error floor is introduced. This error floor is poorer than the error floor from the case of zero-extinction ratio. It is shown that the power penalty is considerably increased if a nonzero-extinction ratio and RIN are present in the system. The decision threshold at the decision circuit is an important parameter. If this parameter is set improperly, a vertical offset from an optimum threshold occurs and subsequently results in a power penalty to the system as shown in Figure 3.13.

The effect of system bandwidth on intersymbol interference (ISI) has been evaluated numerically in chapter 4. Transfer functions of transmitter, fiber, and receiver are modeled as Butterworth filters (orders of 1, 2, and 1, respectively). The effect of fiber bandwidth on ISI is similar to the effect of transmitter and receiver bandwidths on ISI. That is, for low bandwidth, ISI is high. If bandwidth increases, ISI becomes smaller and finally approaches zero. The number of interfering bits is a parameter that can affect the

computation. It is shown that the minimum number of interfering bits is 4. The number of following bits that interfere the bit at time t=0 is less than the number of preceding bits since the impulse response of the system is not symmetric in time as shown in Figure 4.2.3. Comparing between Butterworth filters and raised cosine-rolloff filters, it is shown that raised cosine-rolloff filters give much better performance for ISI than Butterworth filters at particular bandwidths. However, if the transmitter and receiver bandwidths are not matched and are not equal to these bandwidths, the achieved ISI from raised cosine-rolloff filters is much higher than that from Butterworth filters.

The power penalty from ISI has been studied. The power penalty from the normalized maximum ISI is determined by the eye diagram approach whereas the power penalty from the normalized RMS ISI is determined by using Gaussian approximation as shown in chapter 3. It is shown that the power penalty from the normalized RMS ISI is more pessimistic and less useful than that from the normalized maximum ISI. Assuming that the transmitter and receiver bandwidths are matched and fixed to be a constant, a minimum ISI can be achieved if the ratio of fiber bandwidth to bit rate is 0.85 as shown in Figure 4.21.

Future work may involve other approaches to model noise in the system because some types of noise such as shot noise are not appropriate to be used in the Gaussian approximation. These approaches will give alternatives to analyze noises and their effects on system performance. It is also interesting to compare the analyzed result from the thesis to the actual results from experiments. This may give us more understanding on the effect of noise in the system and may lead to a more accurate way to analyze the system.

In chapter 4, only three components are modeled and combined to be a system. However, for a more detailed examination, other components such as optical amplifier and equalizer may be modeled and added to the system. The intersymbol interference of such system should be evaluated and compared to that of the system in the chapter.

Appendix A: Effect of signal-dependent noise in shot noise limit.

In this section, the photodetector is an avalanche photodetector (APD) with a multiplication factor of M. For APDs, shot noise dominates the system; thus, we are in the shot noise limit. Similar to chapter 3, the Gaussian approximation will be used to evaluate the average number of photons per bit although the Gaussian approximation is questionable in the shot noise limit. Assuming zero-extinction ratio, the average currents for bit 0 and bit 1 are given by

$$\langle i_0 \rangle = 0 \tag{A.1}$$

$$\langle i_1 \rangle = MI_1 \tag{A.2}$$

Assuming there is only shot noise in the system, the variances of current for bit 0 and bit 1 are given by [1]

$$\langle i_0^2 \rangle = 0 \tag{A.3}$$

$$\langle i_1^2 \rangle = 2qM^2 I_1 F_A(\Delta f) \tag{A.4}$$

where F_A is the excess noise factor of the APD.

Substituting the average currents and their variances into equation (3.1.10) and expressing I_1 in terms of $\overline{N}_p$, the average number of photons per bit is given by

$$\overline{N}_p = \left(\frac{k^2}{\eta}\right)\left(\frac{\Delta f}{B}\right)F_A \tag{A.5}$$

If relative intensity noise is present in the on-state, the variance of current for bit 1 is changed to be

$$\left\langle i_1^2 \right\rangle = 2qM^2 I_1 F_A(\Delta f) + RIN(0)(\Delta f) M^2 I_1^2 \qquad \text{(A.6)}$$

Substituting the average currents and their variances into equation (3.1.10) and expressing I_1 in terms of $\overline{N}_p$, the average number of photons per bit is given by

$$\overline{N}_p = \left[\frac{1}{1 - RIN(0)(\Delta f)k^2}\right]\left(\frac{k^2}{\eta}\right)\left(\frac{\Delta f}{B}\right)F_A \qquad \text{(A.7)}$$

From equation (A.7) and (A.5), the power penalty from RIN in shot noise limit is given by

$$\delta_{RIN}(dB) = 10\log_{10}\left[\frac{1}{1 - RIN(0)(\Delta f)k^2}\right] \qquad \text{(A.8)}$$

Comparing equation (A.8) to equation (3.2.25), it is seen that the effects of signal-dependent noise in the thermal noise limit and the shot noise limit are the same, assuming the Gaussian approximation applies in both cases.

References

[1] G. P. Agrawal, " *Fiber-optic Communication Systems*" , second edition, John Wiley &Sons, Inc., 1997.

[2] G. Keiser, " *Optical fiber communications*" , second edition, McGraw-Hill, Inc., 1991.

[3] J. H. Winters, R. D. Gitlin, and S. Kasturia, " Reducing the Effects of transmission impairments in Digital Fiber Optic Systems" , *IEEE Communications Magazine*, June, 1993, pp.68-76.

[4] H. Tsai and C. Liu, " Harmonic noise characterization of p-i-n diodes under optical illumination" , *Journal of Physics D.*, Vol.28, 1995, pp.1992-1996.

[5] Ira Jacobs, " Optical Fiber Communication Technology and System Overview" , *Trends in Optical Fiber Metrology and Standards*, NATO ASI Ser E, Vol.285, pp.567-592, Kluwer, Academic Publishers, 1994.

[6] H.-A. Bachor and P. T. H. Fisk, " Quantum Noise – A Limit in Photodetection" , *Journal of Applied Physics B.*, Vol.49, 1989, pp.291-300.

[7] A. M. Bacon, H. Z. Shao, L. J. Wang, and J. E. Thomas, " Microwatt shot-noise measurement" , *Applied Optics*, Vol.34, No.24, 20 August 1995, pp.5326-5330.

[8] H. Tsai and C. Liu, " Harmonic noise characterization of p-i-n diodes under optical illumination" , *Journal of Physics D.*, Vol.28, 1995, pp.1992-1996.

[9] A. R. Mickelson and A. Weierholt, " Modal noise-limited signal-to-noise ratios in multimode optical fibers" , *Applied Optics*, Vol.22, No.19, 1 October 1983, pp.3084-3089.

[10] D. R. Hjelme,and A. R. Mickelson, " Microbending and modal noise" , *Applied Optics*, Vol.22, No.23, 1 December 1983, pp.3874-3879.

[11] T. Kanada, " Evaluation of modal noise in multimode fiber-optic systems" , *Journal of Lightwave Technology*, Vol.LT-2, No. 1, February 1984, pp.11-17.

[12] S. Das, C.G. Englefield, and P. A. Goud, " Modal noise and distortion caused by a longitudinal gap between two multimode fibers" , *Applied Optics*, Vol.23, No. 7, 1 April 1984, pp.1110-1115.

[13] S. Das, C.G. Englefield, and P. A. Goud, " Power loss, modal noise and distortion due to microbending of optical fibers" , *Applied Optics*, Vol.24, No. 15, 1 August 1985, pp.2323-2334.

[14] T. Tanifuji, " Modal noise arising from slightly nonuniform quantum efficiency of a detector" , *Journal of Optical Society of America A.*, Vol.2, No.11, November 1985, pp.1852-1856.

[15] A. M. Koonen, " Bit-error-rate degradation in a multimode fiber optic transmission link due to modal noise" , *IEEE Journal on Selected Areas in Communications*, Vol.SAC-4, No. 9, December 1986, pp.1515-1521.

[16] P. Chan and T. T. Tjhung, " Bit error rate performance for optical fiber systems with modal noise" , *Journal of Lightwave Technology*, Vol.7, No.9, September 1989, pp.1285-1289.

[17] Y. Okano, K. Nagakawa, and T. Ito, " Laser mode partition noise evaluation for optical fiber transmission" , *IEEE Transactions on Communications*, Vol. COM-28, No.2, February 1980, pp.238-243.

[18] K. Ogawa, " Analysis of mode partition noise in transmission systems" , *IEEE Journal of Quantum Electronics*, Vol.QE-18, No.5, May 1982, pp.849-855.

[19] K. Ogawa and R.S. Vodhanel, " Measurements of mode partition noise of laser diodes" , *IEEE Journal of Quantum Electronics*, Vol.QE-18, No.7, July 1982, pp.1090-1093.

[20] A.K. Laughton, " Mode partition noise in gain-guided lasers and its effect on a multimode fiber optic system" , *IEE Proceedings*, Vol.132, Pt.J, No.6, December 1985, pp.359-363.

[21] S.E. Miller, " On the injection laser contribution to mode partition noise in fiber telecommunication systems" , *IEEE Journal of Quantum Electronics*, Vol.25, No.8, August 1989, pp.1771-1781.

[22] S.E. Miller, " On the prediction of the mode-partitioning floor in injection lasers with multiple side modes at 2 and 10 Gb/s" , *IEEE Journal of Quantum Electronics*, Vol.26, No.2, February 1990, pp.242-249.

[23] T. Fujita, J. Ohya, H. Serizawa, H. Sato, and K. Fujito, " Correlation between intensity noise and longitudinal modes of a semiconductor laser coupled to an external cavity" , *Journal of Applied Physics*, Vol.57, No.5, March 1, 1985, pp.1753-1758.

[24] M. Port and K. J. Ebeling, " Intensity noise dependence on the injection current of laser diodes with optical feedback" , *IEEE Journal of Quantum Electronics*, Vol.QE-22, No.11, November 1986, pp.2107-2114.

[25] J. Wang and K. Petermann, " Noise characteristics of PCM-modulated single-mode semiconductor laser diodes with distant optical feedback" , *IEE Proceedings*, Vol.137, Pt.J, No.6, December 1990, pp.385-390.

[26] J. L. Gimlett and N. K. Cheung, " Effects of phase-to-intensity noise conversion by multiple reflections on Gigabit-per-second DFB laser transmission systems" , *Journal of Lightwave Technology*, Vol.7, No. 6, June 1989, pp.888-895.

[27] Y. Nakano, Y. Deguchi, K. Ikeda, Y. Luo, and K. Tada, " Reduction of Excess Intensity noise induced by external reflection in a gain-coupled distributed feedback semiconductor laser" , *IEEE Journal of Quantum Electronics*, Vol.27, No.6, June 1991, pp.1732-1735.

[28] M. M. Choy, J. L. Gimlett, R. Welter, L.G. Kazovsky, and N. K. Cheung, " Interferometric conversion of laser phase noise to intensity noise by single-mode fibre optic components" , *Electronics Letters*, Vol.23, No.21, 8th October 1987, pp.1151-1152.

[29] J. L. Gimlett, J. Young, R. E. Spicer, and N. K. Cheung, " Degradations in Gbit/s DFB laser transmission systems due to phase-to-intensity noise conversion by multiple reflection points" , *Electronics Letters*, Vol.24, No.7, 31st March 1988, pp.406-408.

[30] L. W. Couch, " *Digital and analog communication systems*" , 5th edition, Prentice Hall, Upper Saddle River, NJ, 1997.

[31] M. K. Liu, A. C. Vrahas, and M. B. Moretti, " Saddle point bit error rate computations for optical communications systems incorporating equalizers" , *IEEE Transactions on Communications*, Vol.43, No.2, February, 1995, pp.989-1000.

Vita

Surachet Kanprachar was born in Hadyai, Thailand. He attended Chulalongkorn University in Bangkok (1992-1996) and received a B.S. degree (1^{st} class honors) in Electrical Engineering. In 1996, he spent one year as a lecturer at the Faculty of Engineering, Naresuan University in Phitsanuloke, then was awarded a grant from the Royal Thai Government (1997) to further his studies in Electrical Engineering. He is currently a graduate student at Virginia Polytechnic Institute and State University, working toward his Master's degree.